Publications

1. Liu, P., **Meng, L.,** Zhang, H., Chen, J., and Wang, X. (2002) Involvement of camp in ABA Signal Transduction in Tobacco Suspension Cells. Acta Botanica Sinica. 44(12): 1432-37.
Cited by 3

2. **Meng, L.,** Yasumoto, H., and Tsai, R.Y. (2006). Multiple controls regulate nucleostemin partitioning between nucleolus and nucleoplasm. J Cell Sci 119(24): 5124-36.
Cited by 61 IF 6.43

3. Yasumoto, H., **Meng, L.,** Lin, T., Zhu, Q., and Tsai, R.Y. (2007). GNL3L inhibits activity of estrogen-related receptor gamma by competing for coactivator binding. J Cell Sci 120: 2532-43.
Cited by 22 IF 6.38

4. **Meng, L.,** Zhu, Q., and Tsai, R.Y. (2007). Nucleolar trafficking of nucleostemin family proteins: common versus protein-specific mechanisms. Mol Cell Biol 27: 8670-82.
Cited by 50 IF 6.42

5. Ni, S., **Meng, L.,** Zhao, J., Wang, X., and Chen, J. (2008) Isolation and Characterization of the Trichome-specific AtTSG1 Promoter from Arabidopsis thaliana. Plant Mol Biol Rep. 26(4): 263-276.

Cited by 9 IF 0.74

6. **Meng, L.,** Lin, T., and Tsai, R.Y. (2008). Nucleoplasmic mobilization of nucleostemin stabilizes MDM2 and promotes G2-M progression and cell survival. J Cell Sci 121(24): 4037-46.
Cited by 48 IF 6.25

7. Zhu, Q., **Meng, L.,** Hsu, J.K., Lin, T., Teishima, J., and Tsai, R.Y. (2009). GNL3L stabilizes the TRF1 complex and promotes mitotic transition. J Cell Biol 185(5): 827-39. (**Zhu, Q. and Meng, L. contributed equally to this work**)
Cited by 39 IF 9.58

8. Tsai, R.Y., and **Meng, L.** (2009). Nucleostemin: a latecomer with new tricks. Int J Biochem Cell Biol 41: 2122-24.
Cited by 35 IF 4.89

9. Lin, T., **Meng, L.,** Li, Y., and Tsai, R.Y. (2010). Tumor-initiating function of nucleostemin-enriched mammary tumor cells. Cancer Res 70(22): 9444-52.
Cited by 43 IF 8.23

10. **Meng, L.,** Hsu, J.K., and Tsai, R.Y. (2011). GNL3L depletion destabilizes MDM2 and induces p53-dependent G2/M arrest. Oncogene 30(14): 1716-26.
Cited by 21 IF 6.37

11. Lin, T., **Meng, L.,** and Tsai, R.Y. (2011). GTP depletion synergizes the anti-proliferative activity of chemotherapeutic agents in a cell type-dependent manner. Biochem Biophys Res Commun 414(2): 403-08.
Cited by 2 IF 2.48

12. **Meng, L.,** Hsu, J.K., Zhu, Q., Lin, T., and Tsai, R.Y. (2011). Nucleostemin Inhibits TRF1 Dimerization and Shortens Its Dynamic Association with The Telomere. J Cell Sci 124(21): 3706-14.
Cited by 18 IF 6.11

13. **Meng, L.,** Lin, T., Peng, G., Hsu, J.K., Lee, S., Lin, S.Y. and Tsai, R.Y. (2013). Nucleostemin deletion reveals an essential mechanism that maintains the genomic stability of stem and progenitor cells. Proc Natl Acad Sci 110(28): 11415-20.
Cited by 23 IF 9.81

14. Lin, T., **Meng, L.**, Lin, T.C., Wu, L.J., Pederson, T. and Tsai, R.Y. (2014) Nucleostemin and GNL3L exercise distinct functions in genome protection and ribosome synthesis, respectively. J Cell Sci. 127(10): 2302-12
Cited by 8 IF 5.43

15. **Meng, L.,** Park, J.E., Kim, T.S., Lee, E.H., Park, S.Y., Zhou, M., Bang, J.K. and Lee, K.S. (2015). Bimodal Interaction of Mammalian Polo-Like Kinase 1 and a Centrosomal Scaffold, Cep192, in the Regulation of Bipolar Spindle Formation. Mol Cell Biol, 35(15): 2626-40
Cited by 2 IF 4.43

16. Park, J.E., Kim, T.S., **Meng, L.**, Bang, J.K., Kim, B.Y. and Lee, K.S. (2015) Putting a bit into the polo-box domain of polo-like kinase 1. J Anal Sci Technol. 6(1): 27.

17. Huang, G., **Meng, L.** and Tsai, R.Y. (2015) p53 Configures the G2/M Arrest Response of Nucleostemin-Deficient Cells. Cell Death Discov. 1:15060. (**Huang, G. and Meng, L. contributed equally to this work**)
Cited by 2

Nucleostemin deletion reveals an essential mechanism that maintains the genomic stability of stem and progenitor cells

Lingjun Meng[a,1], Tao Lin[a,1], Guang Peng[b], Joseph K. Hsu[a], Sun Lee[a], Shiaw-Yih Lin[c], and Robert Y. L. Tsai[a,2]

[a]Center for Cancer and Stem Cell Biology, Institute of Biosciences and Technology, Texas A&M Health Science Center, Houston, TX 77030; and [b]Department of Clinical Cancer Prevention, Unit 1013, and [c]Department of Systems Biology, Unit 950, University of Texas M. D. Anderson Cancer Center, Houston, TX 77054

Edited by Solomon H. Snyder, The Johns Hopkins University School of Medicine, Baltimore, MD, and approved May 8, 2013 (received for review January 25, 2013)

Stem and progenitor cells maintain a robust DNA replication program during the tissue expansion phase of embryogenesis. The unique mechanism that protects them from the increased risk of replication-induced DNA damage, and hence permits self-renewal, remains unclear. To determine whether the genome integrity of stem/progenitor cells is safeguarded by mechanisms involving molecules beyond the core DNA repair machinery, we created a nucleostemin (a stem and cancer cell-enriched protein) conditional-null allele and showed that neural-specific knockout of nucleostemin predisposes embryos to spontaneous DNA damage that leads to severe brain defects in vivo. In cultured neural stem cells, depletion of nucleostemin triggers replication-dependent DNA damage and perturbs self-renewal, whereas overexpression of nucleostemin shows a protective effect against hydroxyurea-induced DNA damage. Mechanistic studies performed in mouse embryonic fibroblast cells showed that loss of nucleostemin triggers DNA damage and growth arrest independently of the p53 status or rRNA synthesis. Instead, nucleostemin is directly recruited to DNA damage sites and regulates the recruitment of the core repair protein, RAD51, to hydroxyurea-induced foci. This work establishes the primary function of nucleostemin in maintaining the genomic stability of actively dividing stem/progenitor cells by promoting the recruitment of RAD51 to stalled replication-induced DNA damage foci.

DNA damage repair | homologous recombination | conditional knockout | replication fork stalling | neural development

Stem and progenitor cells play critical roles in embryonic organogenesis, adult tissue regeneration, and tumor development. To maintain self-renewing proliferation, they must be protected from replication-induced DNA damage that limits the proliferative lifespan of most dividing cells. Replication-induced DNA damage may occur spontaneously as a result of stalled and collapsed replication forks, caused by the slowing of the DNA replication machinery over replication "trouble" zones or previously unrepaired damage sites (1–3). Alternatively, replication stalling can be triggered by drugs that deplete the endogenous nucleotide pool (e.g., hydroxyurea) or inhibit the activity of DNA replication (e.g., camptothecin). Prolonged replication stalling will lead to the collapse of replication machinery and double-strand DNA breaks (DSBs), causing cell cycle arrest and genomic instability (4, 5). To date, it remains unclear how stem and progenitor cells survive the increased risk of replication-induced DNA damage during this hyperactive mitotic window of embryogenesis.

Nucleostemin (NS) is a stem cell-enriched nucleolar protein (6). Its biological significance has been illustrated by the early embryonic lethal phenotype of NS germ-line knockout mice (7), which ineluctably hinders further analyses of its in vivo function beyond the blastula stage. To date, the mechanism of NS action in vivo remains unclear. Although some suggested a connection to the p53 pathway (6, 8–10), others have shown that NS is functionally indispensable even in p53-null cells (11, 12). We recently discovered a function of NS in preventing DNA damage on interstitial and telomeric chromosomes, which, by far, best recapitulates its obligatory role in biology (13). Although the telomere-protecting function of NS is mediated by telomeric repeat binding factor 1 (TRF1) SUMOylation and promyelocytic leukemia protein isoform IV (PML-IV) recruitment (13), the role of NS in protecting nontelomeric chromosomes is yet unknown. We hypothesize that NS may formulate a unique mechanism that protects stem/progenitor cells from spontaneous DNA damage as a result of DNA replication. To investigate this idea, we created the NS-flox (NS^{f}) allele and two NS conditional-knockout (NS^{cko}) mouse models. Analyses of these mouse models revealed that neural-specific deletion of NS increases the frequency of spontaneous DNA damage and eliminates neural stem cells (NSCs) in the developing neuroepithelium. DNA damage triggered by NS deletion occurs in a replication-dependent manner and independently of the p53 status or ribosomal RNA (rRNA) synthesis. More importantly, NS is capable of being recruited to DNA damage sites and is required for the efficient recruitment of RAD51 to stalled replication-induced damage foci. This work signifies a primary role of NS in maintaining the genomic stability of stem and progenitor cells.

Results

Creation of a NS Conditional-Knockout Allele. The gene-targeting strategy was used to generate ES cells with a $NS^{floxneo}$ (NS^{fn}) allele, which contains a loxP site linked to an frt-flanked phosphoglycerate kinase-neomycin (pgk-neo) cassette at 820 bp upstream of the first exon and a second loxP site in the second intron (Fig. 1*A* and Fig. S1*A*). After germ-line transmission, the pgk-neo cassette was deleted from the NS^{fn} allele to generate the NS^{flox} (NS^{f}) allele (Fig. S1 *B–D*). $NS^{f/f}$ homozygotes manifest normal developmental, growth, and reproductive activities, and homozygous deletion of the floxed sequence (NS^{null}) results in early embryonic lethality at embryonic day (E) 3.5 (Fig. S1*E*). These findings confirm that the NS^{f} allele is a bona fide conditional-null allele.

Neural-Specific Deletion of NS Triggers DNA Damage and Decreases NSCs in Vivo. To study the NS function in the developing brain, a nestin promoter-driven Cre (Cre^{nestin}) (14) was used to delete NS in the neuroepithelial stem/progenitor cells ($neNS^{cko}$).

Author contributions: L.M., T.L., and R.Y.L.T. designed research; L.M., T.L., G.P., J.K.H., S.L., and R.Y.L.T. performed research; L.M., T.L., G.P., and R.Y.L.T. analyzed data; G.P. and S.-Y.L. contributed new reagents/analytic tools; and R.Y.L.T. wrote the paper.

The authors declare no conflict of interest.

This article is a PNAS Direct Submission.

[1]L.M. and T.L. contributed equally to this work.

[2]To whom correspondence should be addressed. E-mail: rtsai@ibt.tamhsc.edu.

This article contains supporting information online at www.pnas.org/lookup/suppl/doi:10.1073/pnas.1301672110/-/DCSupplemental.

CELL BIOLOGY

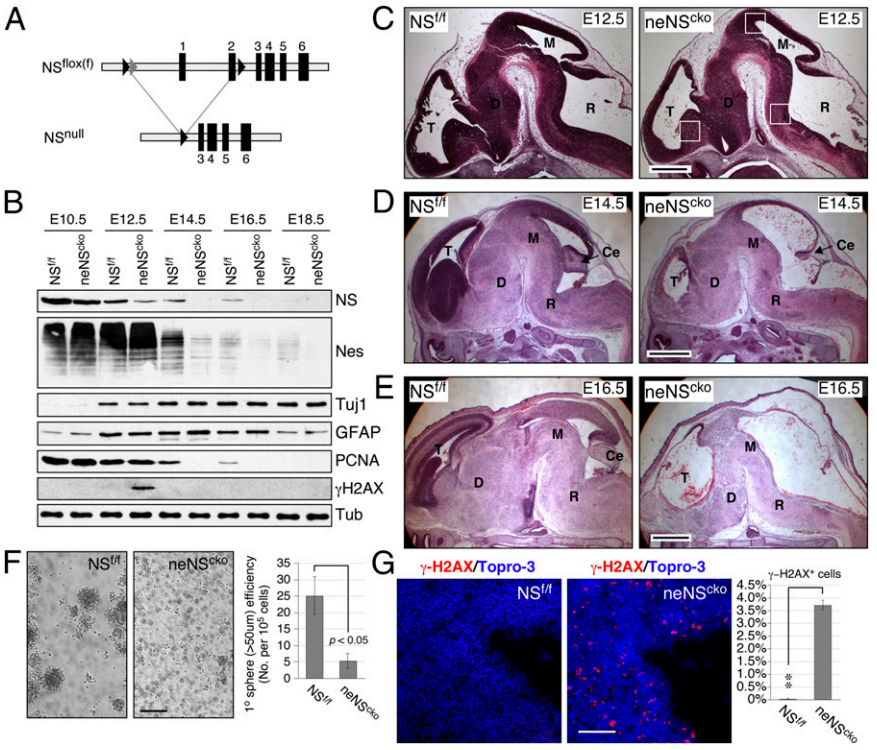

Fig. 1. Neural-specific deletion of nucleostemin (NS) induces DNA damage, decreases embryonic neural stem cells (NSCs), and causes severe brain defects in vivo. (*A*) Diagrams of the NS-flox (NS^{f}) and null (NS^{null}) alleles. Black arrowheads, loxP; gray arrowheads, frt. (*B*) Cre^{nestin}-driven NS deletion ($neNS^{cko}$) decreases its protein in the developing forebrain from embryonic day 12.5 (E12.5). The levels of nestin and PCNA proteins are reduced from E14.5. An increase of γ-H2AX proteins is noted in the $neNS^{cko}$ forebrain at E12.5. Tuj1, neuron-specific β-tubulin; GFAP, glial fibrillary acid protein. (*C*) Compared with control $NS^{f/f}$ embryos, $neNS^{cko}$ embryos begin to show a decreased cellularity in the telencephalic (T), diencephalic (D), mesencephalic (M), and rhombencephalic (R) neuroepithelium at E12.5. Squares indicate regions shown in *G* and Fig. S2*B*. At E14.5 (*D*) and E16.5 (*E*), $neNS^{cko}$ embryos exhibit severe brain defects throughout the neural axis. Ce, cerebellar primordium. (*F*) At E12.5, the forebrains of $neNS^{cko}$ embryos contain much less sphere-forming NSCs than that of $NS^{f/f}$ embryos. (*G*) A notable phenotype of NS deletion is the increase of γ-$H2AX^{+}$ cells in the ventricular zone of the E12.5 neuroepithelium. The region shown here is close to the midbrain roof. (Scale bars: 500 μm in *C*, 1 mm in *D* and *E*, and 100 μm in *F* and *G*.) Bar graphs, mean ± SEM; $*P < 0.01$; $**P < 0.001$; $***P < 0.0001$.

Homozygous $neNS^{cko}$ mice die immediately after birth due to respiratory failure. Western blots showed that Cre^{nestin}-driven NS deletion reduces NS proteins in the developing forebrain most significantly at E12.5 and older, followed by the decrease of nestin and proliferative cell nuclear antigen (PCNA) proteins in E14.5 and older embryos (Fig. 1*B*). The delayed onset of PCNA down-regulation compared with that of NS suggests a delayed cell cycle exit following the loss of NS. To investigate the neural defects of $neNS^{cko}$ mice, embryos were collected at consecutive developmental stages. Histological analyses showed that the neuroepithelial morphology of $neNS^{cko}$ embryos appears the same as that of $NS^{f/f}$ embryos at E10.5 (Fig. S2*A*) but begins to show reduced cellularity throughout the neural axis at E12.5 (Fig. 1*C*). At E14.5 and E16.5, $neNS^{cko}$ embryos show major defects in the telencephalic cortex, ganglionic eminence, cerebellar primordium, midbrain tectum, smaller diencephalon, midbrain and hindbrain tegmentum, and spinal cord compared with their $NS^{f/f}$ littermates (Fig. 1 *D* and *E*). Associated with those defects is a decrease of NSCs in $neNS^{cko}$ neuroepithelium at E12.5 (Fig. 1*F*). We also noticed that E12.5 $neNS^{cko}$ embryos show a significant increase of γ-H2AX proteins and γ-$H2AX^{+}$ cells in their neuroepithelium (Fig. 1 *B* and *G* and Fig. S2*B*).

NS Protects NSCs from DNA Damage and Maintains Their Self-Renewal. NSCs were isolated from the E12.5 forebrain cortex and grown as neurospheres in suspension culture. Confocal analyses showed that most $nestin^{+}$, NS^{+}, and BrdU-labeled cells are found in the peripheral region of the sphere (Fig. 2*A*). The siRNA-based knockdown approach allows a 60% reduction of NS proteins in neurospheres (Fig. 2*B1*) and produces a striking increase of γ-$H2AX^{+}$ cells spontaneously ($P < 0.0001$, Fig. 2 *B2* and *B3*). This NS RNAi (siNS)-mediated knockdown (NSKD) efficiency for the whole neurosphere is moderate compared with what we've seen in monolayer cultures (80–90%), which may be due to the three-dimensional structure of neurospheres. DNA replication is one major source of spontaneous DNA damage that occurs in the S-phase cells. We noted that NSKD causes more DNA damage on S-phase ($BrdU^{+}$) neurosphere cells compared with non–S-phase ($BrdU^{-}$) cells (Fig. 2*C*). Conversely, overexpression of NS can reduce the amount of DNA damage caused by hydroxyurea (HU) in NSCs (Fig. 2*D*). Along with its DNA damage effect, NS depletion also impairs the self-renewal of NSCs, as indicated by the decreased tertiary sphere formation from secondary neurosphere cells (358.3 versus 61.3 spheres per 10^5 plated cells) (Fig. 2*E*). These results demonstrate that NS plays an important role in maintaining the self-renewal of NSCs by protecting them from replication-dependent DNA damage.

NSKO-Induced DNA Damage Does Not Depend on p53 or Affect rRNA Synthesis. To define the role of p53 in the NSKO event, a TAM-inducible NS^{cko} mouse model ($inNS^{cko}$) was created by introducing the Cre^{ER} transgene (15) into $NS^{f/f}$ mice, followed by breeding of $inNS^{cko}$ and $NS^{f/f}$ mice into the p53-null background (16). Mouse embryonic fibroblast (MEF) cells were prepared from E13.5 embryos. Western blots showed that TAM treatment (0.1 μM) decreases the NS protein level by 70% in p53-wild type $inNS^{cko}$ cells (lanes 3 and 4) and by >90% in p53-null $inNS^{cko}$ cells (lanes 7 and 8), but has no effect on $NS^{f/f}$ cells (Fig. 3*A*). Cell growth studies showed that loss of NS impairs the long-term proliferative potential of MEF cells, as shown by the reduced population doubling level (PDL) and early growth plateau (Fig. 3*B*), and that p53 deletion allows NS wild-type MEF cells to escape senescence but significantly shortens the lifespan of NSKO cells (Fig. 3*C*). DNA damage analyses showed that NS deletion increases the percentage of γ-$H2AX^{+}$ MEF cells regardless of their p53 status ($P < 0.0001$) (Fig. 3*D*), indicating that the p53 activity is not required for the NSKO-induced DNA damage. To verify that the DNA damage phenotype of NSKO cells is caused specifically by the loss of NS, we restored the NS expression by introducing a recombinant NS-GFP into NSKO MEF cells, and confirmed that the expression of NS-GFP can reduce the γ-$H2AX^{+}$ percentage of NSKO MEF cells (3.1%) compared with the expression of GFP (19.6%, $P < 0.0001$) (Fig. 3*E*). In addition, the NSdB mutant of NS, which lacks the

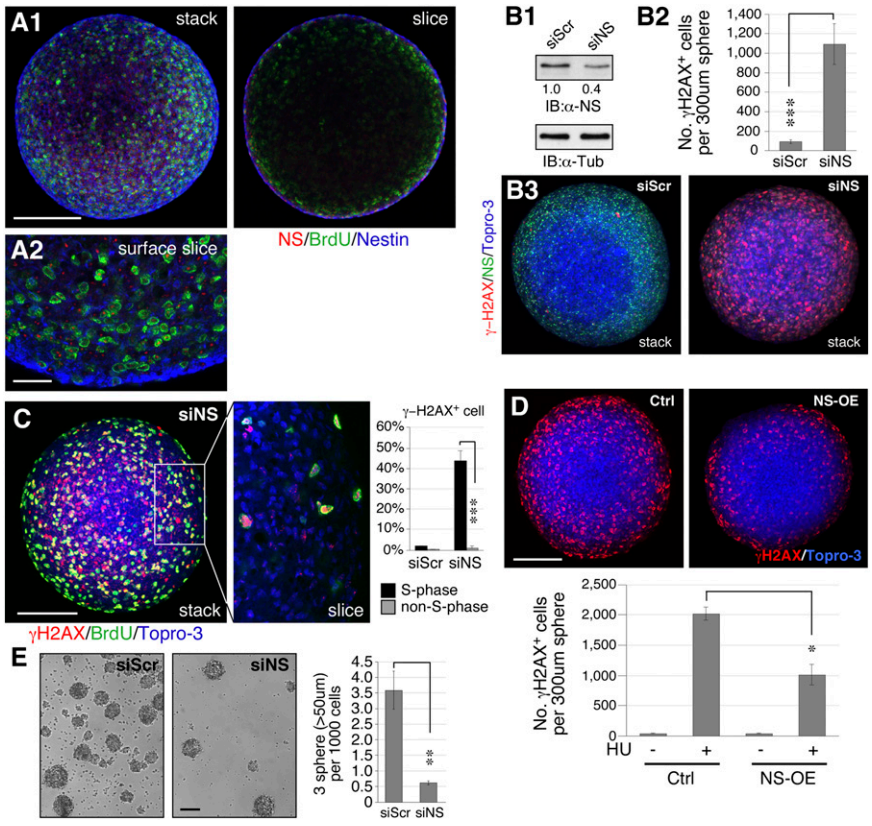

Fig. 2. Loss of NS induces DNA damage and perturbs self-renewal in NSCs. (*A*) NSCs were isolated from the E12.5 cortex of $NS^{f/f}$ embryos and cultured as neurospheres. Dividing neuroepithelial precursors ($BrdU^+$ [green] and $nestin^+$ [blue]) are found in the peripheral zone of the sphere and coincide mostly with the NS signal (red). (*A1*) shows a stacked image (*Left*) and a single slice through the center (*Right*). (*A2*) shows an enlarged view of a single slice close to the surface. (*B1*) RNAi-based NS knockdown (siNS) gives a 60% knockdown efficiency in the whole neurosphere. (*B2* and *B3*) Loss of NS significantly increases the number of γ-$H2AX^+$ cells in neurospheres. (*C*) The S-phase ($BrdU^+$) cells are much more susceptible to the DNA damage effect of NSKD than the non–S-phase ($BrdU^-$) cells. (*D*) NS overexpression protects neurosphere cells from hydroxyurea (HU)-induced DNA damage (γ-$H2AX^+$). (*E*) NSKD by siNS significantly diminishes the ability of secondary neurosphere cells to form tertiary neurospheres. *y* axis indicates the number of tertiary neurospheres formed for every 1,000 secondary neurosphere cells plated. (Scale bars: 100 μm in *A1* and *B–E*, 25 μm in *A2*.) Bar graphs (see description in Fig. 1).

nucleolar localization signal and hence is distributed in the nucleoplasm, retains the same ability as wild-type NS to rescue the DNA damage effect of NSKO, suggesting that nucleolar localization is not a prerequisite for the genome-protecting function of NS. To address the issue of whether NSKO may cause DNA damage secondarily to the perturbation of ribosomal synthesis, we measured the NSKO effect on the levels of pre-rRNA transcripts containing the processing site-1 (PS-1), PS-2, PS-3, or 18S rRNA sequences by real-time RT-PCR (Fig. 3*F*, *Left*). The different PS-containing products represent precursor species that exist before the splicing events occurring at different stages of pre-rRNA processing. Although NSKO reduces NS transcripts

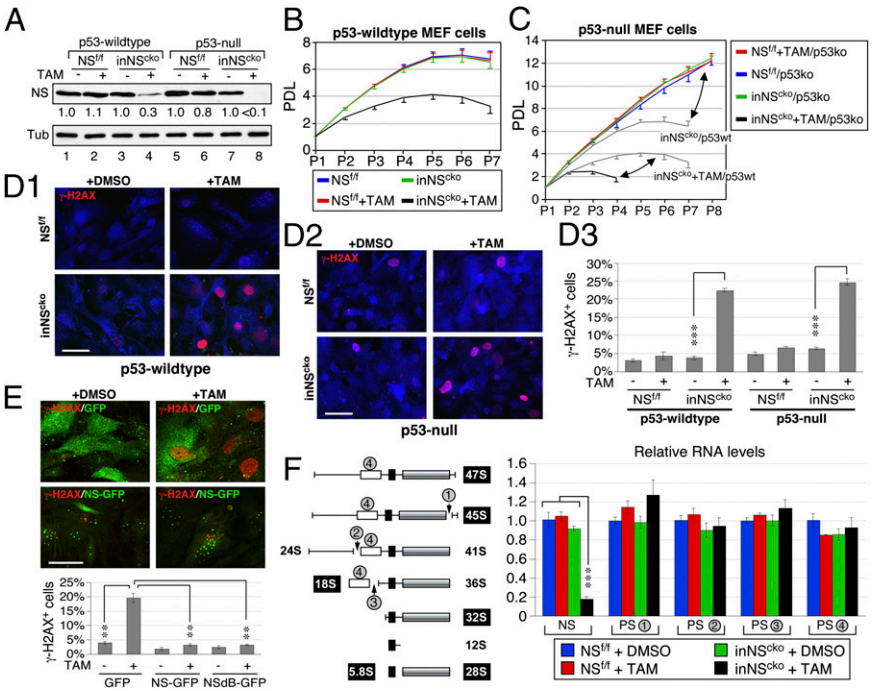

Fig. 3. NSKO-induced DNA damage does not depend on p53 or rRNA synthesis. (*A*) A tamoxifen (TAM)-inducible NS conditional-KO model ($inNS^{cko}$) was generated. TAM treatment (0.1 μM, 4 d) reduces NS proteins in p53 wild-type and null $inNS^{cko}$ MEF cells. (*B*) The population doubling level (PDL) of p53-wildtype MEF cells is decreased by NSKO. (*C*) Deletion of p53 increases the PDL of NS wild-type cells (red, green, blue) and decreases the PDL of NS-null cells (black) compared with their respective p53wt controls (gray). (*D*) TAM-induced NSKO increases the percentage of γ-$H2AX^+$ cells in p53 wild-type and null MEF cells. (*E*) Transfection of NS-GFP or NSdB-GFP reduces the γ-$H2AX^+$ percentage in transfected NSKO MEF cells compared with GFP-transfected NSKO cells. (Scale bars, 50 μm.) (*F Left*) Diagram of the pre-rRNA–processing step and the primer-targeting sites for the processing site-1 (PS-1), PS-2, PS-3, and the 18S-containing transcripts (PS-4). (*Right*) Quantitative RT-PCR shows that NSKO reduces the NS transcript but has no effect on the PS-1, PS-2, and PS-3 events. Neither does it reduce the total amount of pre-rRNAs and rRNAs (PS-4). The transcript levels are quantified by referencing to high mobility group protein 14 (HMG-14) and compared with the DMSO-treated $NS^{f/f}$ samples.

CELL BIOLOGY

and elicits a clear DNA damage response, it has no effect on the splicing events occurring on the 47S pre-rRNA or at the junctions of 5′ETS-18S (PS-2) or 18S-ITS1 (PS-3). Neither does it reduce the total amount of pre-rRNAs and rRNAs, as measured by the PS-4 qRT-PCR (Fig. 3*F*, *Right*). These results prove that the DNA damage effect of NSKO does not depend on the p53 activity and nor is it caused by the impairment of rRNA synthesis.

Loss of NS Triggers Replication-Induced DNA Damage. We noticed that NSKD in MEF cells increases not only the percentage of γ-H2AX$^+$ cells (from 4.1% to 16.6%, $P < 0.0001$) but also the percentages of ataxia telangiectasia and Rad3-related (ATR)$^+$ (from 3% to 21%, $P < 0.01$) and replication protein A-32 (RPA32)$^+$ cells (from 4% to 23%, $P < 0.01$) (Fig. 4 *A* and *B*). Most of the ATR$^+$ and RPA32$^+$ foci colocalize with each other. NSKD also increases the number of DNA damage foci labeled by γ-H2AX, ATR, or breast cancer type 1 (BRCA1) in dysplastic oral keratinocytes cells (Fig. S3). We noted that 55.7% of the NS-depleted MEF cells in S-phase show γ-H2AX$^+$ signals and only 7.8% of the non–S-phase cells are γ-H2AX$^+$. This DNA damage profile resembles that of HU treatment (Fig. 4*C*). To bolster the link between NSKD-triggered damage and DNA replication, we performed propidium iodide-γ-H2AX–doubled labeled flow cytometry on control-KD (siScr) and NSKD (siNS) MEF cells. The flow cytometry results confirm that NSKD significantly increases the percentage of γ-H2AX$^+$ cells compared with the control-KD samples (Fig. S4*A*). Cell cycle analyses on the γ-H2AX–labeled (Fig. S4*B1*) versus γ-H2AX–nonlabeled subpopulation (Fig. S4*B2*) of NSKD cells also prove that a significant portion of NSKD-induced DNA damage occurs in the S-phase cells. By pooling the S-phase cells from both the γ-H2AX–labeled and nonlabeled populations, we find that 80.1% of the S-phase cells show γ-H2AX$^+$ signals, whereas only 25.5% of the non–S-phase cells show γ-H2AX$^+$ signals ($P < 0.01$, Fig. S4*C*). To further support the idea, we demonstrated that the DNA damage effect of NSKD is greatly reduced in slowly dividing MEF cells grown under the serum deprivation condition (1.9%) compared with those grown in 10% (vol/vol) serum (16.6%), and shows no difference from the scrambled RNAi (siScr)-treated cells grown in low-serum medium (1.3%) (Fig. 4*D*, *Left*). This lack of siNS effect in slowly dividing MEF cells is not caused by a decreased NSKD efficiency (Fig. 4*D*, *Right*). To determine

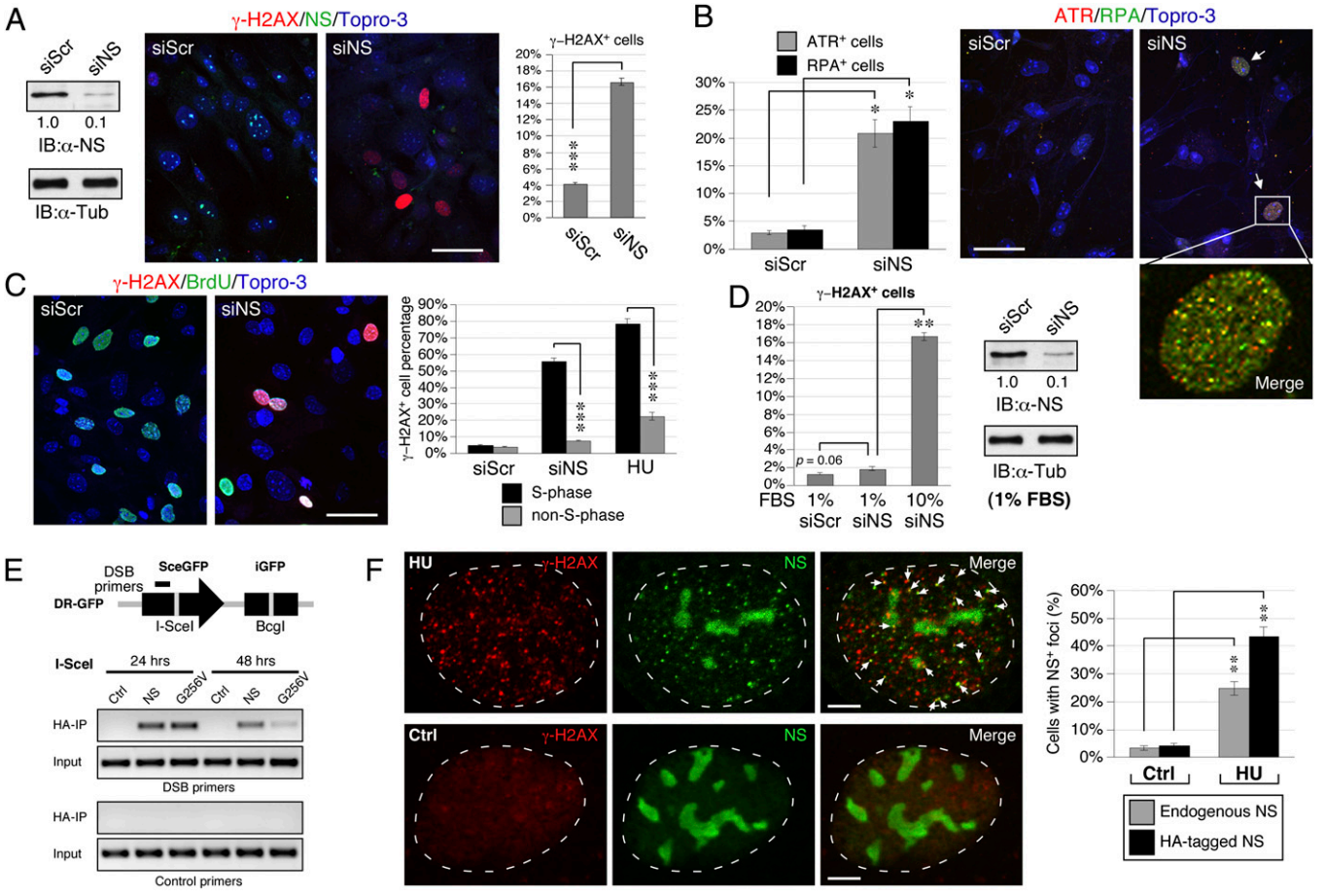

Fig. 4. NS depletion triggers replication-induced DNA damage. (*A*) The siNS treatment produces a 90% protein knockdown efficiency in MEF cells and a significant increase of γ-H2AX$^+$ cells. (*B*) NSKD also increases the percentages of ATR$^+$ and RPA32$^+$ cells. Most of the ATR$^+$ and RPA32$^+$ foci are colocalized. (*C*) S-phase (BrdU$^+$) cells are much more susceptible to the DNA damage effect of NSKD than non–S-phase cells, which resembles the DNA damage profile of HU treatment. (*D*) The siNS-induced DNA damage is significantly diminished in MEF cells grown in low serum-containing medium. The siNS-mediated KD efficiency for the low-serum culture condition is the same as that for the normal-serum culture condition. (*E*) DR-GFP U2OS cells (upper panel) were transfected with the empty vector or HA-tagged NS plasmid. After introducing DSB at the I-SceI site, ChIP analyses were performed by precipitation with anti-HA antibody and PCR amplification with DSB-specific or control primers. The DSB-ChIP assay demonstrates that NS is physically associated with DSB sites. (*F*) HU treatment (in U2OS cells) induces the foci formation of endogenous NS (detected by Ab2438) in the nucleoplasm without apparently diminishing its nucleolar signals. The percentages of cells showing ≥ 5 foci of colocalized NS (green) and γ-H2AX (red) signals are quantified by confocal analyses (gray bars), and independently confirmed by using the HA-tagged NS recombinant protein (black bars). (Scale bars: 50 μm in *A*–*C*; 5 μm in *F*.)

whether NS is directly involved in the response and/or repair of DNA damage, we performed the DSB-chromatin coimmunoprecipitation (ChIP) assay in DR-GFP-U2OS cells (17). The DR-GFP-U2OS cells were stably transfected with the SceGFP transgene, which contains an internal I-SceI site (depicted in Fig. 4*E*, *Upper*). DSBs were introduced specifically at the I-SceI site by the expression of I-SceI enzyme. Primers were designed to detect the DNA sequence localized at 500 bp upstream to the I-SceI site. The DSB-ChIP results showed that immunoprecipitating HA-tagged NS can physically pull down the I-SceI–cut DSB site on the SceGFP locus at the 24-h and 48-h time points following the expression of I-SceI. Compared with the wild-type NS, the non–GTP-binding mutant of NS (G256V) shows a faster clearance from the I-SceI–cut site (Fig. 4*E*, *Lower*). In consistence, confocal studies demonstrated that, following the HU treatment, the endogenous NS protein in 25% of the cells forms discrete foci in the nucleoplasm without losing its nucleolar signals, and 44% of the cells overexpressing HA-tagged NS shows foci formation by the recombinant protein (Fig. 4*F*). Some NS^+ and $NS\text{-}HA^+$ foci are colocalized with the $\gamma\text{-}H2AX^+$ signals. These data indicate that NS may play a direct and primary role in reducing the amount of spontaneous DNA damage associated with the DNA replication process.

NS Depletion Perturbs the Recruitment of RAD51 to Stalled Replication-Induced Damage Foci. Increased DNA damage by NS depletion may be caused by an increased source of DNA damage, induced secondarily by stress, or by impaired DNA damage repair. In the latter case, one should be able to identify the point of perturbation in the DNA repair axis. As homologous recombination (HR) is the main mechanism responsible for repairing replication-induced DNA damage (18) and knockout of the core HR protein, RAD51, shows the same early embryonic lethal phenotype as does NSKO (19), we hypothesize that the recruitment of RAD51 to DNA damage sites may be a target of NS regulation. To date, only a handful of proteins (i.e., BRCA2, RPA70, Bloom's syndrome protein, and RAD52) are implicated in the loading of RAD51 to DNA damage sites. To look for the potential targets of NS, we tested the ability of BRCA2, RPA70 and RAD51 in rescuing the DNA damage phenotype of NSKO MEF cells, and found that only RAD51, but not BRCA2 or RPA70, is capable of doing so (Fig. 5*A*), suggesting that RAD51 may be a direct target of NS. Indeed, coimmunoprecipitation assays confirm that the endogenous NS and RAD51 proteins can interact with each other in vivo (Fig. 5*B*). To determine the role of NS in regulating the recruitment of RAD51, control-KD and NSKD MEF cells were treated with HU (2 mM) for 24 h and assayed for their RAD51 recruitment efficiency. The results showed that, in control-KD MEF cells, HU treatment significantly increases the percentages of $\gamma\text{-}H2AX^+$ (28.0%, $P < 0.0001$, Fig. 5*C*) and $RAD51^+$ cells (30.4%, $P < 0.0001$, Fig. 5*D*) over the non–HU-treated MEF cells (4.1% for $\gamma\text{-}H2AX^+$ cells and 3.8% for $RAD51^+$ cells). In contrast, HU treatment of NSKD MEF cells increases $\gamma\text{-}H2AX^+$ cells significantly (33.6%, Fig. 5*C*), but its effect on triggering $RAD51^+$ foci is greatly reduced (12.4%) compared with its effect in control-KD cells (30.4%, $P < 0.0001$) (Fig. 5*D*). Finally, we performed DSB-ChIP experiments to confirm that NS is required for the physical recruitment of RAD51 to DSB sites (Fig. 5*E*). The ChIP results showed that the recruitment of RAD51 to I-SceI–induced DSB sites at the 24-h and 48-h time points is much attenuated by NS knockdown. These findings, in conjunction with the lack of RAD51 foci formation in NS-depleted cells, establish the importance of NS in promoting RAD51 recruitment to DSB sites and refute the possibility that the DNA damage effect of NS depletion is caused secondarily by increased cellular stress.

Discussion

This study identifies NS as an essential player in protecting stem/progenitor cells from replication-induced DNA damage in vivo and demonstrates its ability to bind and promote the recruitment of RAD51 to stalled replication-induced damage foci. The $neNS^{cko}$ mouse model shows that deleting NS in the neural stem/progenitor cell population increases the frequency of DNA damage, reduces the number of stem/progenitor cells, and causes major developmental defects in the embryonic brain. DNA damage triggered by $neNS^{cko}$ becomes most prominent at E12.5. This window of appearance may be determined collectively by the activity of nestin promoter and the differentiation and dying of NS-deleted neural progenitor cells. As a result, the peak of the NSKO event should parallel or immediately follow the highest of nestin expression at E10.5 and E12.5 (6). The more DNA damage events in the E12.5 compared with the E10.5 neuroepithelium of $neNS^{cko}$ embryos may be caused by the increased frequency of homozygous deletion of NS (evidenced by the amount of NS protein reduction) and the increased frequency of replication stalling events over additional rounds of cell division. The lack of γ-H2AX signals in the E14.5 or older forebrains may be due to the rapid loss of proliferative neural precursors. In support of these in vivo findings, NS depletion by siNS triggers massive DNA damage in NSCs and MEF cells and greatly reduces their ability to self-renew or propagate in culture. The self-renewing activity of NSCs is indicated by their ability to form spheres over multiple passages. Given its role in promoting

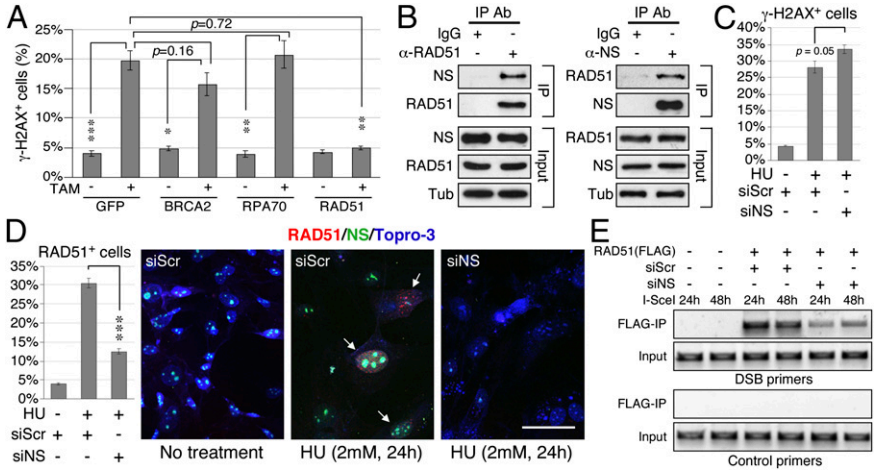

Fig. 5. NS binds RAD51 and promotes its recruitment to DNA damage foci. (*A*) Overexpression of RAD51, but not that of BRCA2 or RPA70, rescues the $\gamma\text{-}H2AX^+$ cell percentage of NSKO MEF cells. (*B*) CoIP of endogenous NS and RAD51 by anti-RAD51 (left) or anti-NS antibody (right) confirms that these two proteins interact with each other in vivo. (*C*) HU treatment increases the percentages of $\gamma\text{-}H2AX^+$ in both siScr- and siNS-treated MEF cells. siNS-treated cells show more DNA damage events than siScr-treated cells. (*D*) The HU effect on triggering $RAD51^+$ foci in siNS-treated MEF cells is significantly reduced compared that in siScr-treated cells. (Scale bar: 50 μm.) (*E*) DSB-ChIP assays show that the physical recruitment of RAD51 to I-SceI–induced DSBs is significantly attenuated by NSKD (siNS) at the 24 and 48-h time points following the induction of I-SceI expression.

the RAD51 recruitment during DNA damage repair, loss of NS is expected to reduce the protection of NSCs against spontaneous DNA damage caused by DNA replication, thereby introducing cell cycle arrest and perturbing the formation of tertiary neurospheres from secondary neurospheres. Notably, restoring the NS expression can reverse the DNA damage phenotype of NS-deleted MEF cells, which supports the specific effect of NS depletion in causing spontaneous DNA damage in vitro and in vivo. Finally, we establish the direct role of NS in the response/repair of DNA damage by showing that NS is physically recruited to the DSB sites and that the DNA damage effect of NSKO depends neither on the p53 status nor on the synthesis of rRNAs.

The two major sources of cell-intrinsic DNA damage are oxidative stress and replication stalling. We noted that the S-phase cells are much more susceptible to the NSKO effect than the non–S-phase cells, a feature also shared by the HU treatment. This idea that NS deletion leads to replication-dependent DNA damage is supported by the lack of DNA damage effect of NSKD on slowly dividing MEF cells and the protective effect of NS against HU-induced DNA damage in NSCs. Further analyses identify RAD51 as a direct molecular target of NS with the ability to rescue the NSKO-induced phenotype. More importantly, loss of NS perturbs the recruitment efficiency of RAD51 to stalled replication-induced damage foci and DSB sites, which refutes that the DNA damage effect of NS depletion arises secondarily due to increased cellular stress. Because the DNA damage phenotype of NSKO cells can be compensated by overexpressing RAD51 alone, we reason that NS more likely plays a promoting role than a determining role in the RAD51 recruitment and that the NS-promoted RAD51 recruitment should be inactive without the preexisting DNA damage event, which, otherwise, would incur nonspecific recombination and genomic instability. This NS function, although modulatory in nature, becomes indispensable for cells that undergo extended DNA replication, such that both NSKO and RAD51-KO mice show the same phenotype of early embryonic lethality (19). In addition, we noted that this obligatory function of NS does not require its nucleolar localization and that the damage-induced foci formation of NS occurs without the apparent translocation of its protein from the nucleolus to the nucleoplasm, suggesting that DNA damage may activate the nucleoplasmic NS via a posttranslational mechanism.

This newly discovered function of NS parallels the one in which NS protects against DNA damage on the telomere by regulating telomeric repeat binding factor 1 (TRF1) SUMOylation and the recruitment of PML-IV (13). Together, these two mechanisms help protect the genome integrity of stem/progenitor cells throughout their proliferative lifespan. NS has also been noted to regulate the p53 pathway via a direct mouse double minute 2 homologue (MDM2) interaction (9, 10). The MDM2-regulatory mechanism of NS, however, cannot account for its essential role in cell proliferation and development, as these events do not require the presence of p53 (11). We have observed that this MDM2-stabilizing function of NS is mostly silent under the normal condition and becomes activated only when the nucleolar organization is disrupted by stress signals (10). Therefore, our current view is that the DNA/telomere-protecting function of NS is required for continuously dividing cells under normal growth conditions and is operated by the nucleoplasmic pool of NS in a damage-dependent manner, whereas its MDM2-stabilizing function is only turned on under nucleolar stress conditions and is operated by the NS protein released from the disassembled nucleolus.

In conclusion, both in vivo and in vitro studies show that loss of NS predisposes stem and progenitor cells to spontaneous DNA damage closely related to the DNA replication event. This essential function of NS operates independently of p53 or rRNA synthesis and acts by promoting the DSB recruitment of RAD51. These discoveries suggest that cells with a robust DNA replication program may need additional molecules to enhance the core HR-based repair activity to safeguard their genome integrity.

Materials and Methods

Animal Studies. All animals were housed by the Program for Animal Resources at the Texas A&M Health Science Center (Houston, TX) and handled in accordance with the principles of the Guide for the Care and Use of Laboratory Animals and the procedures approved by the Institutional Animal Care and Use Committee.

ChIP at DSB Sites. DR-GFP U2OS cells (17) were transfected with the indicated plasmid or treated with the siRNA duplex. After 24 h, DSBs were introduced at the I-SceI site on the SceGFP transgene by transfecting with the I-SceI plasmid, crosslinked with formaldehyde, and subjected to five rounds of sonication (8 s) with 1-min interval using the 60 Sonic Dismembrator. Immunoprecipitation was performed using the anti–HA- or FLAG-agarose beads. See *SI Materials and Methods* for primer sequences.

Other Methods. See *SI Materials and Methods* for details.

ACKNOWLEDGMENTS. This work was supported by National Cancer Institute–Public Health Service Grant R01 CA113750 and Texas A&M Research Development and Enhancement Award (to R.Y.L.T.).

1. Tercero JA, Diffley JF (2001) Regulation of DNA replication fork progression through damaged DNA by the Mec1/Rad53 checkpoint. *Nature* 412(6846):553–557.
2. Katou Y, et al. (2003) S-phase checkpoint proteins Tof1 and Mrc1 form a stable replication-pausing complex. *Nature* 424(6952):1078–1083.
3. Pacek M, Tutter AV, Kubota Y, Takisawa H, Walter JC (2006) Localization of MCM2-7, Cdc45, and GINS to the site of DNA unwinding during eukaryotic DNA replication. *Mol Cell* 21(4):581–587.
4. Saintigny Y, et al. (2001) Characterization of homologous recombination induced by replication inhibition in mammalian cells. *EMBO J* 20(14):3861–3870.
5. Hanada K, et al. (2006) The structure-specific endonuclease Mus81-Eme1 promotes conversion of interstrand DNA crosslinks into double-strands breaks. *EMBO J* 25(20): 4921–4932.
6. Tsai RY, McKay RD (2002) A nucleolar mechanism controlling cell proliferation in stem cells and cancer cells. *Genes Dev* 16(23):2991–3003.
7. Zhu Q, Yasumoto H, Tsai RY (2006) Nucleostemin delays cellular senescence and negatively regulates TRF1 protein stability. *Mol Cell Biol* 26(24):9279–9290.
8. Ma H, Pederson T (2007) Depletion of the nucleolar protein nucleostemin causes G1 cell cycle arrest via the p53 pathway. *Mol Biol Cell* 18(7):2630–2635.
9. Dai MS, Sun XX, Lu H (2008) Aberrant expression of nucleostemin activates p53 and induces cell cycle arrest via inhibition of MDM2. *Mol Cell Biol* 28(13):4365–4376.
10. Meng L, Lin T, Tsai RY (2008) Nucleoplasmic mobilization of nucleostemin stabilizes MDM2 and promotes G2-M progression and cell survival. *J Cell Sci* 121(Pt 24):4037–4046.
11. Beekman C, et al. (2006) Evolutionarily conserved role of nucleostemin: Controlling proliferation of stem/progenitor cells during early vertebrate development. *Mol Cell Biol* 26(24):9291–9301.
12. Jafarnejad SM, Mowla SJ, Matin MM (2008) Knocking-down the expression of nucleostemin significantly decreases rate of proliferation of rat bone marrow stromal stem cells in an apparently p53-independent manner. *Cell Prolif* 41(1):28–35.
13. Hsu JK, Lin T, Tsai RY (2012) Nucleostemin prevents telomere damage by promoting PML-IV recruitment to SUMOylated TRF1. *J Cell Biol* 197(5):613–624.
14. Tronche F, et al. (1999) Disruption of the glucocorticoid receptor gene in the nervous system results in reduced anxiety. *Nat Genet* 23(1):99–103.
15. Hayashi S, McMahon AP (2002) Efficient recombination in diverse tissues by a tamoxifen-inducible form of Cre: A tool for temporally regulated gene activation/inactivation in the mouse. *Dev Biol* 244(2):305–318.
16. Donehower LA, et al. (1992) Mice deficient for p53 are developmentally normal but susceptible to spontaneous tumours. *Nature* 356(6366):215–221.
17. Peng G, et al. (2009) BRIT1/MCPH1 links chromatin remodelling to DNA damage response. *Nat Cell Biol* 11(7):865–872.
18. Helleday T (2008) Amplifying tumour-specific replication lesions by DNA repair inhibitors - a new era in targeted cancer therapy. *Eur J Cancer* 44(7):921–927.
19. Tsuzuki T, et al. (1996) Targeted disruption of the Rad51 gene leads to lethality in embryonic mice. *Proc Natl Acad Sci USA* 93(13):6236–6240.

MCB
Journals.ASM.org

Bimodal Interaction of Mammalian Polo-Like Kinase 1 and a Centrosomal Scaffold, Cep192, in the Regulation of Bipolar Spindle Formation

Lingjun Meng,[a] Jung-Eun Park,[a] Tae-Sung Kim,[a] Eun Hye Lee,[a] Suk-Youl Park,[a] Ming Zhou,[b] Jeong K. Bang,[c] Kyung S. Lee[a]

Laboratory of Metabolism, National Cancer Institute, National Institutes of Health, Bethesda, Maryland, USA[a]; Laboratory of Proteomics and Analytical Technologies, Leidos Biomedical Research, Inc., Frederick National Laboratory for Cancer Research, Frederick, Maryland, USA[b]; Division of Magnetic Resonance, Korea Basic Science Institute, Ochang, South Korea[c]

Serving as microtubule-organizing centers, centrosomes play a key role in forming bipolar spindles. The mechanism of how centrosomes promote bipolar spindle assembly in various organisms remains largely unknown. A recent study with *Xenopus laevis* egg extracts suggested that the Plk1 ortholog Plx1 interacts with the phospho-T46 (p-T46) motif of *Xenopus* Cep192 (xCep192) to form an xCep192-mediated xAurA-Plx1 cascade that is critical for bipolar spindle formation. Here, we demonstrated that in cultured human cells, Cep192 recruits AurA and Plk1 in a cooperative manner, and this event is important for the reciprocal activation of AurA and Plk1. Strikingly, Plk1 interacted with Cep192 through either the p-T44 (analogous to *Xenopus* p-T46) or the newly identified p-S995 motif via its C-terminal noncatalytic polo-box domain. The interaction between Plk1 and the p-T44 motif was prevalent in the presence of Cep192-bound AurA, whereas the interaction of Plk1 with the p-T995 motif was preferred in the absence of AurA binding. Notably, the loss of p-T44- and p-S995-dependent Cep192-Plk1 interactions induced an additive defect in recruiting Plk1 and γ-tubulin to centrosomes, which ultimately led to a failure in proper bipolar spindle formation and mitotic progression. Thus, we propose that Plk1 promotes centrosome-based bipolar spindle formation by forming two functionally nonredundant complexes with Cep192.

As the major microtubule-organizing center in somatic animal cells, centrosomes play a critical role in establishing bipolar spindles. Centrosomes consist of a pair of centrioles surrounded by electron-dense pericentriolar material (PCM), which is thought to serve as a scaffold for recruiting various proteins that are critical for microtubule (MT) assembly. Prior to entering mitosis, centrosome size increases dramatically by recruitment of the γ-tubulin ring complex (γ-TuRC) and other PCM proteins, and this process, called centrosome maturation, confers to centrosomes a greater ability to nucleate MTs.

Centrosome maturation occurs through the actions of various PCM scaffolding proteins and regulatory kinases. One of the PCM scaffolds important for this process is a conserved centrosomal protein called Cep192. Early in the cell cycle, Cep192 is detected as an inner PCM ring structure with a diameter of ~300 to 400 nm (1–3). As cells enter mitosis, the level of Cep192 increases severalfold, and it accumulates on mitotic PCM (4). Interestingly, depletion of Cep192 results in the almost complete loss of centrosome-associated γ-tubulin, whereas overexpression of Cep192 leads to the formation of ectopic puncta in the cytoplasm. These ectopic puncta are capable of recruiting γ-tubulin and other key components that are important for γ-tubulin recruitment. However, how Cep192 functions as a scaffold to support centrosomal maturation and how its function is integrated into the cell cycle have remained elusive.

Besides centrosomal scaffolds that serve as a platform for centrosome maturation, phosphorylation by kinases appears to play an important regulatory role in promoting this event. Data obtained from various studies show that two mitotic Ser/Thr kinases, Plk1 and AurA (and their orthologs in various organisms), play a key role in recruiting γ-tubulin and promoting bipolar spindle formation (5–9). Interestingly, recent studies with *Xenopus laevis* egg extracts revealed that xCep192 binds to and activates xAurA, and this event is important for the interaction with Plx1 (*Xenopus* Plk1 ortholog) and for promoting γ-tubulin recruitment to centrosomes (9, 10). In addition, studies with human HeLa cells suggested that these Cep192-mediated processes are largely conserved (9). Since AurA has been shown to function as an upstream kinase of Plk1 at the time of mitotic entry (11, 12), the formation of the xCep192-xAurA complex appears to be a key step in promoting Plx1-dependent centrosome maturation. Notably, however, the *Xenopus* xCep192(T46A) mutant, lacking T46-dependent Plx1 binding, or the xCep192Δ(543–747) mutant, lacking AurA binding, still maintained a large fraction (~70%) of its MT-nucleating activity (9). These observations suggest the presence of an alternative pathway(s) that regulates the function of xCep192 in the *Xenopus* system.

In this study, we investigated the underlying mechanism of how human Cep192 functions together with Plk1 to promote γ-tubulin recruitment and bipolar spindle formation at mitotic

Received 20 January 2015 **Returned for modification** 13 February 2015
Accepted 14 May 2015

Accepted manuscript posted online 26 May 2015

Citation Meng L, Park J-E, Kim T-S, Lee EH, Park S-Y, Zhou M, Bang JK, Lee KS. 2015. Bimodal interaction of mammalian polo-like kinase 1 and a centrosomal scaffold, Cep192, in the regulation of bipolar spindle formation. Mol Cell Biol 35:2626–2640. doi:10.1128/MCB.00068-15.

Address correspondence to Kyung S. Lee, kyunglee@mail.nih.gov.

L.M., J.-E.P., and T.-S.K. contributed equally to this work.

doi:10.1128/MCB.00068-15

centrosomes. Our results showed that in human cells, Plk1 is recruited to centrosomes through an interaction with either the p-T44 or the p-S995 motif of Cep192 and that the loss of both the T44- and S995-dependent interactions results in an additive defect in γ-tubulin recruitment and bipolar spindle formation. Remarkably, in the presence of Cep192-bound AurA, Plk1 preferentially interacted with the T44 motif by self-phosphorylating this site, whereas in the absence of Cep192-bound AurA, Plk1 favored the S995-dependent interaction. Based on these observations, we propose that Plk1 interacts with Cep192 in a bimodal fashion to localize to centrosomes and promote γ-tubulin recruitment and bipolar spindle formation.

MATERIALS AND METHODS

Plasmid construction. To generate the pCI-neo-$FLAG_3$-Plk1 (pKM3789), pCI-neo-$FLAG_3$-Plk1(H538A K540M) (pKM3790), or pCI-neo-$FLAG_3$-Plk1(K82M) (pKM3791) construct, the respective KpnI (end-filled)-XhoI fragment of Plk1 prepared from either pUC19-Plk1 (pKM3464), pUC19-Plk1(H538A K540M) (pKM3465), or pUC19-Plk1(K82M) (pKM3611) was subcloned into a pCI-neo-$FLAG_3$ vector digested by PmeI and XhoI. The pCI-neo-HA-AurA (pKM4459) and pCI-neo-HA-AurA(T288A) (pKM4460) constructs were generated by inserting the respective PCR products into a modified pCI-neo-HA vector (2) digested by PmeI and NotI. The green fluorescent protein (GFP)-Bora construct was kindly provided by Dong Zhang (New York Institute of Technology, Old Westbury, NY).

The pEGFP-C2-Cep192 (pKM3105) construct encoding residues 1 to 2538 of Cep192 was generated by inserting a reverse transcription-PCR (RT-PCR)-generated N-terminal fragment of Cep192 into the pCR3.1-EGFP-Cep192(507–2538) (numbers indicate amino acid residues) construct (a gift from David Sharp, Albert Einstein College of Medicine, Bronx, NY). To generate the pEGFP-C1-Cep192 (pKM3552) and pCI-neo-HA-Cep192 (pKM3360) constructs, a SalI fragment containing full-length Cep192 was subcloned into a pEGFP-C1 vector (Clontech) digested by SalI and a pCI-neo-HA vector digested by XhoI, respectively. A pEGFP-C1-Cep192 construct containing the S43A (pK4623), T44A (pK4229), R47A (pK4624), D48A (pK4625), R49A (pK4626), or S995A (pKM3553) mutation or the T44A S995A double mutation (pKM4230) was generated by inserting a PCR-generated SalI fragment containing each respective mutation into the pEGFP-C1 vector digested by the same enzyme. The pCR3.1-EGFP-Cep192(507–1065)(S995A) construct (pKM3119) was generated by replacing the wild-type sequence with an HpaI-BamHI fragment containing the S995A mutation. A bacterial construct containing either Plk1 (pKM5548) or Cep192(1–1093) (pKM5552) was generated by inserting each respective XhoI-NotI fragment of the PCR product into the pET28b vector (Novagen) digested by SalI and NotI. The glutathione *S*-transferase (GST)-fused form of Cep192(1–647) (pKM3156) was cloned by inserting a SalI-digested fragment into the pGEX-4T3 vector (GE Healthcare) digested by the same enzyme. The pET32b-Aurora A construct was a kind gift from Takeshi Urano (Shimane University School of Medicine, Izumo, Japan).

For the construction of Cep192 deletion mutants, a SalI fragment containing Cep192 P1(1–647) (pKM3290), Cep192 P3(507–1400) (pKM3287), or Cep192 P6(1700–2538) (pKM3289) or a PmeI-SmaI fragment containing Cep192 P5(901–1800) (pKM3288) was cloned into the pEGFP-C1 vector digested by either SalI or SmaI, respectively.

A lentiviral Cep192-*sil* construct containing either the untagged wild type (WT) (pKM3235), the T44A (pKM4560) or S995A (pKM3236) mutation, or the T44A S995A double mutation (pKM4558) was generated by inserting each respective SalI fragment into a modified pHR′.J-CMV-SV-puro vector (pKM2994) (2) digested by the corresponding enzyme. To generate constructs for tandem affinity purification, an AscI-EcoRV fragment containing Cep192 P1(1–647) (pKM3291), Cep192 P3(507–1400) (pKM3292), Cep192 P5(901–1800) (pKM3293), or Cep192 P6(1700–2538) (pKM3294) was cloned into the pHR′.J-CMV-$FLAG_3$-TEV-ZZ vector (pKM3045) digested by AscI and PmeI. The ZZ tag is a derivative of *Staphylococcus* protein A, which has a high affinity for IgG. The TEV sequence provides a cleavage site for a highly site-specific protease found in tobacco etch virus (TEV).

Cell culture and transfection. HeLa, U2OS, and HEK293T cells were cultured as recommended by the American Type Culture Collection. Transfections into these cells were carried out by using either Lipofectamine 2000 (Invitrogen) for protein overexpression or Lipofectamine RNAiMAX (Invitrogen) for small interfering RNA (siRNA)-based knockdowns. For the production of lentiviruses, transfection was performed by using a calcium phosphate coprecipitation method (13). To effectively deplete Cep192 proteins, U2OS cells were transfected twice with an siRNA against Cep192 (siCep192) (nucleotide positions 2407 to 2427) (14) and cultured for a total period of 96 h. To trap the majority of cells in either the S or M phase, cells were treated with 2.5 mM thymidine (Sigma-Aldrich) or 666 nM nocodazole (Sigma-Aldrich) for 20 h, respectively.

Lentivirus generation and infection. Lentiviruses were generated by cotransfecting HEK293T cells with pHR′-CMVΔR8.2Δvpr-, pHR′-CMV-VSV-G (protein G of vesicular stomatitis virus)-, and pHR′-CMV-SV-puro-based constructs containing the target gene. Stable U2OS cell lines were generated by infecting the cells with lentiviruses expressing the gene of interest and were selected with 2 μg/ml of puromycin (Sigma-Aldrich). The selected cells were then transfected with siRNAs to deplete RNA interference (RNAi)-sensitive endogenous proteins.

Tandem affinity purification of Cep192-binding proteins. HEK293T cells stably expressing various Cep192-$Flag_3$-TEV-ZZ constructs, namely, P1(1–647), P3(507–1400), P5(901–1800), and P6(1700–2538), were generated by using the appropriate lentiviruses and then treated with 666 nM nocodazole to enrich mitotic targets. The resulting cells were lysed in TBSN buffer (20 mM Tris-Cl [pH 8.0], 150 mM NaCl, 0.5% NP-40, 5 mM EGTA, 1.5 mM EDTA, 0.5 mM Na_3VO_4, 20 mM *p*-nitrophenyl phosphate, and a protease inhibitor cocktail [Roche]) (15) and subjected to tandem affinity purification as previously described (14).

GST-PBD and peptide pulldown assays. To carry out Plk1 polo-box domain (PBD) pulldown assays, bacterially expressed, bead-bound GST, the GST-PBD WT, or GST-PBD(H538A K540M) (gifts from Michael B. Yaffe, Massachusetts Institute of Technology, Cambridge, MA) was incubated with an equal amount of mitotic HeLa cell lysates in TBSN buffer for 2 h and then precipitated. The resulting precipitates were washed four times with TBSN buffer and analyzed by immunoblotting with the indicated antibodies.

Peptide-based pulldown assays were carried out as previously described (16).

Antibody production. Rabbit polyclonal antibodies were generated against the synthesized phospho-T44 (p-T44) (residues 34 to 53; SNLGL PVAVS**pT**LARDRSSTD [p-T44 is indicated in boldface type]) or phospho-S995 (p-S995) (residues 986 to 1004; PSTSPLSHS**pS**PSEISGTSS [p-S995 is indicated in boldface type]) peptide at Young In Frontier Co., Ltd. (Seoul, South Korea). Affinity purification of these antibodies was carried by out using C-$(CH_2)_6$-conjugated phosphopeptides and nonphosphopeptides that were immobilized separately on SulfoLink coupling resin (Pierce).

Rabbit anti-Cep192 was previously described (14). Other antibodies used in this study were purchased from commercial sources: rabbit anti-GFP, mouse anti-Plk1, and goat anti-γ-tubulin antibodies were obtained from Santa Cruz Biotechnologies; mouse anti-Flag antibody was obtained from Sigma-Aldrich; rat antihemagglutinin (anti-HA) antibody was obtained from Roche; and both rabbit anti-AurA and rabbit anti-AurA p-T288 antibodies were obtained from Cell Signaling.

***In vitro* kinase assay and GST pulldown.** For the experiments shown in Fig. 6E, kinase assays were carried out with kinase reaction buffer (50 mM Tris-HCl [pH 7.5], 10 mM $MgCl_2$, 2 mM dithiothreitol [DTT], 2 mM EGTA, and 20 mM *p*-nitrophenyl phosphate) in the presence or absence of 1 mM ATP. Bacterially expressed, purified His-Cep192(1–1097) and His-AurA were first incubated in kinase reaction buffer for 30 min at 30°C. Purified His-Plk1 was then added to the reaction mixture and incu-

bated for an additional hour at 30°C. Reactions were terminated by mixing with SDS sample buffer and analyzed.

For the GST pulldown experiments shown in Fig. 2D, kinase reactions were performed as described above except that bead-bound GST-Cep192(1–647) or the GST control was used. Reacted samples were diluted in TBSN buffer (20 mM Tris-Cl [pH 8.0], 150 mM NaCl, 0.5% NP-40, 5 mM EGTA, 1.5 mM EDTA, 0.5 mM Na_3VO_4, and 20 mM *p*-nitrophenyl phosphate) and then subjected to GST pulldown. After mixing of the glutathione (GSH)-agarose precipitates with SDS sample buffer, samples were separated by 10% SDS-PAGE and analyzed by immunoblotting.

Coimmunoprecipitation and immunoblotting. Cells were lysed in TBSN buffer, and the resulting lysates were incubated with the primary antibody for 1 h at 4°C, followed by an additional 2 h of incubation with protein G-Sepharose beads (Santa Cruz). Where indicated, 20 μM the Plk1 PBD-binding PLHSpT phosphopeptide (17) was provided to competitively inhibit the interaction between the Plk1 PBD and its target. Immunoprecipitates were washed five times with TBSN buffer, separated by 10% SDS-PAGE (7% to detect Cep192), transferred onto a polyvinylidene difluoride (PVDF) membrane, and then detected by immunoblotting with the indicated antibodies using an enhanced chemiluminescence detection system (Pierce). The signal intensities of the protein bands of interest were quantified by using ImageJ software.

Size exclusion chromatography. Size exclusion chromatography was performed with the Akta Explorer instrument (GE Healthcare), which was equipped with a HiLoad 16/60 Superdex 200 prep-grade column (GE Healthcare). The column was preequilibrated with loading buffer (20 mM Tris-HCl [pH 7.5], 1 mM $MgCl_2$, 1 mM EGTA, and 150 mM NaCl) and then applied with 1 ml (2 mg/ml) of precleared cell lysates. Gel filtration was carried out with loading buffer at 1 ml/min, and fractions were collected every 2 min (2 ml/fraction). The resulting samples were then subjected to immunoblot analysis.

Immunofluorescence microscopy and quantification. Immunostaining analysis was carried out essentially as previously described (16), using the indicated primary antibodies and appropriate secondary antibodies (Alexa Fluor 488 or 594) from Invitrogen. Confocal images were obtained by using the Zeiss LSM 780 system mounted on a Zeiss Observer Z1 microscope. To quantify the fluorescence signal intensities, images of unsaturated fluorescence signals were acquired with the same laser intensity at 512 by 512 pixels and with a 12-bit resolution. The intensities of the fluorescence signals were quantified by using Zeiss ZEN confocal software and then plotted by using the GraphPad Prism 6 program.

RESULTS

Mammalian Plk1 PBD interacts with Cep192 in a phospho-dependent manner. In our effort to better understand the function of Cep192 during the M phase of the cell cycle, we isolated Cep192-binding proteins by performing tandem affinity purification with HEK293T cells expressing various ligands and treated with nocodazole to enrich mitotic targets (Fig. 1A). Mass spectrometry analyses revealed that both the Cep192 P3(507–1400) and P5(901–1800) fragments specifically coprecipitated Plk1, whereas the Cep192 P1(1–647) fragment efficiently interacted with AurA (Fig. 1B). In good agreement with data from a previous report (9), a systematic analysis revealed that human Cep192 (401–647) was necessary for AurA binding (data not shown). These data suggest that AurA and Plk1 bind to distinct regions on Cep192. A relatively low efficiency of Plk1 binding to Cep192, compared to that of AurA binding to Cep192, could be attributed to the fact that Plk1 binding requires the prior generation of a phosphoepitope on its target (18), whereas AurA binding does not (19).

Previous studies showed that Cep192 localizes to centrosomes throughout the cell cycle and becomes most abundant at these sites during the M phase of the cell cycle (2, 4). Centrosome-localized Plk1 is detected as early as the late S phase and sharply peaks at mitotic centrosomes (15, 20). Consistent with these findings, the localization of Cep192 to centrosomes preceded that of Plk1 to centrosomes (Fig. 1C), suggesting that Cep192 could serve as a scaffold that recruits Plk1 to these structures. Since both Cep192 and Plk1 have been shown to play important roles in mitotic spindle assembly (4, 9, 10, 21), we therefore chose to investigate the physiological significance of the Cep192-Plk1 interaction during the cell cycle.

To examine whether Cep192 interacts with Plk1 at its endogenous levels, we performed coimmunoprecipitation analysis using HeLa cells treated with either thymidine (S-phase arrest) or nocodazole (M-phase arrest). Immunoprecipitation of Cep192 coprecipitated Plk1 from M-phase but not S-phase cells, whereas it coprecipitated AurA from both S- and M-phase cells (Fig. 1D). These observations suggest that under physiological conditions, Cep192 interacts with AurA prior to interacting with Plk1. Notably, Cep192 showed markedly retarded electrophoretic mobility in M phase (Fig. 1D, third panel), likely due to AurA- and Plk1-dependent phosphorylation (see below). Since the Plk1 PBD binds to a phosphorylated epitope (18), Plk1 may interact with phosphorylated Cep192 during M phase. Consistent with this view, the provision of a Plk1 PBD-binding phosphopeptide PLHSpT (17) but not its respective nonphosphopeptide, greatly diminished the level of the Cep192-Plk1 interaction, whereas it failed to alter the level of the Cep192-AurA interaction within the same sample (Fig. 1E).

In a second experiment, the H538A K540M (AM) mutation, which cripples the ability of the Plk1 PBD to recognize its phospho-target (18), completely annihilated the interaction between cotransfected Plk1 and Cep192 (Fig. 1F) or between the recombinant GST-PBD and endogenous Cep192 (Fig. 1G). Furthermore, the GST-fused Plk1 PBD, but not its respective PBD(AM) mutant, interacted with the Cep192 P5(901–1800) fragment (Fig. 1H). Analyses of 11 potential Plk1 PBD-binding phosphopeptides visually identified from the Cep192 primary sequence revealed that the p-S995-containing peptide was capable of efficiently interacting with endogenous Plk1 (Fig. 1I), hinting that the S995 residue is phosphorylated *in vivo*, and this event is likely important for the Cep192-Plk1 interaction.

Synergism in the formation of the Cep192-AurA-Plk1 ternary complex. Studies with *Xenopus* egg extracts have shown that xAurA binds to xCep192, and the resulting xCep192-xAurA complex activates Plx1 to induce bipolar spindle assembly (9, 10). However, how Cep192, AurA, and Plk1 interact with one another to elicit this event remains uninvestigated. To examine the molecular nature of their interactions, we performed gel filtration chromatography using cotransfected HEK293T cells treated with nocodazole for 20 h. Because the level of endogenous Cep192 is low and because both AurA and Plk1 bind to many targets under physiological conditions, the use of cotransfected cell lysates was necessary. In the presence of GFP-fused Cep192 (i.e., GFP-Cep192), the majority of AurA coeluted with Cep192 in high-molecular-weight fractions (fractions 21 to 23) (Fig. 2A, arrowheads) immediately following the void volume (i.e., fraction 19) (Fig. 2A), suggesting that Cep192 and AurA form a high-molecular-weight complex. The ability of Cep192 and AurA to form a high-molecular-weight complex may stem from the capacity of Cep192 to establish homomeric interactions under nocodazole- and thymi-

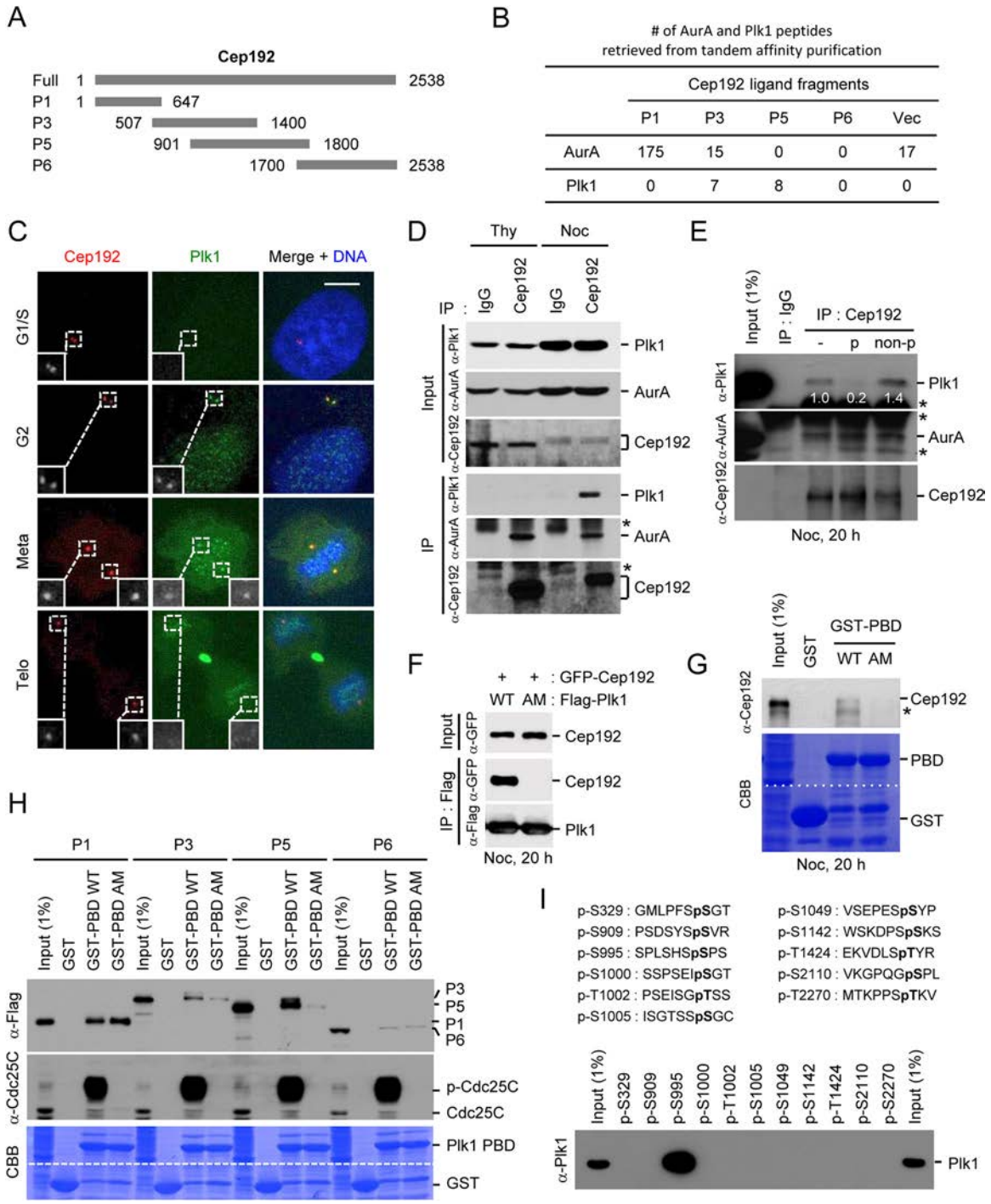

FIG 1 The Plk1 PBD interacts with Cep192 in a phospho-dependent manner. (A) Cep192 constructs used for tandem affinity purification. (B) Numbers of AurA and Plk1 peptides retrieved by mass spectrometry analysis. (C) Immunostaining was carried out with asynchronously growing U2OS cells. Bar, 5 μm. (D) Immunoprecipitation (IP) analysis was carried out with HeLa cells treated with thymidine or nocodazole for 20 h. Samples were then immunoblotted to detect endogenous proteins. Asterisks indicate cross-reacting proteins. (E) Immunoprecipitation analysis was carried out with nocodazole-treated HeLa cell lysates preincubated with buffer (−) or 20 μM either a Plk1 PBD-binding phosphopeptide (p), PLHSpT (17), or its respective nonphosphopeptide (non-p). Numbers indicate relative signal intensities, and asterisks indicate cross-reacting proteins. (F) Immunoprecipitation analysis was carried out with HEK293T cells transfected with the indicated constructs. AM, H538A K540M double mutant. (G) A GST pulldown assay was carried out by using nocodazole-treated HeLa lysates. The asterisk indicates a cross-reacting protein. CBB, Coomassie brilliant blue. The dotted line in the Coomassie brilliant blue gel indicates merged gels. (H) GST pulldown was carried out by using HEK293T cells transfected with the constructs described above for panel A and treated with nocodazole for 20 h. The resulting precipitates were immunoblotted with the indicated antibodies. p-Cdc25C precipitated with the Plk1 PBD served as a positive control. (I) A pulldown was carried out by using the indicated bead-immobilized phosphopeptides (top) and nocodazole-treated HeLa lysates, and the samples were then subjected to immunoblot analysis to detect coprecipitated endogenous Plk1. Phosphorylated residues are indicated in boldface type.

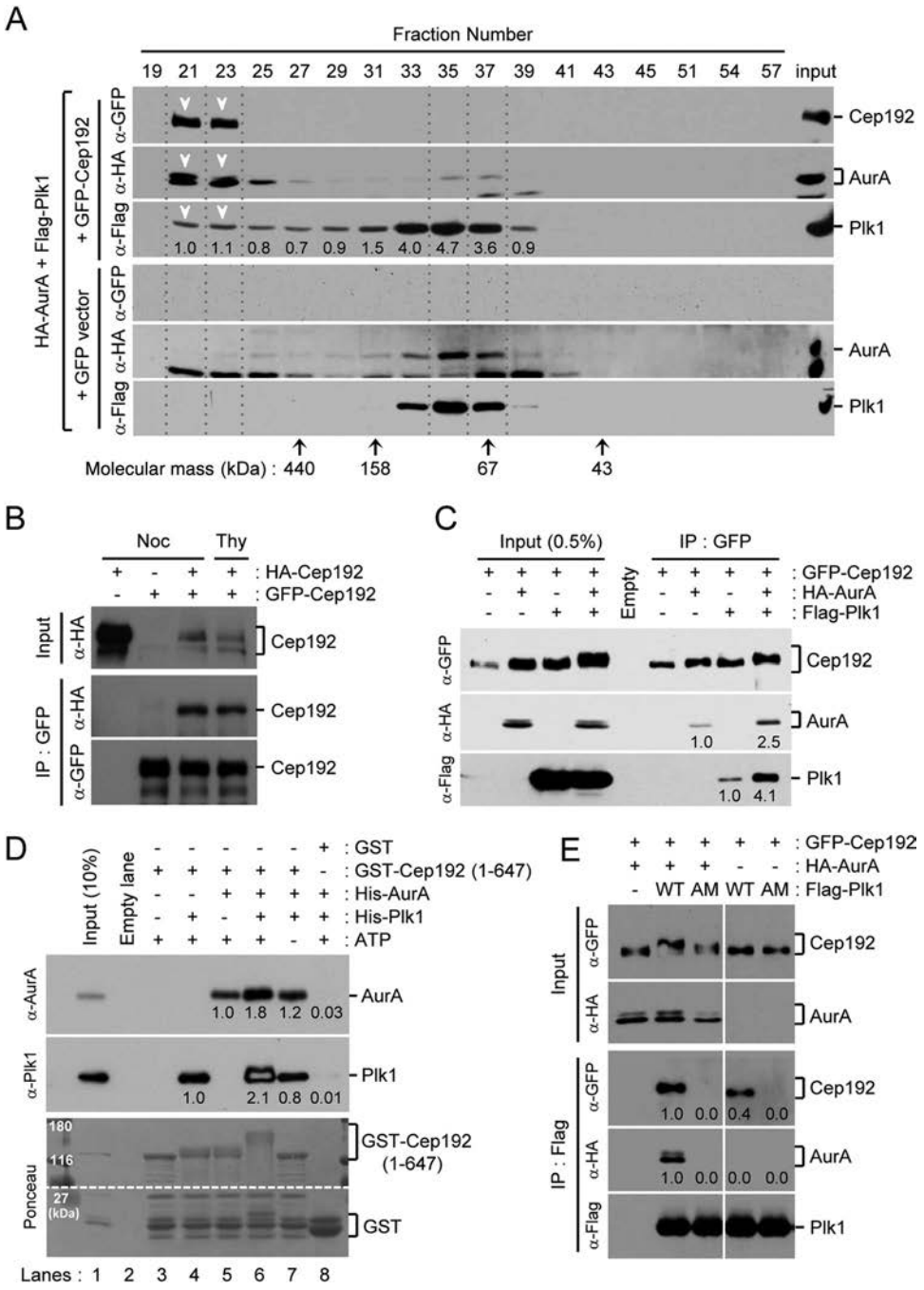

FIG 2 AurA and Plk1 form a ternary complex with Cep192 in a cooperative manner. (A) Immunoblot analysis was carried out by using lysates fractionated on a Superdex 200 gel filtration column. Arrowheads indicate fractions 21 to 23, which contain cofractionated Cep192, AurA, and Plk1. Numbers indicate relative signal intensities. (B and C) Immunoprecipitation analysis was carried out by using transfected HEK293T cells. Cells in panel B were treated with thymidine or nocodazole for 20 h. Numbers in panel C indicate relative signal intensities. (D) *In vitro* kinase assays were carried out, and the resulting samples were subjected to GST pulldown. To detect their cooperative binding to the GST-Cep192(1–647) ligand, limited amounts of AurA and Plk1 were added to the reaction mixture to ensure that ligands are in excess, and coprecipitated AurA and Plk1 were detected by immunoblotting. Numbers indicate relative signal intensities. (E) Immunoprecipitation analysis was carried out with cotransfected HEK293T cells as described above for panels B and C. AM, H538A K540M double mutant. Numbers indicate relative signal intensities.

dine-treated conditions (Fig. 2B). As expected if Plk1 formed a complex with Cep192 and AurA, a significant fraction of coexpressed Plk1 was enriched in fractions 21 to 23 (Fig. 2A, arrowheads), while the majority of Plk1 was detected as a monomeric 68-kDa protein (Fig. 2A). The relatively low level of Plk1 coeluted with the high-molecular-weight Cep192-AurA complex (fractions 21 to 23) could be attributed in part to the fact that the generation of a phosphorylated epitope is a prerequisite step for the complex's interaction with the Plk1 PBD (18). In control GFP vector-transfected cells, both AurA and Plk1 failed to form a high-

molecular-weight complex (Fig. 2A, bottom three panels), suggesting that AurA and Plk1 associate with each other through Cep192.

If Cep192, AurA, and Plk1 indeed form a thermodynamically stable ternary complex, the presence of either AurA or Plk1 may promote the binding of the other to Cep192. In support of this notion, expression of AurA greatly increased the Cep192-Plk1 interaction, while expression of Plk1 also enhanced the Cep192-AurA interaction but at a somewhat reduced level (Fig. 2C, right). Notably, the expression of either AurA or Plk1 moderately decreased the electrophoretic mobility of GFP-Cep192, whereas the expression of both AurA and Plk1 greatly decreased it (Fig. 2C, input). In a second experiment, we were able to reconstitute the findings shown in Fig. 2C by performing *in vitro* kinase reactions followed by GST pulldown (Fig. 2D) and demonstrated the formation of a ternary Cep192-AurA-Plk1 complex using bacterially expressed purified proteins (Fig. 2D, lane 6). Judging from the Ponceau-stained gel, it was apparent that AurA and Plk1 cumulatively phosphorylate Cep192 (Fig. 2D, bottom). These findings suggest that AurA and Plk1 directly phosphorylate Cep192 in an additive manner and that they cooperatively promote the formation of a Cep192-based ternary complex. In addition, consistent with the PBD-dependent Plk1-Cep192 interaction (Fig. 1F to H), WT Plk1, but not its respective Plk1(AM) mutant, coimmunoprecipitated Cep192 or the Cep192-AurA complex, and the coexpression of AurA substantially increased the Cep192-Plk1 interaction (Fig. 2E, compare lanes 2 and 4).

Cep192 mediates the interaction between and the reciprocal activation of AurA and Plk1. The synergistic formation of a ternary Cep192-AurA-Plk1 complex raises the question of how Cep192 serves as a platform to regulate AurA and Plk1. To directly determine whether Cep192 serves as a scaffold that mediates the interaction between AurA and Plk1, we carried out coimmunoprecipitation analyses using cotransfected HEK293T cells that express AurA and Plk1 in the presence or absence of GFP-Cep192. In the total lysates, coexpression of Cep192 resulted in the generation of p-T288 epitope-containing activated AurA (22) (Fig. 3A, input, third panel) and p-T210 epitope-containing activated Plk1 (23) (Fig. 3A, input, bottom). Coimmunoprecipitation analyses under these conditions revealed that AurA and Plk1 reciprocally coprecipitated each other only in the presence of Cep192 (Fig. 3A, right panels). These findings demonstrated that Cep192 mediates the AurA-Plk1 interaction and that the formation of the Cep192-AurA-Plk1 complex could be important for activating AurA and Plk1. Notably, treatment of cells with either thymidine or nocodazole did not significantly alter the levels of activated AurA and Plk1 and the degree of the Cep192-dependent AurA-Plk1 interaction (Fig. 3A). These results hint that the formation of an active ternary Cep192-AurA-Plk1 complex can occur without the involvement of a third element, which may influence AurA or Plk1 function, in S- or M-phase-arrested cell lysates. Therefore, except where indicated, we used asynchronously cultured cells for further analysis.

To determine whether AurA and Plk1 can reciprocally activate each other in the presence of Cep192, we examined the level of activated AurA or Plk1 in total lysates coexpressing either Plk1 or AurA, respectively (Fig. 3B). Consistent with the results shown in Fig. 3A, coexpression of AurA markedly increased the level of p-T210 epitope-containing activated Plk1. In addition, as expected if Plk1 promoted the Cep192-AurA interaction shown in Fig. 2C, Plk1 coexpression increased the level of p-T288 epitope-containing activated AurA in the total lysates (Fig. 3B, compare the third panel with the total amount of AurA in the second panel). Although the degree of Plk1-dependent AurA activation was not as prominent as that of AurA-dependent Plk1 activation, these findings hint that AurA and Plk1 reciprocally activated each other in the presence of Cep192.

We then investigated whether the reciprocal activation of AurA and Plk1 required the kinase activity of each enzyme. To this end, HEK293T cells were cotransfected with either the WT or its respective kinase-inactive form of AurA or Plk1 and subjected to immunoblot analysis. The Cep192(S995A) mutant deprived of the p-S995 motif-dependent interaction with Plk1 (Fig. 1I) was included
for comparison. The results showed that the expression of WT AurA, but not its kinase-inactive T288A mutant (22), efficiently induced the p-T210 epitope on Plk1 but only in the presence of Cep192 (Fig. 3C). In addition, WT Plk1, but not its kinase-inactive K82M mutant (15), was required to achieve the full activation of AurA, again in the presence of Cep192 (Fig. 3C). Notably, the Cep192(S995A) mutant, which is expected to abrogate the p-S995-dependent Cep192-Plk1 interaction, still possessed a significant capacity to promote AurA-dependent Plk1 p-T210 generation (Fig. 3C, compare lane 3 to lanes 1 and 2), suggesting that the S995 motif may not be the sole source of the interaction between Cep192 and Plk1 (see below).

To further investigate whether the kinase activities of AurA and Plk1 are important for their interactions with Cep192, we performed coimmunoprecipitation analysis using samples prepared as for Fig. 3C. We observed that cells expressing either the kinase-inactive AurA(T288A) or Plk1(K82M) mutant showed a markedly diminished level of interaction between Cep192 and Plk1, compared to cells expressing the respective WT AurA or WT Plk1 (Fig. 3D). In addition, Cep192(S995A)-expressing cells showed a much higher level of the Cep192-Plk1 interaction than did AurA(T288A)- or Plk1(K82M)-expressing cells (Fig. 3D), further suggesting the existence of an S995-independent Cep192-Plk1 interaction.

We next investigated whether AurA and Plk1 reciprocally activate each other at their endogenous levels and whether this event requires Cep192. To do this, HeLa cells enriched in M phase were treated with pharmacological inhibitors against AurA (MLN8237) or Plk1 (BI2536) for 1 h and then immunostained. To examine the effect of Cep192 depletion on cross-activation between AurA and Plk1, cells treated with Cep192 siRNA (siCep192) were also included. Quantification of the level of the centrosome-localized AurA p-T288 or Plk1 p-T210 epitope was performed by using cells with metaphase chromosome morphology to indirectly assess the overall AurA or Plk1 kinase activity at this location. The results showed that treatment of cells with MLN8237, which greatly diminished the level of the p-T288 epitope, also significantly reduced the level of the p-T210 epitope (Fig. 3G). In addition, treatment with BI2536 led to similar degrees of cross-reductions for p-T210 and p-T288 signals (Fig. 3G), thus confirming the results obtained with transfected lysates (Fig. 3C). Depletion of Cep192 drastically diminished the levels of centrosome-localized p-T288 and p-T210 signals (Fig. 3E to G), indicating that Cep192 is required for the cross-activation of AurA and Plk1 at their endogenous sites. In cotransfected HEK293T cells, GFP-fused Bora, a nuclear activator of AurA (24), was capable of activating coexpressed AurA and Plk1 but only marginally (judging from the

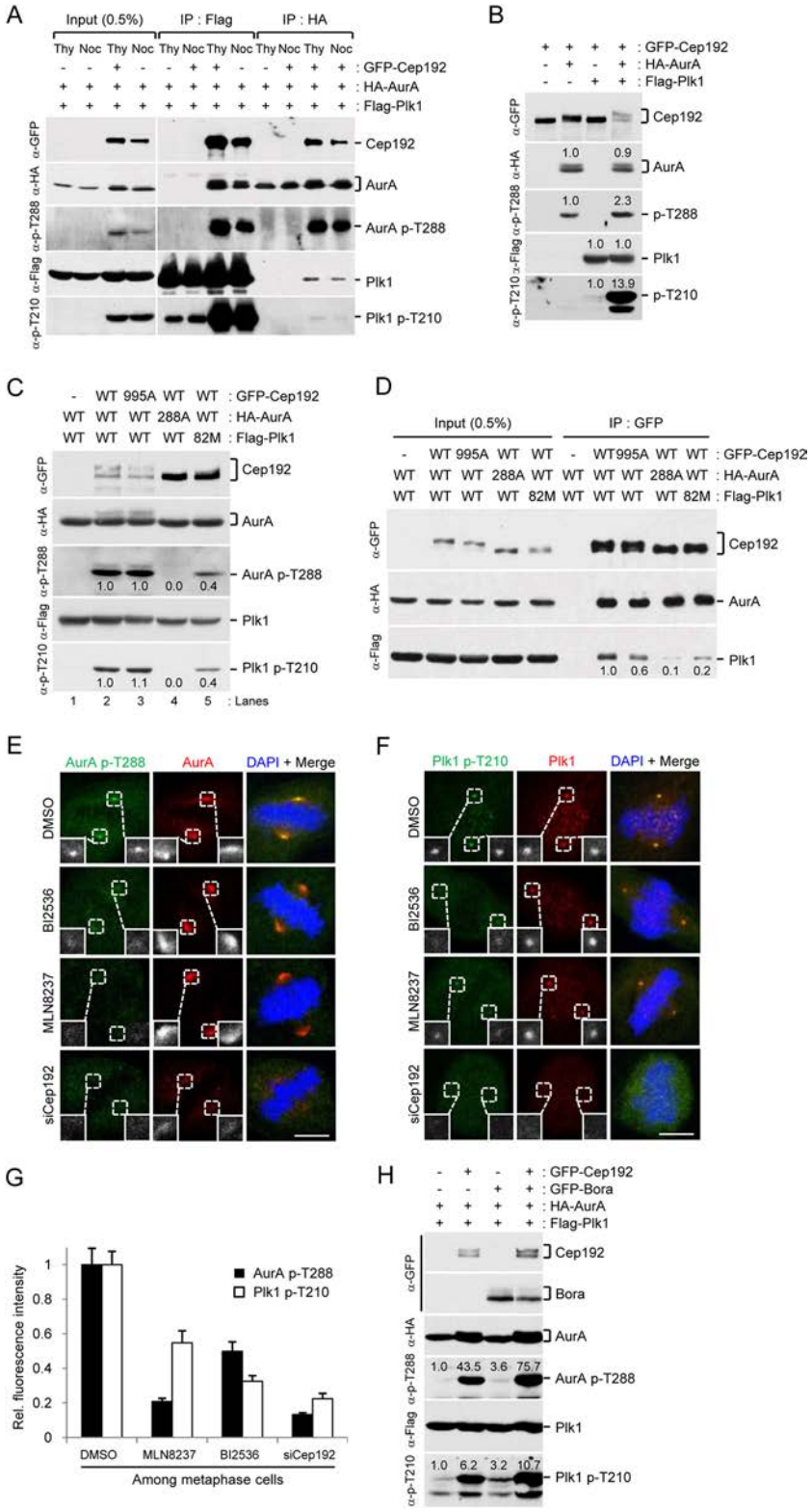

FIG 3 Cep192-dependent reciprocal activation of AurA and Plk1 is required for the proper Cep192-Plk1 interaction. (A) Immunoprecipitation analysis was carried out by using transfected HEK293T cells treated with thymidine or nocodazole for 20 h. (B and C) Immunoblot analysis was carried out by using HEK293T cells transfected with the indicated constructs. (D) Immunoprecipitation analysis was carried out by using transfected HEK293T cells. Numbers in panels B to D indicate relative signal intensities. 995A, S995A mutant; 288A, T288A mutant; 82M, K82M mutant. (E and F) HeLa cells released from a DT block for 9 h were treated with control dimethyl sulfoxide (DMSO), 0.5 μM MLN8237, or 0.1 μM BI2536 for 1 h and then harvested for immunostaining analysis. Cells treated with Cep192 siRNA (siCep192) were included for comparison. Costaining with either anti-AurA (E) or anti-Plk1 (F) antibody was carried out to assess the total level of centrosome-localized AurA or Plk1 signals. Representative images are shown. Bars, 5 μm. DAPI, 4′,6-diamidino-2-phenylindole. (G) Quantification of centrosome-localized p-T210 or p-T288 signals was carried out with metaphase HeLa cells, prepared as described above for panels E and F, from three independent experiments ($n \geq 20$ per sample/experiment). Error bars indicate standard deviations. (H) Immunoblot analysis was carried out by using HEK293T cells transfected with the indicated constructs. Numbers indicate relative signal intensities.

levels of the activational p-T288 and p-T210 epitopes, respectively) (Fig. 3H, compare lanes 1 and 3). Under conditions where GFP-Cep192 and GFP-Bora were expressed at similar levels, GFP-Cep192 activated coexpressed AurA and, in turn, Plk1 more efficiently than did GFP-Bora (Fig. 3H, compared lanes 2 and 3).

Plk1 interacts with Cep192 in both AurA-dependent and -independent manners. While we were searching for additional Plk1-binding motifs, Joukov et al. demonstrated that in *Xenopus* egg extracts, Plx1 interacts with the T46 motif of xCep192 and promotes microtubule recruitment (9). Notably, the analogous human T44 motif does not closely resemble the previously proposed Plk1 PBD-binding motif (Φ/P-Φ-T/Q/H/M-S-pS/pT-P/X, where X is any amino acid residue and Φ is a hydrophobic residue) (18) and therefore was not included in our phosphopeptide screens for Plk1 PBD binding (Fig. 1I). However, we found that a p-T44 peptide immobilized on beads precipitated endogenous Plk1 from mitotic HeLa cell lysates as efficiently as the p-S995 peptide, whereas their respective non-phospho-S995 and -T44 peptides did not detectably precipitate endogenous Plk1 from the same lysates (Fig. 4B). Furthermore, mutational analyses of the purportedly PBD-binding T44 motif and its neighboring residues confirmed that both the T44 and, somewhat less importantly, S43 residues were critical for Plk1 binding, while their downstream residues were not (Fig. 4A). The importance of a Ser residue at the −1 position and the nonessential role of residues downstream of the SpT dipeptide have been previously demonstrated (17, 18). These data strongly suggest that in addition to the S995 motif (Fig. 1I), the T44 motif is required for the Cep192-Plk1 interaction in humans. Highlighting the importance of both T44- and S995-dependent Plk1 PBD binding, these two residues are conserved among higher eukaryotic organisms (Fig. 4C).

To investigate the functional relationship between the T44- and the S995-dependent Cep192-Plk1 interactions, we closely examined the significance of these interactions under different conditions. When only Plk1 and Cep192 were coexpressed, we found that the S995A mutation greatly diminished the Cep192-Plk1 interaction, whereas the T44A mutation only mildly crippled the interaction (Fig. 4D). In contrast, under conditions where Cep192, AurA, and Plk1 were all coexpressed, the T44A mutation caused a much more pronounced defect in the Cep192-Plk1 interaction than did the S995A mutation (Fig. 4E). The T44A S995A (AA) double mutations appeared to cripple the Cep192-Plk1 interaction in an additive manner (Fig. 4D and E). These results suggest that Plk1 binds to two distinct phospho-motifs (i.e., the p-T44 and p-S995 motifs) on Cep192 and that the binding is contingent upon the presence or absence of AurA.

Since both AurA and Plk1 activities were required for the efficient formation of the Cep192-AurA-Plk1 ternary complex (Fig. 3D), we next investigated the relationship between AurA activity and T44- or S995-dependent Cep192-Plk1 interactions. Using cotransfected HEK293T cells expressing either WT AurA or the kinase-inactive AurA(T288A) mutant, we confirmed that AurA activity was required for the Cep192-Plk1 interaction (Fig. 4F, compare lanes 1 and 2). Under these conditions, the Cep192 (S995A) mutant, which still bears the T44 motif, coprecipitated Plk1 in an AurA activity-dependent manner (Fig. 4F, lanes 3 and 4). In contrast, the Cep192(T44A) mutant, which contains the S995 motif, bound to Plk1 regardless of the presence or absence of AurA activity, although the level of the Cep192(T44A)-Plk1 interaction in AurA(T288A)-expressing cells was somewhat diminished (Fig. 4F, compare lanes 5 and 6). This finding suggests that unlike the T44-dependent Cep192-Plk1 interaction, the S995-dependent interaction is largely independent of AurA kinase activity. As expected, the Cep192(T44A S995A) double mutant failed to coprecipitate Plk1 because of the lack of both AurA-dependent (i.e., T44-dependent) and AurA-independent (i.e., S995-dependent) interactions between Cep192 and Plk1. Whether the AurA-dependent interaction between the T44 motif of Cep192 and Plk1 is regulated by either AurA activity itself or AurA-activated Plk1 activity is addressed below.

Cell cycle-dependent regulation of the p-T44 and p-S995 motifs and generation of the "self-primed" p-T44 epitope by AurA-activated Plk1. The two distinct modes of Plk1 binding to either the T44 or S995 motif of Cep192 (Fig. 4) suggest that phosphorylation of the T44 and S995 residues could be differentially regulated. To investigate this possibility, we generated phospho-T44 and -S995 antibodies (Fig. 5) and carried out immunostaining analyses using cells released synchronously from a double-thymidine (DT) block. These results showed that the levels of both the p-T44 and p-S995 signals were hardly detectable or very low at interphase centrosomes (Fig. 6A). However, the levels of these signals increased sharply during M phase, peaking at metaphase centrosomes before precipitously decreasing in late mitosis (Fig. 6A). Interestingly, unlike the p-S995 epitope, which was detectable mostly at metaphase centrosomes, a significant level of the p-T44 epitope was detectable even at prophase centrosomes (Fig. 6A). This observation suggests that under physiological conditions, the p-T44-dependent formation of the Cep192-AurA-Plk1 complex could occur at this stage.

Since AurA and Plk1 cooperated to form the Cep192-AurA-Plk1 ternary complex, and both AurA and Plk1 appeared to additively phosphorylate Cep192 (Fig. 3), we investigated whether their kinase activities are required to generate the p-T44 and p-S995 epitopes. Because the S995 residue is followed by a Pro residue at the +1 position, we also examined whether a Pro-directed mitotic kinase, Cdc2 (25), contributes to the production of the p-S995 epitope. To this end, HeLa cells enriched in mitosis from DT release were additionally treated with pharmacological inhibitors against AurA (MLN8237 and VX680) (26, 27), Plk1 (BI2536) (28), or Cdc2 (BMI1026) (29). Interestingly, although the treatment of cells with an AurA-selective inhibitor, MLN8237, or a pan-Aur inhibitor, VX680, only modestly reduced the level of the p-T44 signal, both inhibitors greatly diminished the level of the p-S995 signal (Fig. 6B). On the other hand, the treatment of cells with a Plk1 inhibitor, BI2536, selectively abolished the p-T44 epitope but not the p-S995 signal. Cells treated with a Cdc2 inhibitor, BMI1026, exhibited somewhat reduced levels of both the p-T44 and p-S995 signals (Fig. 6B). A short (20-min) treatment was required to minimize the degree of unscheduled mitotic exit by Cdc2 inhibition (29).

To further investigate whether AurA or Plk1 contributes to the production of the p-T44 or p-S995 epitope, HEK293T cells expressing Cep192 were coexpressed with either Plk1 or AurA and harvested for immunoblot analysis (we were not able to detect endogenous p-T44 and p-S995 epitopes with our antibodies). The results showed that coexpression of WT Plk1 but not its respective kinase-inactive K82M mutant efficiently induced the p-T44 epitope in Cep192 (Fig. 6C, lanes 1 and 2). Interestingly, the level of the p-T44 epitope remained unaltered by the Cep192(S995A)

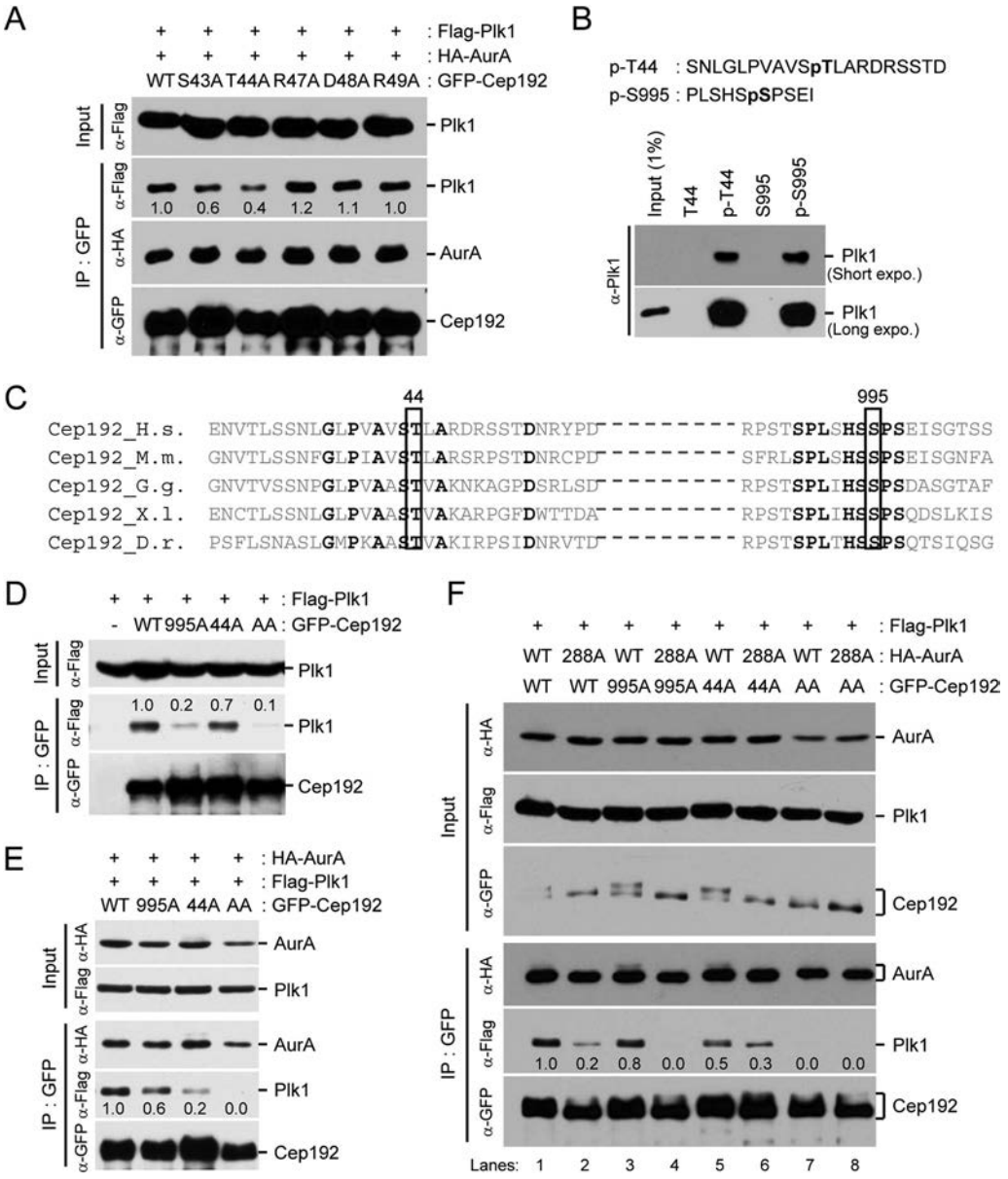

FIG 4 Two distinct modes of the Cep192-Plk1 interaction in the absence or presence of AurA. (A) Immunoprecipitation analysis was carried out by using cotransfected HEK293T cells lysates. The numbers indicate the relative levels of Plk1 coprecipitated with Cep192 and AurA. Because the p-T44-dependent Cep192-Plk1 interaction requires a prior Cep192-AurA interaction, AurA was cotransfected. (B) Peptide pulldown assays were carried out by using bead-immobilized nonphosphopeptides or their respective phospho-T44 (p-T44) or phospho-S995 (p-S995) peptides. Sequences of synthesized T44 or S995 peptides are shown at the left. The p-T44 and p-S995 residues are indicated in boldface type. (C) Sequence alignment of the T44 and S995 regions of Cep192 orthologs in *Homo sapiens* (H.s.), *Mus musculus* (M.m.), *Gallus gallus* (G.g.), *Xenopus laevis* (X.l.), and *Danio rerio* (D.r.). Identical residues are marked by boldface type. (D to F) Immunoprecipitation analysis was carried out by using HEK293T cells transfected with the indicated constructs. Numbers indicate relative signal intensities. 288A, T288A mutant; 995A, S995A mutant; 44A, T44A mutant; AA, T44A S995A double mutant.

mutation (Fig. 6C, compare lanes 1 and 5), suggesting that Plk1-dependent production of the p-T44 epitope does not require prior phosphorylation at S995. AurA alone failed to detectably induce the p-T44 epitope (Fig. 6C, lanes 9 to 16). Under these conditions, we found that the level of the p-S995 epitope was unaltered by the presence or absence of Plk1 or AurA kinase activity or the T44A mutation (Fig. 6C, lanes 1 to 4 and 9 to 12), suggesting that the production of the p-S995 epitope is independent of AurA, Plk1, and the T44A mutation.

Although AurA activity was required for the T44-dependent Cep192-Plk1 interaction (Fig. 4F, compare lanes 3 and 4), AurA failed to directly induce the p-T44 epitope (Fig. 6C). Thus, we investigated whether AurA contributes to the T44-dependent interaction via Plk1. We found that cell lysates coexpressing Cep192 and Plk1 induced the p-T44 epitope at a modest level, whereas cell lysates coexpressing Cep192, AurA, and Plk1 induced the p-T44 epitope at a substantially (~8.5-fold) increased level (Fig. 6D, compare lanes 2 and 4). Coexpression of the kinase-inactive AurA(T288A) mutant failed to enhance the level of the p-T44 epitope (Fig. 6D, compare lanes 4 and 5), suggesting that the ac-

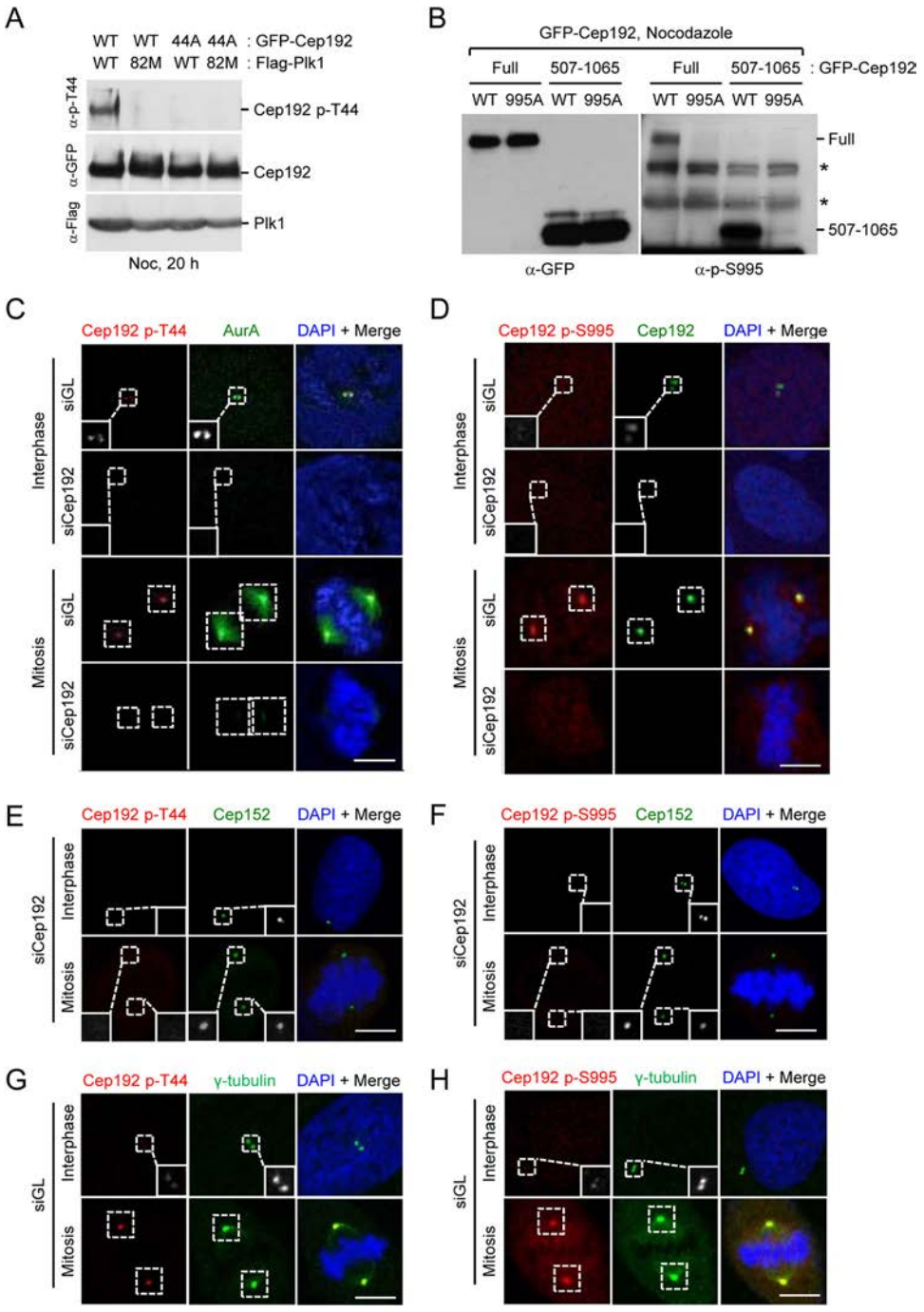

FIG 5 Characterization of Cep192 p-T44 and p-S995 phospho-antibodies. (A and B) HEK293T cells transfected with the indicated constructs were treated with nocodazole for 20 h and then immunoblotted. Unlike the p-S995 epitope, coexpression of Plk1 was necessary to readily detect the p-T44 epitope. 82M, K82M mutant; 44A, T44A mutant; 995A, S995A mutant. Asterisks indicate cross-reacting proteins. (C to H) Immunostaining with Cep192 p-T44 or p-S995 antibodies was carried out by using U2OS cells silenced for either the control luciferase (siGL) or Cep192 (siCep192). The positions of centrosomes are marked by AurA (C), Cep192 (D), Cep152 (E and F), or γ-tubulin (G and H) signals. Bars, 5 μm.

tivation of Plk1 by AurA is critical for the phosphorylation and generation of the p-T44 epitope. Judging from the levels of the AurA p-T288 and Plk1 p-T210 epitopes, the coexpression of AurA and Plk1 significantly cross-activated each other (Fig. 6D, fourth and sixth panels), confirming the findings shown in Fig. 3. In contrast to these findings, the level of the p-S995 epitope remained unchanged by the expression of Plk1, AurA, or both (Fig. 6C and D), implying that the markedly decreased p-S995 signal caused by MLN8237 or VX680 treatment (Fig. 6B) is likely an indirect consequence of AurA inhibition. Consistent with data shown in Fig. 6C and D, *in vitro* kinase assays with purified proteins showed that Plk1 directly phosphorylated and generated the p-T44

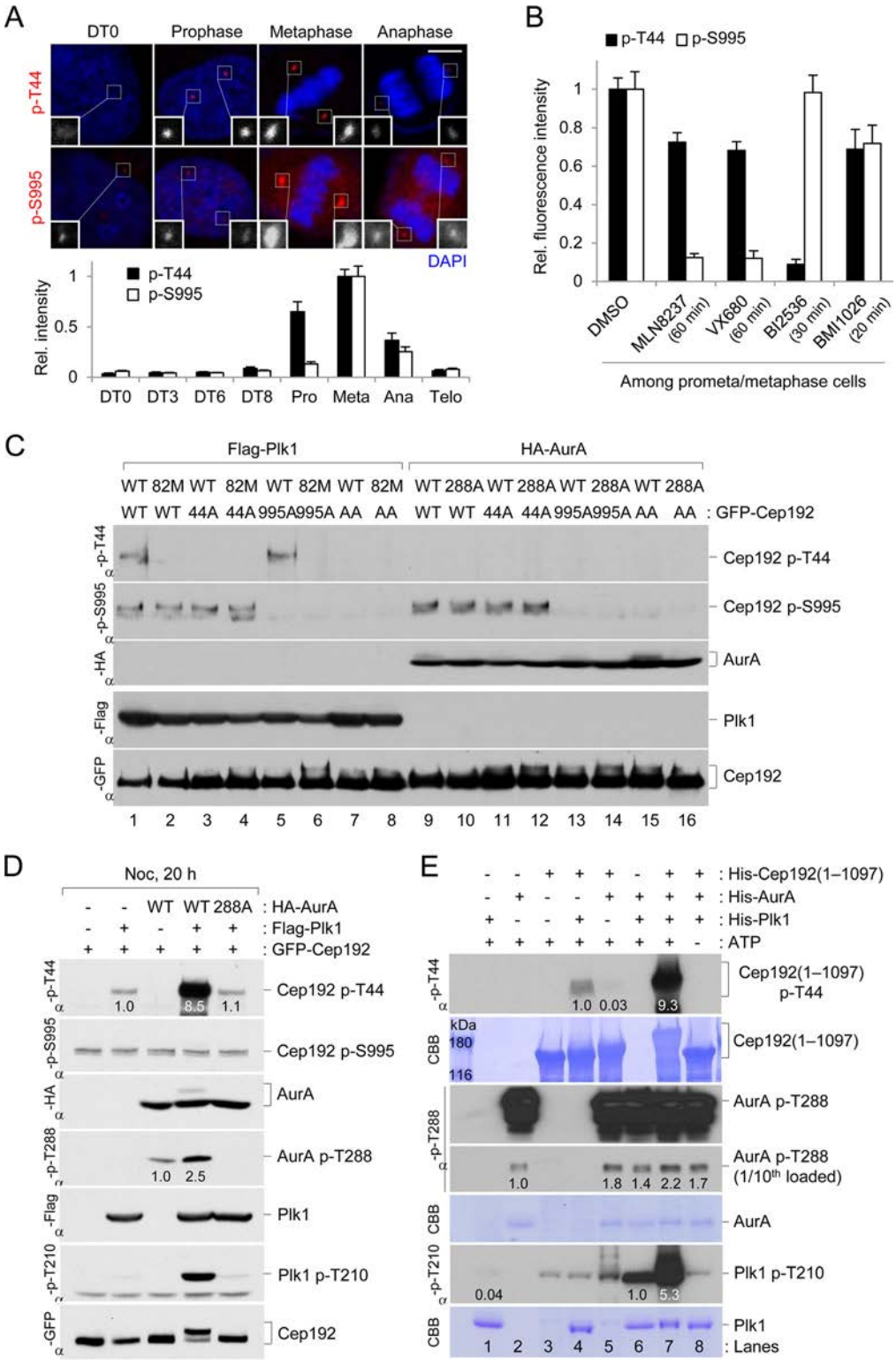

FIG 6 Cell cycle-dependent regulation of the p-T44 and p-S995 epitopes and phosphorylation of the T44 site by AurA-activated Plk1. (A) Immunostaining was carried out by using HeLa cells harvested at the indicated time points (hours) after double-thymidine (DT) release (top), and centrosome-localized p-T44 and p-S995 signals were quantified ($n \geq 20$ per sample at each time point) (bottom). Bar, 5 μm. Error bars indicate standard deviations. (B) Quantification of centrosome-localized p-T44 or p-S995 signals after treatment of HeLa cells with 0.5 μM MLN8237, 0.5 μM VX680, 0.1 μM BI2536, or 0.2 μM BMI1026 ($n \geq 20$ per sample). To enrich the mitotic population, cells released from a DT block for 9 h were used. Error bars indicate standard deviations. (C) Immunoblot analysis was carried out with transfected HEK293T cells treated with nocodazole for 20 h. 82M, K82M mutant; 44A, T44A mutant; 995A, S995A mutant; AA, T44A S995A double mutant; 288A, T288A mutant. (D) Immunoblot analysis was performed by using transfected HEK293T cells treated with nocodazole for 20 h. (E) *In vitro* kinase assays were carried out by using purified protein, as described in Materials and Methods. The resulting samples were immunoblotted. Numbers indicate relative signal intensities.

epitope, whereas AurA did not (Fig. 6E, lanes 4 and 5, respectively). The addition of AurA greatly enhanced (9.3-fold) the ability of Plk1 to generate the p-T44 epitope, closely reflecting the severalfold increased level of the p-T210 epitope on Plk1 (Fig. 6E, compare lanes 4 and 7). The effect of Plk1 on AurA activation was less apparent under these conditions, because bacterially expressed, purified AurA was already highly phosphorylated at its activational T288 residue (Fig. 6E, third panel, lane 2).

Both p-T44- and p-S995-dependent Cep192-Plk1 interactions are required for proper spindle formation and mitotic progression. To determine the physiological significance of T44- and/or S995-dependent interactions between Cep192 and Plk1, U2OS cells expressing a lentivirus-based control vector or various RNAi-insensitive Cep192 (Cep192-*sil*) constructs were silenced for either the control luciferase (siGL) or endogenous Cep192 (siCep192) by siRNA transfection. Immunoblot analysis revealed that the silencing of Cep192 efficiently depleted endogenous Cep192 but not exogenously expressed Cep192-*sil* and that exogenous Cep192-*sil* forms were expressed at a level comparable to that of endogenous Cep192 (Fig. 7A). Immunostaining analysis showed that all Cep192-*sil* forms localized to centrosomes efficiently (Fig. 7B and C), suggesting that both the T44A and S995A mutations do not alter the subcellular localization of Cep192. Under these conditions, cells expressing the Cep192(T44A S995A) mutant exhibited significantly diminished γ-tubulin recruitment to centrosomes, while cells expressing either the Cep192(T44A) or the Cep192(S995A) single mutant displayed a somewhat modest defect in this process (Fig. 7B and C). These findings suggest that the γ-tubulin recruitment defect associated with the T44A or S995A mutation is additive. In line with these results, Cep192(AA)-expressing cells also appeared to exhibit an additive defect in the amount of the total Plk1 population and the active Plk1 p-T210 form recruited to centrosomes (Fig. 7B and C). Interestingly, although the level of centrosome-localized Cep192 remained unchanged by the T44A and S995A mutations, the levels of both centrosomally localized AurA and its active AurA p-T288 form were modestly diminished in cells expressing the Cep192(AA) mutant (Fig. 7B and C), likely because of the loss of the Plk1-promoted Cep192-AurA interaction shown in Fig. 2C. As a consequence of the defects in the proper recruitment of Plk1 and γ-tubulin, Cep192(AA) mutant cells exhibited a significantly increased mitotic block, with monopolar spindle morphology, whereas either Cep192(T44A) or Cep192(S995A) cells displayed these defects somewhat weakly (Fig. 7D to F).

DISCUSSION

AurA and Plk1 cooperation in the formation of the Cep192-AurA-Plk1 ternary complex. While characterizing the physiological function of human Cep192, Gomez-Ferreria et al. proposed that Cep192 serves as a scaffold that is critical for γ-TuRC recruitment to centrosomes and bipolar spindle formation at these structures (4). Later studies with *Xenopus* egg extracts suggested that xCep192 binds to and activates xAurA (10), which in turn activates Plx1 to promote centrosome maturation and bipolar spindle assembly (9). These observations highlight the importance of an xCep192-organized xAurA-Plx1 cascade in regulating γ-TuRC recruitment and MT assembly at centrosomes. However, the molecular mechanism of how Cep192, AurA, and Plk1 orchestrate their functions to elicit these processes in human cells has remained largely uninvestigated. In this study, we demonstrated that AurA and Plk1 are recruited to distinct regions of Cep192 and form a ternary complex in a cooperative manner (Fig. 2). Furthermore, Cep192-bound AurA and Plk1 reciprocally activate each other, although the degree of Plk1-dependent AurA activation was somewhat less substantial than that of AurA-dependent Plk1 activation (Fig. 3B and C). The underlying mechanism of how Plk1 activates Cep192-bound AurA remains to be further investigated. Since AurA functions as an upstream kinase of Plk1 (11, 12), the feedback activation of AurA by Plk1 constitutes a positive amplification loop that ultimately leads to the activation of Plk1 itself. Thus, the formation of a ternary Cep192-AurA-Plk1 complex is likely crucial for the rapid amplification of AurA-dependent Plk1 activation prior to mitotic entry.

The mechanism underlying the cooperative formation of the Cep192-AurA-Plk1 complex remains elusive. Here, we demonstrated that the initial formation of the Cep192-AurA complex does not require AurA or Plk1 kinase activity, but the presence of Plk1 enhances the formation of the Cep192-AurA complex (Fig. 2C and 3D). On the other hand, Plk1 recruitment to the Cep192-AurA complex required both AurA and Plk1 activities (Fig. 3D). Thus, once AurA binds to Cep192, AurA and Plk1 cooperate to generate the Cep192-AurA-Plk1 complex. These observations suggest that AurA- and Plk1-dependent Cep192 phosphorylations likely induce a conformational change in the Cep192 scaffold that allows both AurA and Plk1 to bind more efficiently to Cep192. Since Plx1-dependent xCep192 phosphorylation appears to promote γ-tubulin recruitment and bipolar spindle formation in *Xenopus* egg extracts (9), it will be interesting to further investigate whether AurA- and/or Plk1-dependent phosphorylations on Cep192 cooperatively promote γ-tubulin recruitment to the centrosome-associated Cep192 scaffold in human cells. Identification of Cep192 phosphorylation sites and subsequent investigation of the physiological significance of this event will be necessary for a better understanding of this process.

It should be noted that cells overexpressing Cep192, AurA, and Plk1 form a high-molecular-weight complex, which is significantly larger than the calculated size of the heterotrimeric Cep192-AurA-Plk1 complex (calculated molecular mass of ~393 kDa). This observation suggests that Cep192, AurA, and Plk1 may form a multitrimeric complex under physiological conditions. Unlike in the *Xenopus* system, where xAurA is proposed to form a dimer/multimer (9), we found that Cep192 homomerizes under physiological conditions, whereas AurA and Plk1 do not detectably do so (Fig. 2A and B). Thus, we propose that in human cells, Cep192 homomerization is likely the driving force for the formation of a Cep192-AurA-Plk1 multitrimeric complex.

Two distinct modes of interaction between Cep192 and Plk1. Studies with *Xenopus* egg extracts showed that the xCep192(T46A) mutant lacking T46-dependent Plx1 binding or the xCep192Δ(543–747) mutant lacking xAurA binding still maintained ~70% of its MT-nucleating activity, suggesting the presence of a T46- and xAurA-independent xCep192 function (9). Here, we demonstrated that Plk1 binds to Cep192 through interactions between its C-terminal PBD and one of the two phosphorylated motifs (p-T44 and p-S995) on Cep192. Remarkably, the Plk1 interaction with the p-T44 motif was prevalent when Cep192 was in a complex with AurA, whereas the Plk1 interaction with the p-S995 motif was preferred when Cep192 was in an AurA-unbound homomeric state (Fig. 4). Since AurA phosphorylates Cep192 and retards its gel mobility (Fig. 2 and 3), AurA may have the capacity to induce a conformational change in Cep192 that

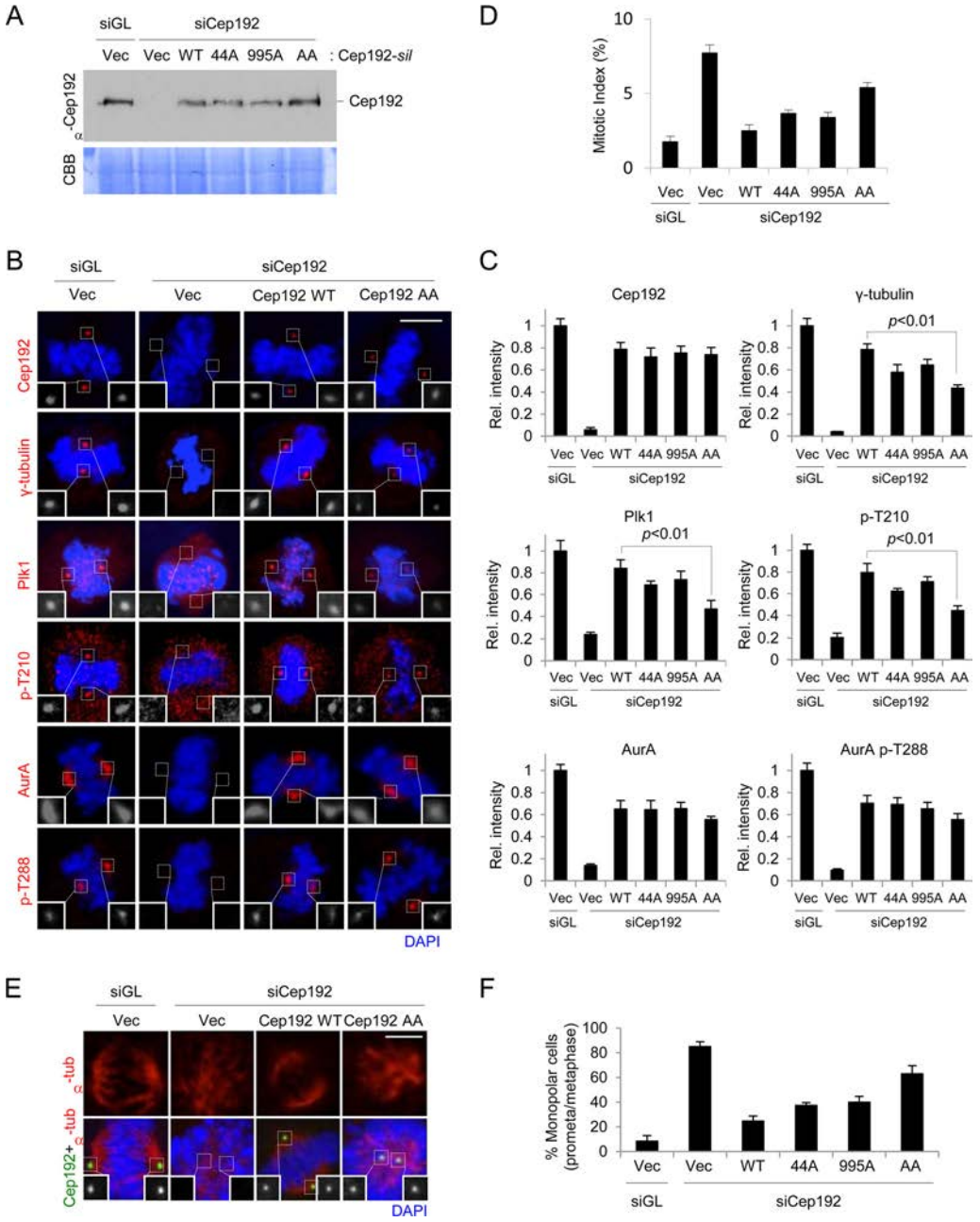

FIG 7 Additive defect of the T44A and S995A mutations in the recruitment of γ-tubulin and the establishment of bipolar spindles. (A) Immunoblotting was carried out for U2OS cells stably expressing RNAi-insensitive Cep192 (Cep192-*sil*) constructs and depleted of endogenous Cep192. CBB, Coomassie brilliant blue. (B to F) The resulting cells from panel A were immunostained (B and E) with the appropriate antibodies, and the fluorescent signal intensities (C) ($n \geq 20$ per sample), numbers of mitotic cells (D) ($n \geq 4{,}000$ per each sample), and numbers of cells with monopolar spindles (E and F) ($n \geq 45$ per each sample) were quantified. Bars, 5 μm (B and E). Error bars in panels C, D, and F indicate standard deviations. 44A, T44A mutant; 995A, S995A mutant; AA, T44A S995A double mutant.

favors the T44 motif-dependent Plk1 interaction. Interestingly, the defect associated with the impairment of T44- and S995-dependent functions appeared to be additive (Fig. 7; also see below). Thus, we propose that the bimodal interactions between Cep192 and Plk1 ultimately lead to the formation of two distinct Cep192-Plk1 complexes that function in parallel pathways to recruit downstream components, such as the γ-TuRC (Fig. 8). In this view, the bimodal formation of the Cep192-Plk1 complex may serve as a crucial step for providing versatility in Plk1-dependent downstream events. As with the importance of the biomodal nature of the Cep192-Plk1 interaction, both the T44 and S995 residues are highly conserved among vertebrates (Fig. 4C).

Then how are the p-T44 and p-S995 epitopes generated on Cep192? We observed that Plk1 expression efficiently induced the p-T44 epitope in the presence of AurA (Fig. 6D), whereas Plk1 inhibition almost completely abolished it (Fig. 6B). These findings

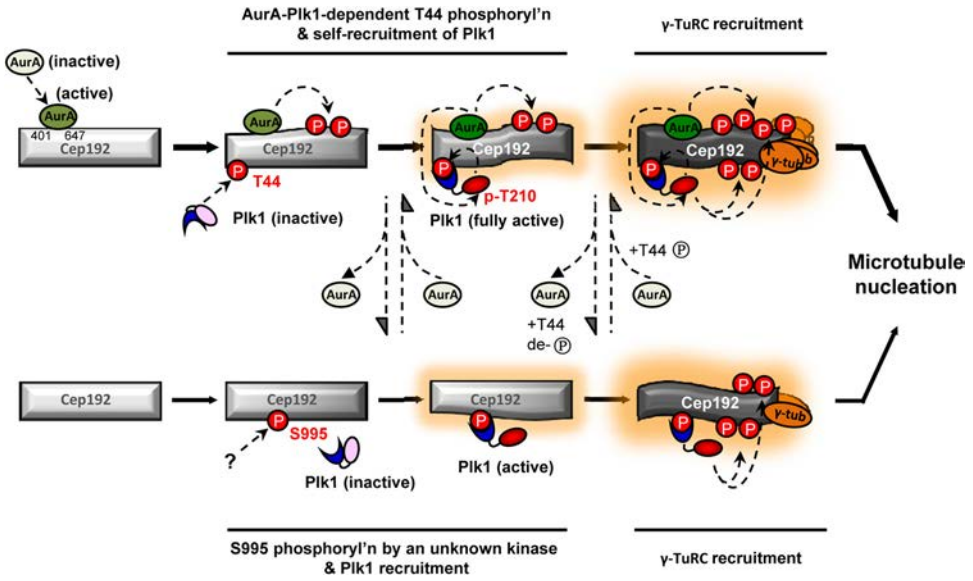

FIG 8 Model illustrating the formation of the AurA-dependent Cep192 p-T44-Plk1 complex and the AurA-independent Cep192 p-S995-Plk1 complex and the regulation of MT nucleation by these complexes. During interphase, AurA binds to the region of Cep192 spanning residues 401 to 647 and becomes activated at centrosomes. In the presence of AurA binding, Plk1 preferentially phosphorylates and interacts with the T44 motif of Cep192 through the "self-priming and binding" mechanism (31, 32). The formation of the Cep192-AurA-Plk1 ternary complex allows efficient AurA-dependent Plk1 activation. Plk1 also reciprocally activates AurA, presumably by phosphorylating Cep192 and enhancing the Cep192-AurA interaction, thus creating a positive feedback loop to further potentiate Cep192-AurA-Plk1-mediated γ-tubulin recruitment and bipolar spindle formation. In the absence of AurA binding to Cep192 (considering a strong interaction between Cep192 and AurA, a minor fraction of Cep192 could be free of AurA at centrosomes), Plk1 binds to the p-S995 motif generated by an unknown kinase and promotes γ-tubulin recruitment and bipolar spindle formation. The resulting Cep192-Plk1 complex may function as a trigger of downstream events (thin arrows) or serve as an intermediate subcomplex for the formation of the Cep192-AurA-Plk1 ternary complex with available AurA. The ternary complex may also revert back to the Cep192-Plk1 binary complex upon AurA dissociation and p-T44 dephosphorylation. Notably, the AurA-Plk1-dependent production of the p-T44 epitope is independent of S995 phosphorylation, while the production of the p-S995 epitope is independent of AurA, Plk1, and T44 phosphorylation. In line with these observations, the loss of both T44- and S995-dependent Cep192-Plk1 interactions induces an additive defect in γ-tubulin recruitment and bipolar spindle formation.

suggest that Cep192-bound AurA, which presumably induces a conformational change in Cep192 through phosphorylation, allows Plk1 to "self-prime" the T44 residue and bind to the resulting p-T44 epitope, thus generating a Cep192-AurA-Plk1 ternary complex (Fig. 8). Contrary to these findings, the mechanism of how the p-S995 epitope is generated remains puzzling at present. Our results showed that although AurA inhibition greatly diminished the level of the p-S995 epitope, AurA expression failed to increase it at all (Fig. 6). Consistent with these results, we found that the primary sequence of the S995 motif does not conform to the canonical AurA consensus phosphorylation site [(K/R)XX(S/T), where X is any residue] (30). Identification of the kinase responsible for generating the p-S995 epitope will be very important for a better understanding of the mechanism underlying the formation of an AurA-independent Cep192-Plk1 complex.

Physiological significance of T44- and S995-dependent Cep192-Plk1 interactions. Prior to mitotic entry, centrosomes recruit various components of the pericentriolar material, including MT-nucleating factors such as the γ-TuRC. This process, called centrosome maturation, is critical for the proper establishment of bipolar spindles during mitosis. Data obtained from studies with various organisms suggest that Plk1 and AurA, and their orthologs, play an important role in this process (5–9). Recently, Cep192 has been proposed to function as an important centrosomal scaffold that promotes centrosome maturation and bipolar spindle formation (4). Subsequent studies with *Xenopus* egg extracts have shown that an xCep192-organized xAurA-Plx1 cascade promotes γ-TuRC recruitment and MT assembly (9).

The molecular mechanisms of how human Cep192 assembles functional complexes with AurA and Plk1 and how the formation of these complexes is regulated are beginning to emerge. Our data showed that the impairment of T44- and S995-dependent Cep192-Plk1 interactions induced additive defects in Plk1 recruitment and activation, γ-tubulin recruitment, and bipolar spindle formation (Fig. 7). These observations suggest that T44- and S995-dependent Cep192-Plk1 interactions function in parallel to promote Plk1-dependent biochemical and cellular processes that are important for bipolar spindle establishment (Fig. 8). Given that AurA efficiently binds to Cep192, as shown in Fig. 2A, the Cep192-Plk1 complex, which preferably forms in the absence of AurA, could serve as an intermediate subcomplex that facilitates the rapid reassembly of the Cep192-AurA-Plk1 ternary complex. However, we cannot exclude the possibility that the Cep192-AurA-Plk1 complex disassembles via AurA dissociation and p-T44 dephosphorylation to regenerate the Cep192-Plk1 binary complex (Fig. 8). In this regard, perhaps the intricate regulation of the two Plk1-bound states (i.e., Cep192-AurA-bound and Cep192-bound states) could be important in helping to maintain the proper levels of Cep192-associated Plk1 and, consequently, Plk1-mediated MT nucleation at centrosomes. A deeper understanding of how the Cep192-Plk1 interaction is regulated during the cell cycle and how this interaction promotes the recruitment of γ-tubulin to centrosomes will be critical for providing new insights into the mechanism of centrosome maturation and bipolar spindle formation at the time of mitotic entry.

ACKNOWLEDGMENTS

We are grateful to Michael B. Yaffe and Gerd Pfeifer for reagents and Susan Garfield for technical assistance in microscopy.

This work was supported in part by National Cancer Institute intramural grants (K.S.L.) and Korea Basic Science Institute grant T33418 (J.K.B.).

REFERENCES

1. **Lawo S, Hasegan M, Gupta GD, Pelletier L.** 2012. Subdiffraction imaging of centrosomes reveals higher-order organizational features of pericentriolar material. Nat Cell Biol **14:**1148–1158. http://dx.doi.org/10.1038/ncb2591.
2. **Park SY, Park JE, Kim TS, Kim JH, Kwak MJ, Ku B, Tian L, Murugan RN, Ahn M, Kim BY, Bang JK, Kim SJ, Oh BH, Erikson RL, Yang W, Lee KS.** 2014. Molecular basis for unidirectional scaffold switching of Plk4 in centriole biogenesis. Nat Struct Mol Biol **21:**696–703. http://dx.doi.org/10.1038/nsmb.2846.
3. **Sonnen KF, Schermelleh L, Leonhardt H, Nigg EA.** 2012. 3D-structured illumination microscopy provides novel insight into architecture of human centrosomes. Biol Open **1:**965–976. http://dx.doi.org/10.1242/bio.20122337.
4. **Gomez-Ferreria MA, Rath U, Buster DW, Chanda SK, Caldwell JS, Rines DR, Sharp DJ.** 2007. Human Cep192 is required for mitotic centrosome and spindle assembly. Curr Biol **17:**1960–1966. http://dx.doi.org/10.1016/j.cub.2007.10.019.
5. **Berdnik D, Knoblich JA.** 2002. Drosophila Aurora-A is required for centrosome maturation and actin-dependent asymmetric protein localization during mitosis. Curr Biol **12:**640–647. http://dx.doi.org/10.1016/S0960-9822(02)00766-2.
6. **Hannak E, Kirkham M, Hyman AA, Oegema K.** 2001. Aurora-A kinase is required for centrosome maturation in Caenorhabditis elegans. J Cell Biol **155:**1109–1116. http://dx.doi.org/10.1083/jcb.200108051.
7. **Dutertre S, Descamps S, Prigent C.** 2002. On the role of aurora-A in centrosome function. Oncogene **21:**6175–6183. http://dx.doi.org/10.1038/sj.onc.1205775.
8. **Lane HA, Nigg EA.** 1996. Antibody microinjection reveals an essential role for human polo-like kinase 1 (Plk1) in the functional maturation of mitotic centrosomes. J Cell Biol **135:**1701–1713. http://dx.doi.org/10.1083/jcb.135.6.1701.
9. **Joukov V, Walter JC, De Nicolo A.** 2014. The Cep192-organized aurora A-Plk1 cascade is essential for centrosome cycle and bipolar spindle assembly. Mol Cell **55:**578–591. http://dx.doi.org/10.1016/j.molcel.2014.06.016.
10. **Joukov V, De Nicolo A, Rodriguez A, Walter JC, Livingston DM.** 2010. Centrosomal protein of 192 kDa (Cep192) promotes centrosome-driven spindle assembly by engaging in organelle-specific Aurora A activation. Proc Natl Acad Sci U S A **107:**21022–21027. http://dx.doi.org/10.1073/pnas.1014664107.
11. **Macùrek L, Lindqvist A, Lim D, Lampson MA, Klompmaker R, Freire R, Clouin C, Taylor SS, Yaffe MB, Medema RH.** 2008. Polo-like kinase-1 is activated by aurora A to promote checkpoint recovery. Nature **455:**119–123. http://dx.doi.org/10.1038/nature07185.
12. **Seki A, Coppinger JA, Jang CY, Yates JR, Fang G.** 2008. Bora and the kinase Aurora a cooperatively activate the kinase Plk1 and control mitotic entry. Science **320:**1655–1658. http://dx.doi.org/10.1126/science.1157425.
13. **Chen C, Okayama H.** 1987. High-efficiency transformation of mammalian cells by plasmid DNA. Mol Cell Biol **7:**2745–2752.
14. **Kim TS, Park JE, Shukla A, Choi S, Murugan RN, Lee JH, Ann M, Rhee K, Bang JK, Kim BY, Loncarek J, Erikson RL, Lee KS.** 2013. Hierarchical recruitment of Plk4 and regulation of centriole biogenesis by two centrosomal scaffolds, Cep192 and Cep152. Proc Natl Acad Sci U S A **110:**E4849–E4857. http://dx.doi.org/10.1073/pnas.1319656110.
15. **Lee KS, Yuan YL, Kuriyama R, Erikson RL.** 1995. Plk is an M-phase-specific protein kinase and interacts with a kinesin-like protein, CHO1/MKLP-1. Mol Cell Biol **15:**7143–7151.
16. **Kang YH, Park JE, Yu LR, Soung NK, Yun SM, Bang JK, Seong YS, Yu H, Veenstra TD, Lee KS.** 2006. Self-regulation of Plk1 recruitment to the kinetochores is critical for chromosome congression and spindle checkpoint signaling. Mol Cell **24:**409–422. http://dx.doi.org/10.1016/j.molcel.2006.10.016.
17. **Yun SM, Moulaei T, Lim D, Bang JK, Park JE, Shenoy SR, Liu F, Kang YH, Liao C, Soung NK, Lee S, Yoon DY, Lim Y, Lee DH, Otaka A, Appella E, McMahon JB, Nicklaus MC, Burke TRJ, Yaffe MB, Wlodawer A, Lee KS.** 2009. Structural and functional analyses of minimal phosphopeptides targeting the polo-box domain of polo-like kinase 1. Nat Struct Mol Biol **16:**876–882. http://dx.doi.org/10.1038/nsmb.1628.
18. **Elia AE, Rellos P, Haire LF, Chao JW, Ivins FJ, Hoepker K, Mohammad D, Cantley LC, Smerdon SJ, Yaffe MB.** 2003. The molecular basis for phospho-dependent substrate targeting and regulation of Plks by the polo-box domain. Cell **115:**83–95. http://dx.doi.org/10.1016/S0092-8674(03)00725-6.
19. **Bayliss R, Sardon T, Vernos I, Conti E.** 2003. Structural basis of Aurora-A activation by TPX2 at the mitotic spindle. Mol Cell **12:**851–862. http://dx.doi.org/10.1016/S1097-2765(03)00392-7.
20. **Golsteyn RM, Mundt KE, Fry AM, Nigg EA.** 1995. Cell cycle regulation of the activity and subcellular localization of Plk1, a human protein kinase implicated in mitotic spindle function. J Cell Biol **129:**1617–1628. http://dx.doi.org/10.1083/jcb.129.6.1617.
21. **Haren L, Stearns T, Lüders J.** 2009. Plk1-dependent recruitment of gamma-tubulin complexes to mitotic centrosomes involves multiple PCM components. PLoS One **4:**e5976. http://dx.doi.org/10.1371/journal.pone.0005976.
22. **Walter AO, Seghezzi W, Korver W, Sheung J, Lees E.** 2000. The mitotic serine/threonine kinase Aurora2/AIK is regulated by phosphorylation and degradation. Oncogene **19:**4906–4916. http://dx.doi.org/10.1038/sj.onc.1203847.
23. **Lee KS, Erikson RL.** 1997. Plk is a functional homolog of *Saccharomyces cerevisiae* Cdc5, and elevated Plk activity induces multiple septation structures. Mol Cell Biol **17:**3408–3417.
24. **Hutterer A, Berdnik D, Wirtz-Peitz F, Zigman M, Schleiffer A, Knoblich JA.** 2006. Mitotic activation of the kinase Aurora-A requires its binding partner Bora. Dev Cell **11:**147–157. http://dx.doi.org/10.1016/j.devcel.2006.06.002.
25. **Wysocka J, Liu Y, Kobayashi R, Herr W.** 2001. Developmental and cell-cycle regulation of Caenorhabditis elegans HCF phosphorylation. Biochemistry **40:**5786–5794. http://dx.doi.org/10.1021/bi010086o.
26. **Görgün G, Calabrese E, Hideshima T, Ecsedy J, Perrone G, Mani M, Ikeda H, Bianchi G, Hu Y, Cirstea D, Santo L, Tai YT, Nahar S, Zheng M, Bandi M, Carrasco RD, Raje N, Munshi N, Richardson P, Anderson KC.** 2010. A novel Aurora-A kinase inhibitor MLN8237 induces cytotoxicity and cell-cycle arrest in multiple myeloma. Blood **115:**5202–5213. http://dx.doi.org/10.1182/blood-2009-12-259523.
27. **Harrington EA, Bebbington D, Moore J, Rasmussen RK, Ajose-Adeogun AO, Nakayama T, Graham JA, Demur C, Hercend T, Diu-Hercend A, Su M, Golec JM, Miller KM.** 2004. VX-680, a potent and selective small-molecule inhibitor of the Aurora kinases, suppresses tumor growth in vivo. Nat Med **10:**262–267. http://dx.doi.org/10.1038/nm1003.
28. **Lenart P, Petronczki M, Steegmaier M, Di Fiore B, Lipp JJ, Hoffmann M, Rettig WJ, Kraut N, Peters JM.** 2007. The small-molecule inhibitor BI 2536 reveals novel insights into mitotic roles of polo-like kinase 1. Curr Biol **17:**304–315. http://dx.doi.org/10.1016/j.cub.2006.12.046.
29. **Seong YS, Min C, Li L, Yang JY, Kim SY, Cao X, Kim K, Yuspa SH, Chung HH, Lee KS.** 2003. Characterization of a novel cyclin-dependent kinase 1 inhibitor, BMI-1026. Cancer Res **63:**7384–7391.
30. **Ferrari S, Marin O, Pagano MA, Meggio F, Hess D, El-Shemerly M, Krystyniak A, Pinna LA.** 2005. Aurora-A site specificity: a study with synthetic peptide substrates. Biochem J **390:**293–302. http://dx.doi.org/10.1042/BJ20050343.
31. **Lee KS, Park JE, Kang YH, Zimmerman W, Soung NK, Seong YS, Kwak SJ, Erikson RL.** 2008. Mechanisms of mammalian polo-like kinase 1 (Plk1) localization: self- versus non-self-priming. Cell Cycle **7:**141–145. http://dx.doi.org/10.4161/cc.7.2.5272.
32. **Park JE, Soung NK, Johmura Y, Kang YH, Liao C, Lee KH, Park CH, Nicklaus MC, Lee KS.** 2010. Polo-box domain: a versatile mediator of polo-like kinase function. Cell Mol Life Sci **67:**1957–1970. http://dx.doi.org/10.1007/s00018-010-0279-9.

OPEN

Citation: Cell Death Discovery (2015) 1, 15060; doi:10.1038/cddiscovery.2015.60

www.nature.com/cddiscovery

ARTICLE

p53 Configures the G2/M arrest response of nucleostemin-deficient cells

G Huang[1,2,4], L Meng[1,4] and RYL Tsai[1,3]

Nucleostemin (NS) protects the genome from replication-induced DNA damage and has an indispensable role in maintaining the continuous proliferation of both p53-wild-type and mutant cells. Yet, some outcomes of NS-deficient cells appear to be shaped by their p53 status, which stimulates conflicting claims on the role of p53 in executing the NS function. This disparity was conveniently attributed to the usual suspect of cell-type variations. To provide a definitive resolution, we investigated the interplay between NS and p53 in two pairs of isogenic cells, that is, genetically modified mouse embryonic fibroblast (MEF) cells and HCT116 human colon cancer cells. In MEF cells, p53 deletion further compromises rather than rescues the proliferative potential of NS-depleted cells without changing their G2/M arrest fate before prophase entry. The detrimental effect of p53 loss in NS-depleted MEF cells correlates with a dramatic increase of polyploid giant cells (PGCs) (up to 24%), which indicates aberrant mitosis. To determine how p53 shapes the response of cells to NS depletion at the molecular level, we showed that p53 turns on the expression of reprimo and MDM2 in NS-deficient MEF cells. In absence of p53, NS-deficient MEF cells exhibit increased levels of phosphorylated cdc2 (Y15) protein and cyclin B1. In cancer (HCT116) cells, NS loss leads to G2/M arrest under both p53wt and p53ko conditions and increases phosphorylated cdc2 more in p53ko than in p53wt cells, as it does in MEF cells. Unlike its effect in MEF cells, NS depletion decreases tumor growth and increases the expression of reprimo and cyclin B1 in a p53-independent manner in HCT116 cells. Our data indicate that the p53 status of NS-deficient cells orchestrates how they respond to G2/M arrest in a normal *versus* cancer cell distinct fashion.

Cell Death Discovery (2015) **1,** 15060; doi:10.1038/cddiscovery.2015.60; published online 23 November 2015

INTRODUCTION

Mammalian nucleostemin (NS) was first discovered as a gene more abundantly expressed by embryonic neural stem cells than their progeny[1] and later found to be highly enriched in many stem cell types and cancer cells.[1–6] The importance of NS has been unequivocally shown in several biological events of fundamental significance, including blastocyst formation,[7,8] embryogenesis,[9] postnatal tissue regeneration,[10,11] cancer development,[5,6,12] and reprogramming to pluripotency.[13] The majority of NS protein is stored in the nucleolus but takes action outside the nucleolus via a GTP-controlled shuttling mechanism.[14,15]

Earlier studies indicated that NS (mostly that of the mammal) and its paralogue is physically associated with MDM2 and functionally linked to p53 inactivation.[1,16–19] If the MDM2-p53 regulation represents a major target of NS action, one may logically infer that p53 loss should partially or completely reverse the detrimental outcome of NS deletion. Yet, several studies have demonstrated that NS remains indispensable for the survival and continuous proliferation of p53-null normal or cancer cells.[8,9,20] We recently discovered a key role of NS in reducing the amount of DNA damage accumulated during the S phase.[4,9,11,21] In accord with the p53 independency of NS, deletion of NS leads to DNA damage to the same extent in p53-wild-type (p53wt) MEF cells as in p53-null (p53ko) cells.[9] Based on the evidence reported so far,[22] we believe that the essential function of NS is best captured by its genome-protective activity, whereas its MDM2 regulatory function occurs mainly in the context of mitosis or nucleolar stress, when the NS protein is released *en masse* from the nucleolus to the nucleoplasm.

This model, however, does not preclude the possibility that p53 may still be involved in guiding the ensuing events after NS depletion. Indeed, we found that the growth of NS-deficient MEF cells becomes more severely prohibited without p53 than with p53.[9] This paradoxical finding certainly refutes the idea that the obligatory function of NS depends on p53 inhibition, but more importantly it supports that the p53 status may influence how cells respond to NS depletion. To date, it is not entirely clear how exactly the outcome of NS-deficient cells is shaped by their p53 status, considering the many genetic variations that exist between the difference cell models used in different studies. To overcome this challenge, we used two pairs of isogenic cell models to understand the interplay between NS and p53 perturbation. Our findings provide new insight into how p53 may shape the response of NS-deficient cells to G2/M arrest.

RESULTS

Loss of p53 aggravates the already diminished proliferation of NS-depleted MEF cells

To determine how p53 regulates the NS-knockdown (NSkd) response of normal cells, we created a tamoxifen (TAM)-inducible NS^{cko} mouse model (inNS^{cko}) by introducing the Cre^{ER} transgene [23] into $NS^{flx/flx}$ mice[9] and then bred inNS^{cko} and $NS^{flx/flx}$ mice into the p53ko background.[24] MEF cells were harvested from E13.5

[1]Institute of Biosciences and Technology, Texas A&M University Health Science Center, Houston, TX, USA; [2]Department of General Surgery, The Fifth Affiliated Hospital of Guangzhou Medical University, Guangzhou 510700, China and [3]Department of Molecular and Cellular Medicine, Texas A&M University Health Science Center, College Station, TX, USA.
Correspondence: RYL Tsai (rtsai@ibt.tamhsc.edu)
[4]These authors contribute equally to this work.
Received 5 October 2015; revised 20 October 2015; accepted 25 October 2015; Edited by AE Sayan

mouse embryos of four genetic backgrounds, i.e. $NS^{flx/flx}$-p53wt, $inNS^{cko}$-p53wt, $NS^{flx/flx}$-p53ko, and $inNS^{cko}$-p53ko, and cultured on a 3- day-passage schedule with or without 0.1 μM TAM. Western blots confirmed a specific decrease of NS protein in TAM-treated $inNS^{cko}$ cells compared with DMSO-treated $inNS^{cko}$ cells or TAM-treated $NS^{flx/flx}$ cells (Supplementary Figure S1a). The proliferative potentials of NS- and/or p53-perturbed MEF cells were determined by calculating the average daily cell expansion ratio during the 3-day period of each passage. TAM-induced NS loss decreases the proliferative potential of p53wt MEF cells by 30–40% in early passages (P1–P4) (Figure 1a). This growth-inhibitory effect of NS loss becomes indiscernible when cells enter late passages (P5–P6). Interestingly, loss of p53 increases the proliferative potential of control MEF cells ($NS^{flx/flx}$ with/without TAM and $inNS^{cko}$ without TAM) but reduces the proliferative potential of NS-depleted MEF cells ($inNS^{cko}$ with TAM) (Figure 1b). This paradoxical effect of p53 deletion on control *versus* NS-deficient MEF cells becomes more evident as the passage number increases from P1 to P4 (Supplementary Figure S1b). These findings indicate that p53wt MEF cells have a higher dependency on NS at early passages than late passages, whereas p53-null MEF cells are progressively more sensitive to the anti-proliferative effect of NSkd at later passages.

NS-deficient MEF cells arrest in the G2/M phase regardless of their p53 status

To determine whether the cell cycle outcome of NS-depleted MEF cells depends on p53, we treated P2 MEF cells with or without TAM (0.1 μM) for 4 days and analyzed their cell cycle profiles. Propidium iodide (PI)-labeled studies showed that TAM-induced NS depletion in p53wt MEF cells ($inNS^{cko}$+TAM) causes a slight decrease in G1 cells and an increase in G2/M and sub-G1 (3–4%) cells (Figure 2a1). This profile indicates a G2/M arrest and is consistent with a partial NSkd effect seen in MDA-MB-231 breast cancer cells.[25] In p53ko MEF cells, NS depletion also results in a G2/M arrest phenotype and a sub-G1 cell increase (~12%) (Figure 2a2). To determine whether NS-depleted cells were checked in the G2 or M phase, we quantified the percentages of MEF cells in the mitotic prophase, metaphase, anaphase, and telophase by their expression of phosphorylated histone H3 (pH3) at serine 10, which occurs exclusively during mitosis in mammalian cells.[26,27] In p53wt MEF cells, decreases in the prophase, metaphase, anaphase, and telophase cells were specifically noted in the TAM-treated $inNS^{cko}$ cells compared with the controls (Figure 2b1). In p53ko MEF cells, the same defect in prophase entry occurs following NS depletion (Figure 2b2). These results indicate that a partial loss of NS results in G2 arrest before mitotic entry and that this event occurs regardless of the p53 status.

Loss of p53 leads to a dramatic increase of PGCs in NS-depleted MEF cells

The slight difference in the degree of G2/M arrest between p53wt-NSkd and p53ko-NSkd cells does not match the major disparity of their proliferative potentials. To search for what might account for the p53ko-aggravated effect in NS-depleted cells, we determined the percentages of senescent cells in P3 MEF cells by SA-β-Gal staining and found that NS depletion does not increase SA-β-Gal^+ cells in the presence of p53 but does so in the absence of p53. However, the increase of SA-β-Gal^+ cells by NSkd in p53ko cells only amounts to $< 1\%$ of the total cells (data not shown), which hardly matches the scale of the decrease in cell proliferation. In contrast, DAPI staining revealed that 24% of the NSkd-p53ko MEF cells show abnormal giant nuclear morphology, which is significantly more abundant than that of NSkd-p53wt cells (1.5%) or NS-wild-type cells ($< 0.5\%$) (Figure 3a). Many abnormal giant cells are associated with small satellite nuclei or lobulated nuclei. PI-labeled flow cytometry confirmed a significant increase of polyploid cells (8 N and 16 N) in NSkd-p53ko MEF cells (Figure 3b). These results indicate that p53 deletion precipitates the frequency of mitotic aberration and the formation of PGCs in NSkd MEF cells.

NS depletion elicits distinct molecular responses in p53ko and p53wt MEF cells

Entry into the M phase is driven by the dephosphorylation of phosphorylated cdc2 and a surge of cyclin B1. Dephosphorylation of cdc2 is triggered by nuclear translocation of cdc25C phosphatase. To gain insight into how p53 regulates the mitotic blockage of NSkd cells, we first measured the level of phosphorylated cdc2 (Tyr15) in response to NS deletion. Our results showed that NS depletion increases the amount of phosphorylated cdc2 protein in p53ko MEF cells but not in p53wt cells (Figure 4a), suggesting that p53 may direct NS-deficient cells toward a G2/M arrest pathway different from that of p53ko cells. To identify the potential targets of p53, we used the quantitative RT-PCR assay to measure the transcript levels of several gene products involved in G1/S arrest, G2/M arrest, apoptosis, or p53 feedback control. We first confirmed that TAM treatment decreases NS transcripts by 74% in p53wt cells and by $> 90\%$ in p53ko cells (Figure 4b). The amounts of several G1/S regulators, including cyclin E1, cyclin A2, and $p27^{kip}$, show no NS-dependent changes in either p53wt or p53ko cells, whereas $p21^{cip}$ is increased only in p53wt cells in a TAM-dependent but NS-independent manner (Figure 4b). Compared with p53wt cells, the baseline levels of cyclin A2 and $p27^{kip}$ in p53ko cells are higher, regardless of their NS status, and their baseline level of $p21^{cip}$ is lower (Figure 4b, gray asterisks). For genes that regulate

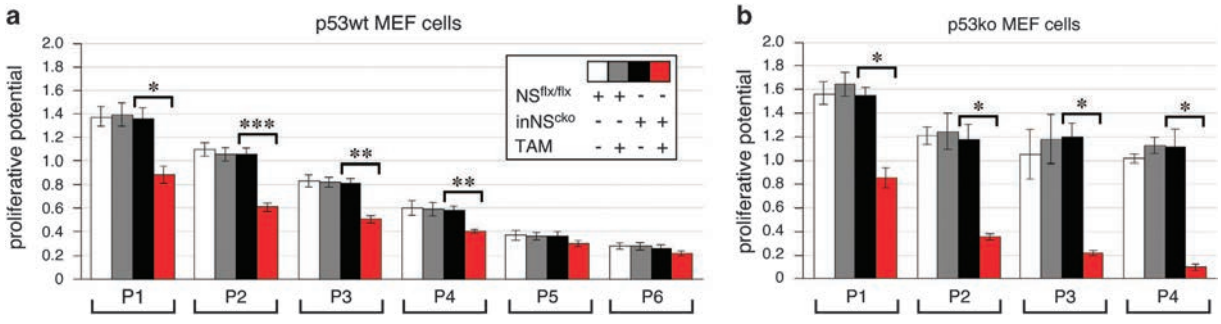

Figure 1. Loss of p53 decreases the proliferative potential of NS-depleted mouse embryonic fibroblast (MEF) cells. MEF cells were prepared from $NS^{flx/flx}$ or $inNS^{cko}$ embryos in the p53-wild-type (p53wt) (**a**) or p53-null (p53ko) (**b**) background and treated with 0.1 μM tamoxifen (TAM) or DMSO from passage 1 (P1) to P4–P6. The proliferative potential was determined as the average daily cell expansion ratio during each passage. Bars and error bars represent the average and s.e.m. $^*P \leqslant 0.01$, $^{**}P \leqslant 0.001$ and $^{***}P \leqslant 0.0001$.

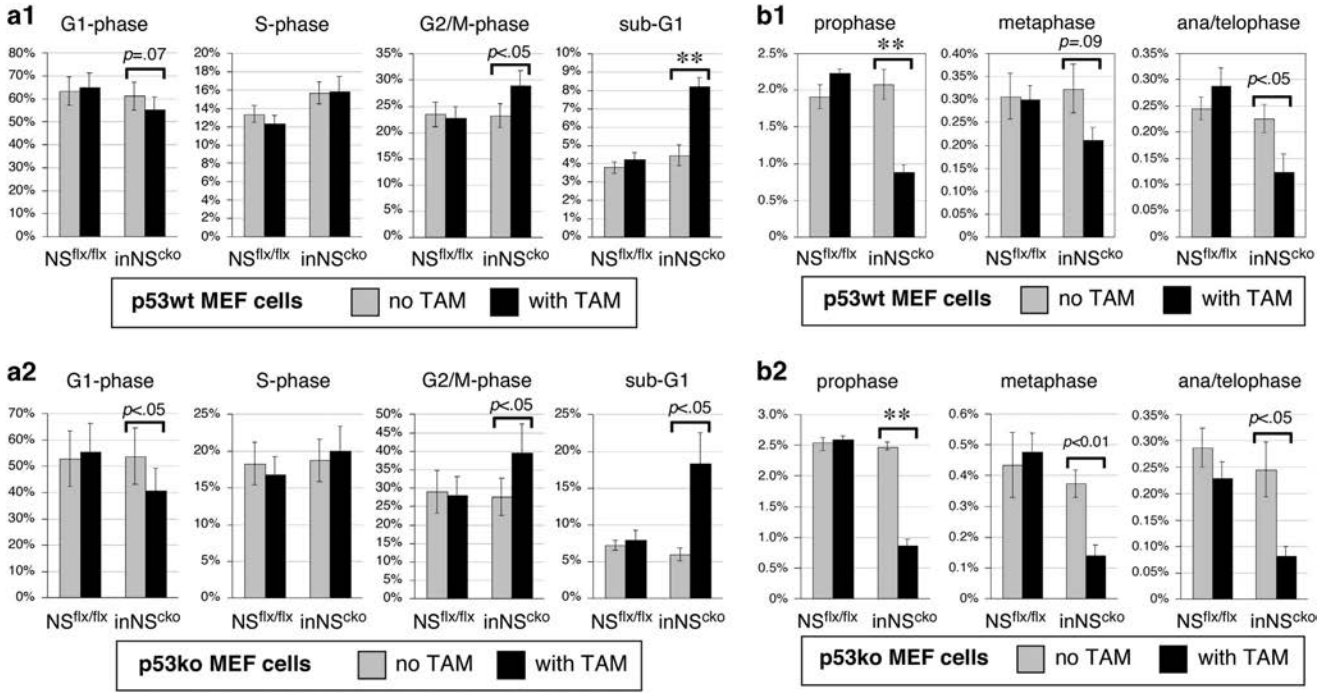

Figure 2. NS depletion triggers G2/M arrest in both p53wt and p53ko MEF cells.(**a**) MEF cells derived from $NS^{flx/flx}$ or $inNS^{cko}$ embryos in the p53wt or p53ko background were treated with DMSO (gray bars) or TAM (0.1 μM, black bars) for 4 days at P2 and analyzed by propidium iodide (PI)-labeled flow cytometry. The averages for p53wt cells ($n = 9$) and p53ko cells ($n = 4$) were shown in (**a1**) and (**a2**), respectively. (**b**) The percentages of prophase, metaphase, anaphase, and telophase cells were quantified by anti-pH3 staining in p53wt (**b1**) and p53ko (**b2**) MEF cells from eight experiments. See Figure 1 for description regarding error bars and asterisks.

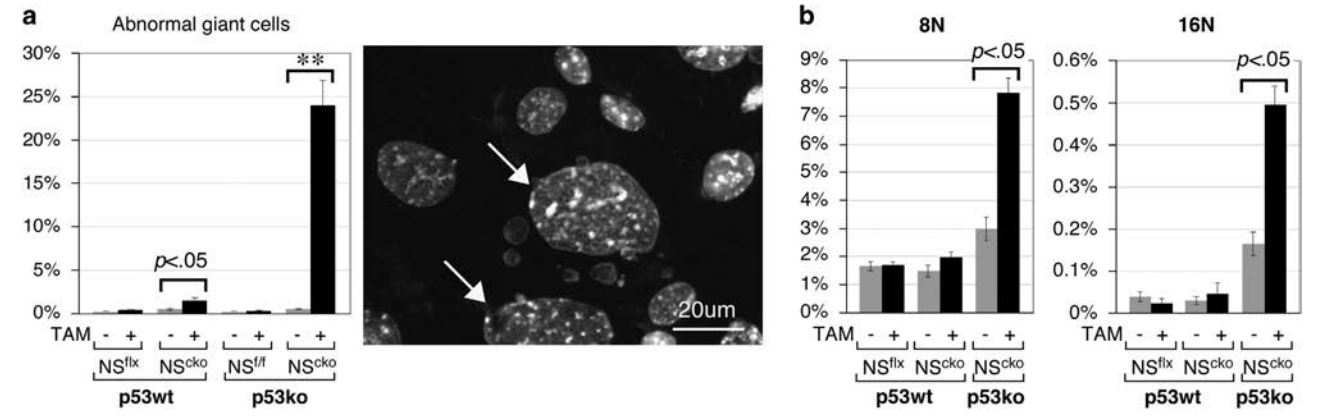

Figure 3. Deletion of p53 enhances polyploid giant cell formation in NS-depleted MEF cells. (**a**) DAPI staining reveals a dramatic increase in cells with an abnormal giant nuclear morphology (nuclear diameter $\geqslant 40\,\mu$m) in NS-p53 double-knockout MEF cells (P3). (**b**) The amounts of polyploid cells (8 N and 16 N) in P2 MEF cells were measured by PI-labeled flow cytometry. $NS^{flx/flx}$ and $inNS^{cko}$ are represented by NS^{flx} and NS^{cko}, respectively. See Figure 1 for description regarding error bars and asterisks.

the G2/M transition, we found that NS loss increases the transcript levels of cdc2 and cyclin B1 only in p53ko cells, but increases the level of reprimo only in p53wt cells (Figure 4c). Compared with p53wt cells, p53ko cells express a higher baseline level of cdc2, cyclin B1, and cdc25C and a lower baseline level of cyclin G1. In addition, NS deletion increases the level of MDM2 only in p53wt cells and the levels of Bax and p63 in both p53wt and p53ko cells (Figure 4d). These results identify p53-dependent *versus* independent changes following NS loss. Specifically, NS depletion upregulates the expression of reprimo and MDM2 in p53wt MEF cells, the levels of phosphorylated cdc2 and cyclin B1 in p53ko cells, and the expression of Bax and p63 in both p53wt and p53ko cells.

Loss of NS blocks both HCT116-8 and HCT116-2 cells at G2/M and reduces their clonogenic survival

p53 mutation is commonly seen in human cancer. We used two isogenic human colorectal cancer cells, HCT116-8 (p53wt) and HCT116-2 (p53ko) cells, to determine how p53 influences the clonogenic survival and cell cycle arrest phenotype of NS-depleted cancer cells. We first showed that siNS treatment reduces NS protein comparably in HCT116-8 and HCT116-2 cells (Figure 5a, left panel). NSkd by siNS decreases the survival of both p53wt and p53ko HCT116 cells (Figure 5a, right panel). Unlike MEF cells, loss of p53 does not further compromise the survival of HCT116 cancer cells, if not slightly improves it (Figure 5a). Cell cycle profile analyses showed that NS depletion decreases the G1 cell

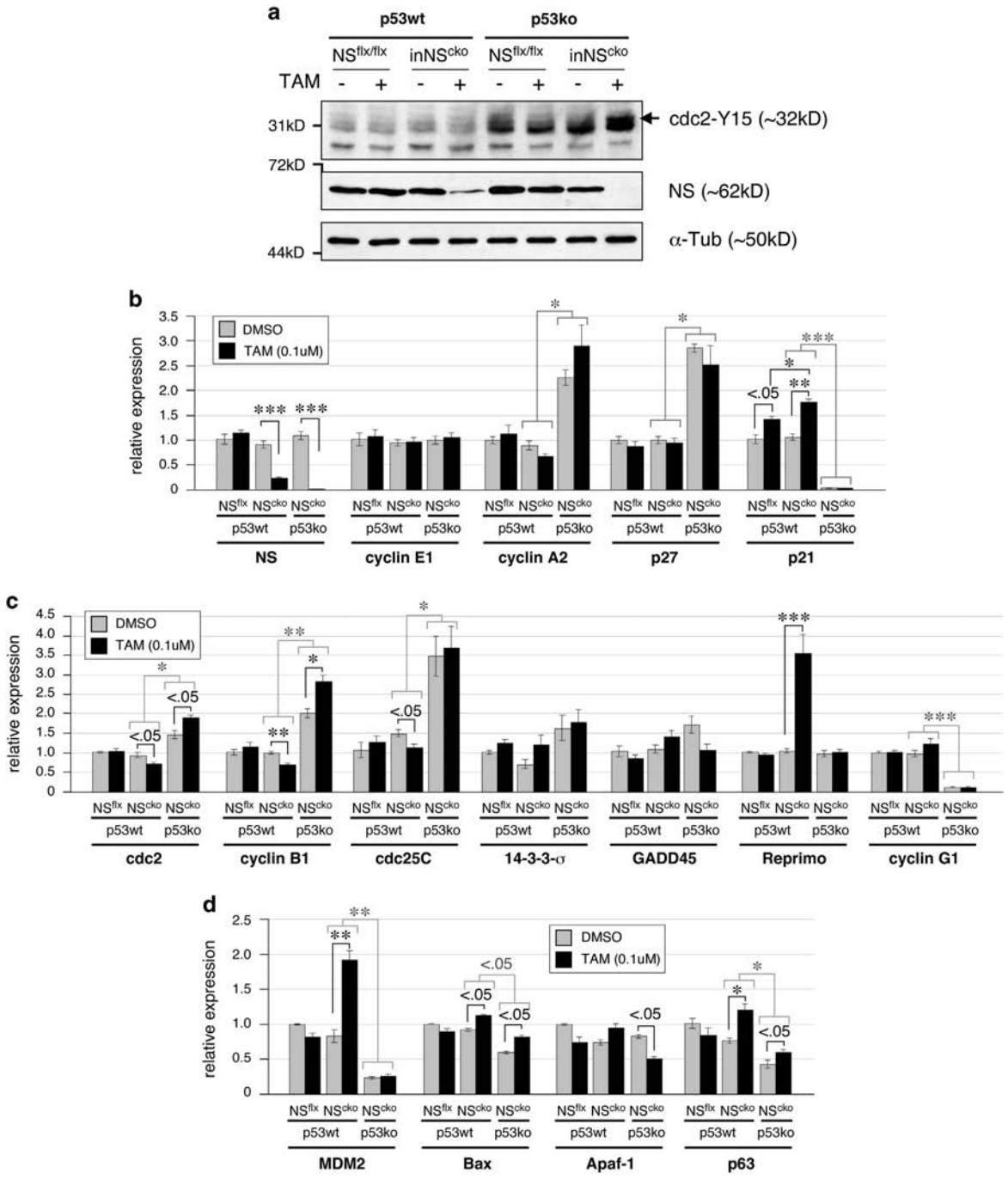

Figure 4. Molecular responses to NS depletion in p53wt and p53ko MEF cells. MEF cells were prepared from four genetic models. P2 cells were treated with DMSO (gray bars) or TAM (0.1 μM, black bars) for 4 days and collected for western blotting (**a**) or quantitative RT-PCR analyses (**b**–**d**). The levels of gene products that are involved in G1/S control (**b**), G2/M control (**c**), apoptosis, and feedback regulation of p53 (**d**) were measured by qRT-PCR ($n=6$). See Figure 1 for description regarding error bars and asterisks.

percentage and increases the G2/M cell percentage in both HCT116-8 and HCT116-2 cells to similar extents (Figure 5b). We also observed an increase in the S-phase cell percentage in HCT116-2 cells but no significant increase in the sub-G1 cell percentage in either cell type following NSkd.

Molecular responses of p53wt and p53ko cancer cells to NS depletion

To determine whether p53 modulates the response of cancer cells to NSkd-induced G2/M arrest in the same way as it does in MEF cells, we analyzed the molecular responses of HCT116 cells to NSkd by qRT-PCR. The results showed that the baseline level of NS is two times higher in HCT116-8 cells than in HCT116-2 cells but the relative NSkd efficiencies are comparable in both cell lines (~60%). Similar to MEF cells, loss of NS upregulates the transcript levels of MDM2 in p53wt cells, cdc2 in p53ko cells, and Bax in both p53wt and p53ko cells, and does not change the p21 level in either p53wt or p53ko HCT116 cells (Figure 6a). Unlike MEF cells, NSkd increases cyclin B1 and reprimo expression in both p53wt and p53ko HCT116 cells. Western blots showed that NS depletion increases the amount of phosphorylated cdc2 (Y15) more in

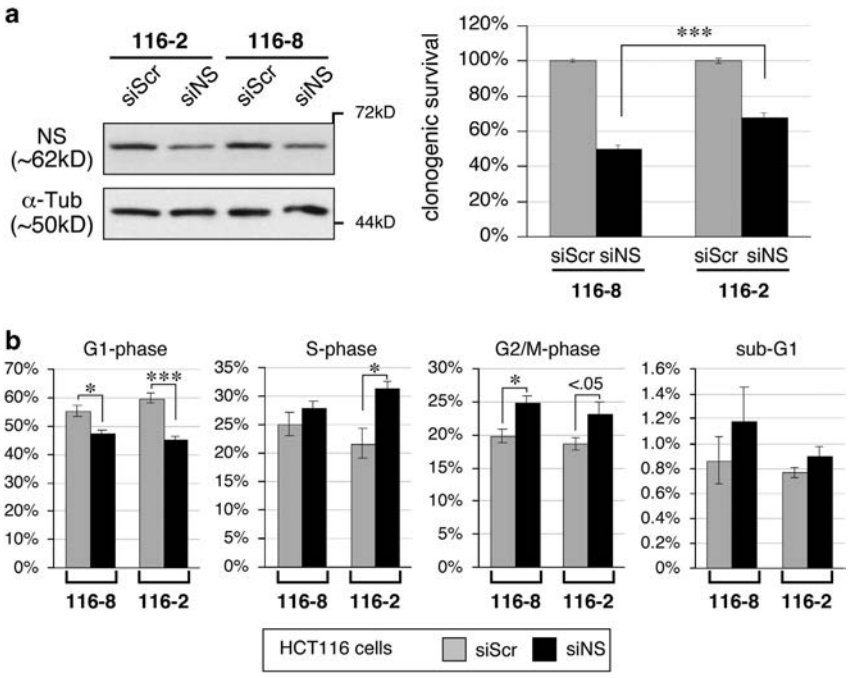

Figure 5. NS depletion reduces the clonogenic survival of HCT116 cells and triggers G2/M arrest in a p53-independent manner. (**a**) Western blots (left panel) and clonogenic survival (right panel) of HCT116-8 (p53wt) and HCT116-2 (p53ko) cells in response to control (siScr) or NS-specific (siNS) siRNA treatment. NS was detected by the Ab138 antibody. (**b**) Flow cytometry analysis of cell cycle profiles ($n = 9$). See Figure 1 for description regarding error bars and asterisks.

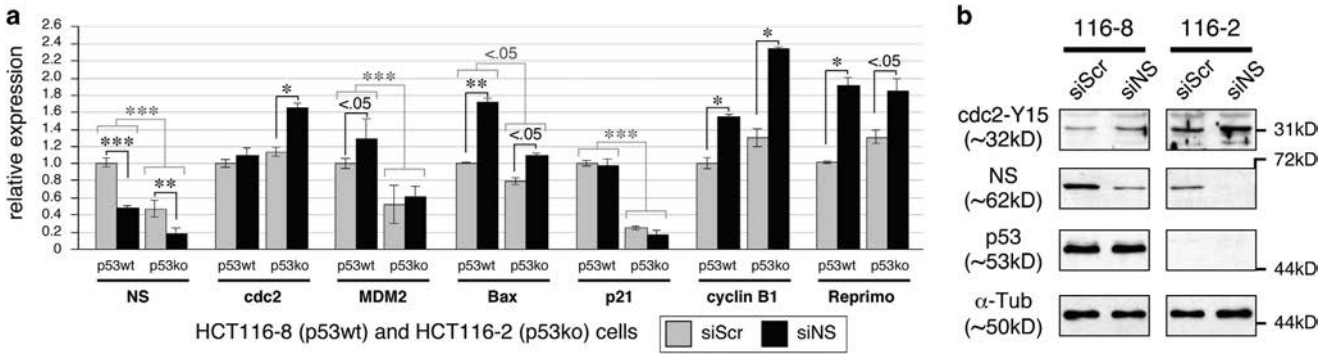

Figure 6. Molecular responses of p53wt and p53ko cancer cells to NS depletion. HCT116-8 (p53wt) and HCT116-2 (p53ko) cells were treated with siScr or siNS for 15 h and collected for analysis after 2 days. (**a**) The mRNA levels of p53-downstream genes were measured by qRT-PCR assays. (**b**) The amount of phosphorylated cdc2 (Y15), NS, and p53 in control (siScr) and NS-knockdown (siNS) HCT116-8 and HCT116-2 cells were measured by western blots. See Figure 1 for description regarding error bars and asterisks.

HCT116-2 cells than in HCT116-8 cells (Figure 6b). These data indicate that HCT-116 cells display a qualitative increase in phosphorylated cdc2, cyclin B1, and Bax in both p53wt and p53ko cells. Quantitatively, p53wt cells show more increase in reprimo and cyclin B1 and less increase in phosphorylated cdc2 compared with p53ko cells. Finally, normal and cancer cells show shared as well as unique molecular responses to NSkd-induced G2 arrest in contingency of their p53 status.

DISCUSSION

How NS intersects with the p53 pathway has always been a perplexing and highly debated issue in quest of the NS mechanism of action. This study illuminates this question by showing how p53 configures the response of cells to damages caused by the loss of NS. In our opinion, one major challenge in synthesizing a coherent model by integrating findings obtained from different cell models is to resolve their genetic heterogeneity. Such an issue exists not only between different cancer cell types but also between cancer and normal cells. To overcome this hurdle, we used two isogenic cell models with genetically perturbed NS and/or p53: one representing normal cells (e.g., MEF) and the other representing cancer cells (HCT116). This design permits the isogenic pairs to differ only in their NS and/or p53 status genetically.

Semipermissive NS deficiency causes G2/M arrest regardless of p53

In both MEF cells and HCT116 cells, loss of NS triggers G2/M arrest and perturbs cell proliferation regardless of their p53 status. Because of its functional proximity to cell proliferation, NS was sometimes referred to as a cell cycle protein. We found that the level of NS protein remains constant throughout the cell cycle under the normal growth condition (Supplementary Figure S2),

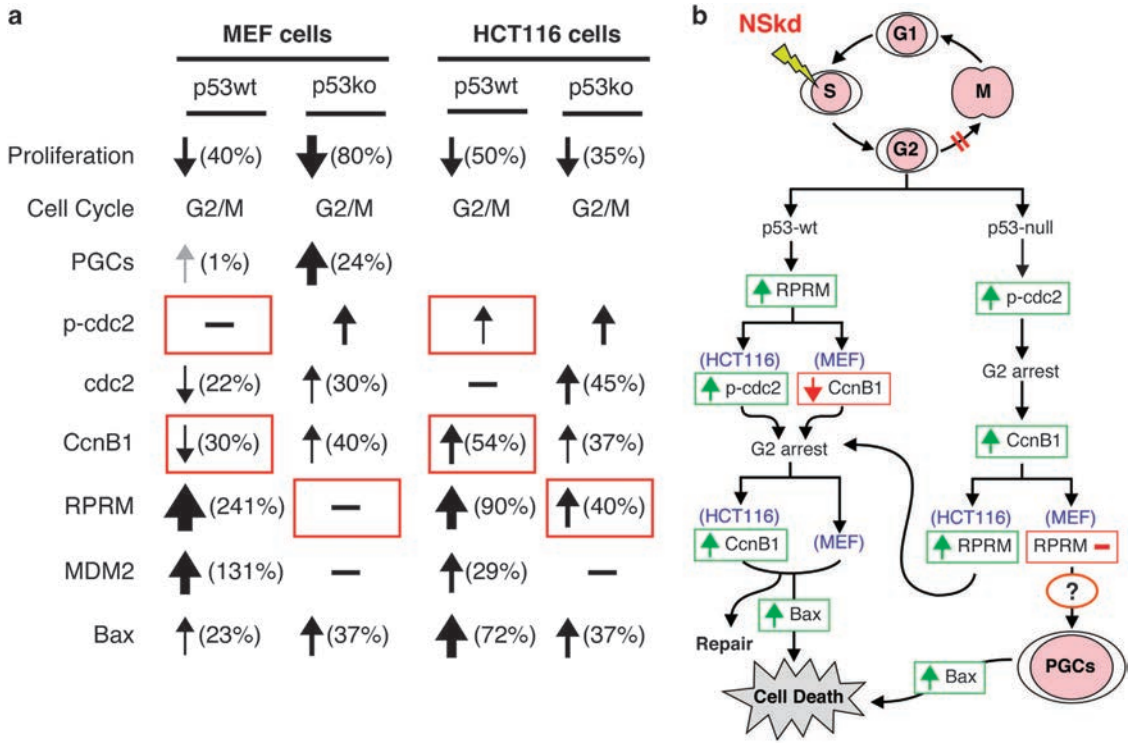

Figure 7. Diagrams of the p53-regulated response of NS-depleted cells to G2/M arrest. (**a**) Molecular and cellular responses of MEF and HCT116 cells to NS deficiency in the presence or absence of p53. Arrows and percentages in parenthesis denote the amount of increase (up arrow) or decrease (down arrow) induced by NS loss (NSkd). Red boxes mark the changes that are different in normal *versus* cancer cells. (**b**) A schematic diagram showing how NSkd affects cell cycling and how NS-deficient cells may respond to the resulting G2/M arrest under the p53wt or p53ko condition. Ccn B1, cyclin B1; PGCs, polypoid giant cells; RPRM, reprimo.

indicating that, at the level of protein expression, NS is neither regulating nor regulated directly by cell cycle progression. Depending on the extent of knockdown, NS-depleted cells may display the phenotypic profile of early S or G2/M arrest under the nonpermissive or semipermissive condition, respectively.[25] The inNS^{cko} MEF cell model resembles the haploinsufficient MEF cells [7] in showing a semipermissive G2/M arrest phenotype. NSkd-triggered cell cycle arrest occurs before entry into mitotic prophase. Molecular analyses provide further insight into how p53 may shape the response of NS-deficient cells to G2/M arrest (Figure 7a). First, mitotic entry is propelled by cdc2 dephosphorylation and cyclin B1 upregulation. Both p53ko MEF and HCT116 cells show a significant increase in cyclin B1 and phosphorylated cdc2 following NS depletion, suggesting that failure to dephosphorylate cdc2 may be a driver and increased cyclin B1 may be a reactor in the event of NSkd-triggered G2/M arrest. With wild-type p53, the responses of cyclin B1 and phosphorylated cdc2 to NS loss are distinctive between normal and cancer cells, with HCT116 cells showing increases in both phosphorylated cdc2 and cyclin B1 and MEF cells showing no change in phosphorylated cdc2 and a decrease in cyclin B1. Some commonly known p53-downstream G2/M regulators (e.g., 14-3-3-σ, GADD45, and cyclin G1) appear not to participate in this process. Instead, the gene that is regulated by p53 and consistently activated by NS depletion in p53wt MEF and HCT116 cells is reprimo. Reprimo has been shown to be upregulated by X-ray irradiation in p53wt MEF cells and suitably involved in G2/M arrest.[28] We therefore propose that NS deficiency arrests cells in the G2/M phase via a p53-dependent upregulation of reprimo or a p53-independent mechanism that blocks the dephosphorylation of cdc2.

p53 reduces the frequency of aberrant mitosis in G2-arrested NS-depleted MEF cells

A combined loss of NS and p53 has a more detrimental effect on cell proliferation in normal (MEF) cells than loss of NS alone. This compounding effect of p53 deletion in NS-depleted cells cannot be accounted for by the rather minor increase of cellular senescence or cell cycle perturbation. Instead, this proliferative crisis is most quantitatively compatible with a dramatic increase of PGCs, which suggests that p53 loss may subject the G2-arrested, NS-depleted cells to endoreplication and mitotic catastrophe. We reason that the molecules suppressing this event should be active in p53wt MEF cells and disabled in p53ko MEF cells. They should also be active in HCT116-8 and HCT116-2 cells, because the compounding effect of p53 deletion is not seen in HCT116 cells. Among the genes examined, only reprimo fits this profile, where its expression is upregulated by NSkd in p53wt MEF cells, HCT116-8 cells, and HCT116-2 cells, but remains unchanged in p53ko MEF cells. These results suggest a potential hypothesis that upregulation of reprimo in response to p53 activation following NS depletion may prevent cells from undergoing endoreplication and becoming PGCs, thereby reducing the risk of mitotic catastrophe.

p53-independent regulation of reprimo and Bax

In the context of NS perturbation, the expression of MDM2, p21, and cyclin G1 shows absolute p53 dependence, in the sense that they display a higher expression levels in p53wt than in p53ko cells. They either do not respond to NSkd specifically (e.g., p21 and cyclin G1) or respond to NSkd in a p53-dependent manner (e.g., MDM2). Conversely, cyclin A2, p27^{kip}, and cdc25C exhibit a p53-inhibited, NS-independent pattern of expression. NSkd

increases Bax expression in both normal and cancer cells regardless of their p53 status. Notably, the expression of reprimo in HCT116 cells can also be increased by NSkd in HCT116-2 (p53ko) cells. Indeed, it has been reported that the expression of reprimo can be regulated by promoter methylation as well as other p53-independent mechanisms in some cancer cells.[29–31]

Differential responses of normal and cancer cells to NS/p53 loss

Notably, MEF and HCT116 cells exhibit some differential responses to NS/p53 perturbation. For example, the NSkd-triggered reprimo response is p53-dependent in MEF cells and p53-independent in HCT116 cells. The cyclin B1 response to NSkd is decreased in p53wt MEF cells and increased in HCT116-8 cells. Another difference between MEF and HCT116 cells relates to their NS expression. In MEF cells, p53 deletion does not affect the basal expression level of NS but appears to sensitize them to TAM-induced NS depletion. Contrarily, loss of p53 reduces the baseline level of NS without affecting their respective sensitivities to NSkd. The exact mechanisms that drive the differential responses of cancer *versus* normal cells to NS/p53 perturbation remain to be determined on a case-by-case basis, but may relate to other cancer-associated mutations, such as p16 inactivation in HCT116 cells. Furthermore, even though the genetic variables of the isogenic cell pairs used in this study are limited to NS and p53 only, they may develop different adaptive responses that alter their expression of genes beyond NS and p53. Finally, there are likely multiple steps in between the NS/p53 perturbation and the readout events (e.g., G2/M arrest, cell death, and PGCs). Nevertheless, given the key positions where NS and p53 sit in cell proliferation and checkpoint monitoring, respectively, they may serve as a valuable predictor of the proliferative fate of normal and cancer cells. Finally, the different responses of normal and cancer cells to the perturbation of NS and/or p53 may potentially be used to design cancer-specific therapies.

CONCLUSION

Our data show that even though p53 loss cannot reverse the damage caused by NS loss or the ultimate fate of NS-deficient cells, it will orchestrate how they respond to the G2/M arrest (Figure 7b). The presence of p53 provides a mechanism for normal G2-arrested cells to reduce the chance of mitotic catastrophe. On the other hand, cancer cells appear to manage the NS loss condition more independently of their p53 status. The differential response of normal and cancer cells to NS deficiency may provide a rationale for developing tumor-selective therapies by targeting the NS activity.

MATERIALS AND METHODS

Cell culture, RNAi knockdown, and synchronization

Genetically modified mouse models were created and described in a previous report.[9] Animals were housed by the Program for Animal Resources at the TAMHSC-Houston campus and handled in accordance with the principles of the Guide for the Care and Use of Laboratory Animals. All procedures were approved by the Institutional Animal Care and Use Committee. MEF cells were prepared from $NS^{flx/flx}$-p53wt, $NS^{flx/flx}$-p53ko, $inNS^{cko}$-p53wt, and $inNS^{cko}$-p53ko embryos at embryonic day 13.5 using the method shown previously.[7] The flow cytometry (Figures 2a and 3b), mitosis (Figure 2b), and qRT-PCR (Figure 4) studies were performed by using the second passage (P2) MEF cells. The SA-β-Gal staining (data not shown) and giant cell studies (Figure 3a) were conducted in P3 MEF cells. HCT116-8 and HCT116-2 cells were obtained from Dr. Bert Vogelstein and cultured in McCoy's 5 A medium plus 10% FBS. HeLa cell lines were maintained in DMEM plus 10% FBS. For NSkd, HCT116 cells were replated for 24 h and then treated with siRNA duplexes (siScr or siNS) at 100 nM in Oligofectamine complex (Invitrogen, Carlsbad, CA, USA) for 15 h. The RNA sequences targeted by the siRNA duplexes are 5′-UGA CGA UCA GAA UGC GAC U-3′ (siScr) and 5′-GAA CUA AAA CAG CAG CAG A-3′ (siNS). Early S-phase synchronization was achieved by incubating HeLa cells with 2 mM thymidine for 20 h. Mitotic arrest was done by incubating cells with 0.5 μM nocodazole for 20 h.

Flow cytometry

At the time of the analysis, cells were washed, trypsinized, and fixed in 72% (vol/vol) ice-cold ethanol overnight. Cells were first processed for propidium iodide staining (50 μg/ml, Sigma, St. Louis, MO, USA) in the presence of 20 μg/ml DNase-free RNase A. Flow cytometry analyses were conducted using a COULTER EPICS XL flow cytometer and the XL System II software in the Flow Cytometry Core Facility at the Texas Children's Hospital. Cell cycle profiles were compiled from 2×10^4 gated events and analyzed using the Multi Cycle AV software. All data represent the average of $\geqslant 4$ independent repeats.

Western blot

Western blot analyses were performed as described previously and repeated twice.[14,32] Primary antibodies used in this study include rabbit polyclonal antibodies to human NS (Ab138, Tsai Laboratory, Houston, TX, USA), p-cdc2 (Y15, Cell Signaling, Danvers, MA, USA), MDM2 (SMP-14, Santa Cruz, Santa Cruz, CA, USA), p53 (DO-1, Santa Cruz), p-histone H3 (S10, Upstate, Lake Placid, NY, USA), and α-tubulin (Sigma). Secondary antibodies were conjugated to peroxidase (Jackson ImmunoResearch, West Grove, PA, USA).

Anti-pH3 staining

To measure the percentages of cells in different mitotic phases, cells were fixed in 4% formaldehyde for 15 min, permeablized by 0.3% Triton X-100, and incubated with anti-p-histone H3 antibody overnight, followed by incubation with FITC-conjugated secondary antibodies for 2 h. Abnormal nuclear morphologies were analyzed by DAPI staining. Fluorescent images were acquired on a Zeiss LSM510 confocal microscope (Göttingen, Germany) using the $\times 40$ or $\times 63$ plan-apochromat objectives. Images were scanned with a 512×512 frame size and $\times 1$ zoom. Detector gain and amplifier offset were adjusted to ensure that all signals were displayed within the linear range. Final data represent the average of three independently performed experiments.

Quantitative RT-PCR analyses

Total RNAs (5μg) were reversed transcribed into first-strand cDNAs using random hexamers and M-MLV reverse transcriptase. For qPCR, the ΔC(t) values between the target message and the reference message (Rplp0) were determined by the MyiQ single-color real-time PCR detection system and supermix SYBR green reagent. The ΔΔC(t) values were measured from three biological replicates and two technical repeats ($n = 6$) to compare the relative expression levels of target sequences between different groups. All final results were confirmed by comparing to a second reference message, HMG-14. Primer sequences are provided in Supplementary Data.

Clonogenic survival assay

HCT116 cells were treated with siRNAs for 24 h, replated at low density (55 cells/cm^2) in six-well plates at a density of 300 cells per well, and grown in normal growth medium for 12 days to allow colony formation. Formed colonies were then visualized by fixing with 3.7% formaldehyde for 15 min at room temperature and staining with 0.25% crystal violet for 30 min. Colonies larger than 1mm in diameter were counted. Final data represent the average of three independently performed experiments and are analyzed by Repeated Measures ANOVA.

ABBREVIATIONS

MEF, mouse embryonic fibroblast; NS, nucleostemin; NSkd, NS-knockdown; PGCs, polyploid giant cells; PI, propidium iodide; pH3, phospho-histone H3; p53wt, p53-wildtype; p53ko, p53-null.

ACKNOWLEDGEMENTS

This work was supported by NCI-PHS grant R01 CA113750 to RYLT. The open access publishing fees for this article have been covered by the Texas A&M University Online

Access to Knowledge (OAK) Fund, supported by the University Libraries and the Office of the Vice President for Research.

COMPETING INTERESTS

The authors declare no conflict of interest.

REFERENCES

1 Tsai RY, McKay RD. A nucleolar mechanism controlling cell proliferation in stem cells and cancer cells. *Genes Dev* 2002; **16**: 2991–3003.
2 Baddoo M, Hill K, Wilkinson R, Gaupp D, Hughes C, Kopen GC *et al.* Characterization of mesenchymal stem cells isolated from murine bone marrow by negative selection. *J Cell Biochem* 2003; **89**: 1235–1249.
3 Ohmura M, Naka K, Hoshii T, Muraguchi T, Shugo H, Tamase A *et al.* Identification of stem cells during prepubertal spermatogenesis via monitoring of nucleostemin promoter activity. *Stem Cells* 2008; **26**: 3237–3246.
4 Yamashita M, Nitta E, Nagamatsu G, Ikushima YM, Hosokawa K, Arai F *et al.* Nucleostemin is indispensable for the maintenance and genetic stability of hematopoietic stem cells. *Biochem Biophys Res Commun* 2013; **441**: 196–201.
5 Tamase A, Muraguchi T, Naka K, Tanaka S, Kinoshita M, Hoshii T *et al.* Identification of tumor-initiating cells in a highly aggressive brain tumor using promoter activity of nucleostemin. *Proc Natl Acad Sci USA* 2009; **106**: 17163–17168.
6 Lin T, Meng L, Li Y, Tsai RY. Tumor-initiating function of nucleostemin-enriched mammary tumor cells. *Cancer Res* 2010; **70**: 9444–9452.
7 Zhu Q, Yasumoto H, Tsai RY. Nucleostemin delays cellular senescence and negatively regulates TRF1 protein stability. *Mol Cell Biol* 2006; **26**: 9279–9290.
8 Beekman C, Nichane M, De Clercq S, Maetens M, Floss T, Wurst W *et al.* Evolutionarily conserved role of nucleostemin: controlling proliferation of stem/progenitor cells during early vertebrate development. *Mol Cell Biol* 2006; **26**: 9291–9301.
9 Meng L, Lin T, Peng G, Hsu JK, Lee S, Lin S-Y *et al.* Nucleostemin deletion reveals an essential mechanism that maintains the genomic stability of stem and progenitor cells. *Proc Natl Acad Sci USA* 2013; **110**: 11415–11420.
10 Shugo H, Ooshio T, Naito M, Naka K, Hoshii T, Tadokoro Y *et al.* Nucleostemin in injury-induced liver regeneration. *Stem Cells Dev* 2012; **21**: 3044–3054.
11 Lin T, Ibrahim W, Peng C-Y, Finegold MJ, Tsai RY. A novel role of nucleostemin in maintaining the genome integrity of dividing hepatocytes during mouse liver development and regeneration. *Hepatology* 2013; **58**: 2176–2187.
12 Sijin L, Ziwei C, Yajun L, Meiyu D, Hongwei Z, Guofa H *et al.* The effect of knocking-down nucleostemin gene expression on the *in vitro* proliferation and *in vivo* tumorigenesis of HeLa cells. *J Exp Clin Cancer Res* 2004; **23**: 529–538.
13 Qu J, Bishop JM. Nucleostemin maintains self-renewal of embryonic stem cells and promotes reprogramming of somatic cells to pluripotency. *J Cell Biol* 2012; **197**: 731–745.
14 Tsai RY, McKay RD. A multistep, GTP-driven mechanism controlling the dynamic cycling of nucleostemin. *J Cell Biol* 2005; **168**: 179–184.
15 Meng L, Zhu Q, Tsai RY. Nucleolar trafficking of nucleostemin family proteins: common versus protein-specific mechanisms. *Mol Cell Biol* 2007; **27**: 8670–8682.
16 Ma H, Pederson T. Depletion of the nucleolar protein nucleostemin causes G1 cell cycle arrest via the p53 pathway. *Mol Biol Cell* 2007; **18**: 2630–2635.
17 Dai MS, Sun XX, Lu H. Aberrant expression of nucleostemin activates p53 and induces cell cycle arrest via inhibition of MDM2. *Mol Cell Biol* 2008; **28**: 4365–4376.
18 Meng L, Lin T, Tsai RY. Nucleoplasmic mobilization of nucleostemin stabilizes MDM2 and promotes G2-M progression and cell survival. *J Cell Sci* 2008; **121**: 4037–4046.
19 Meng L, Hsu JK, Tsai RY. GNL3L depletion destabilizes MDM2 and induces p53-dependent G2/M arrest. *Oncogene* 2011; **30**: 1716–1726.
20 Jafarnejad SM, Mowla SJ, Matin MM. Knocking-down the expression of nucleostemin significantly decreases rate of proliferation of rat bone marrow stromal stem cells in an apparently p53-independent manner. *Cell Prolif* 2008; **41**: 28–35.
21 Hsu JK, Lin T, Tsai RY. Nucleostemin prevents telomere damage by promoting PML-IV recruitment to SUMOylated TRF1. *J Cell Biol* 2012; **197**: 613–624.
22 Tsai RY. Turning a new page on nucleostemin and self-renewal. *J Cell Sci* 2014; **127**: 3885–3891.
23 Hayashi S, McMahon AP. Efficient recombination in diverse tissues by a tamoxifen-inducible form of Cre: a tool for temporally regulated gene activation/inactivation in the mouse. *Dev Biol* 2002; **244**: 305–318.
24 Donehower LA, Harvey M, Slagle BL, McArthur MJ, Montgomery CA Jr., Butel JS *et al.* Mice deficient for p53 are developmentally normal but susceptible to spontaneous tumours. *Nature* 1992; **356**: 215–221.
25 Lin T, Meng L, Wu LJ, Pederson T, Tsai RY. Nucleostemin and GNL3L exercise distinct functions in genome protection and ribosome synthesis, respectively. *J Cell Sci* 2014; **127**: 2302–2312.
26 Gurley LR, D'Anna JA, Barham SS, Deaven LL, Tobey RA. Histone phosphorylation and chromatin structure during mitosis in Chinese hamster cells. *Eur J Biochem* 1978; **84**: 1–15.
27 Wei Y, Yu L, Bowen J, Gorovsky MA, Allis CD. Phosphorylation of histone H3 is required for proper chromosome condensation and segregation. *Cell* 1999; **97**: 99–109.
28 Ohki R, Nemoto J, Murasawa H, Oda E, Inazawa J, Tanaka N *et al.* Reprimo, a new candidate mediator of the p53-mediated cell cycle arrest at the G2 phase. *J Biol Chem* 2000; **275**: 22627–22630.
29 Takahashi T, Suzuki M, Shigematsu H, Shivapurkar N, Echebiri C, Nomura M *et al.* Aberrant methylation of Reprimo in human malignancies. *Int J Cancer* 2005; **115**: 503–510.
30 Vanlandingham JW, Tassabehji NM, Somers RC, Levenson CW. Expression profiling of p53-target genes in copper-mediated neuronal apoptosis. *Neuromolecular Med* 2005; **7**: 311–324.
31 Malik S, Jiang S, Garee JP, Verdin E, Lee AV, O'Malley BW *et al.* Histone deacetylase 7 and FoxA1 in estrogen-mediated repression of RPRM. *Mol Cell Biol* 2010; **30**: 399–412.
32 Meng L, Yasumoto H, Tsai RY. Multiple controls regulate nucleostemin partitioning between nucleolus and nucleoplasm. *J Cell Sci* 2006; **119**: 5124–5136.

Supplemental Information accompanies the paper on the *Cell Death Discovery* website (http://www.nature.com/cddiscovery)

Nucleostemin inhibits TRF1 dimerization and shortens its dynamic association with the telomere

Lingjun Meng*, Joseph K. Hsu*, Qubo Zhu, Tao Lin and Robert Y. L. Tsai‡

Center for Cancer and Stem Cell Biology, Institute of Biosciences and Technology, Texas A&M Health Science Center, Houston, Texas 77030, USA

*These authors contributed equally to this work
‡Author for correspondence (rtsai@ibt.tamhsc.edu)

Accepted 3 June 2011
Journal of Cell Science 124, 3706–3714

doi: 10.1242/jcs.089672

Summary

TRF1 is a key component of the telomere-capping complex and binds double-strand telomeric DNA as homodimers. So far, it is not clear whether TRF1 dimerization coincides with its telomere binding or is actively controlled before it binds the telomere, and in the latter case, how this event might affect its telomere association. We previously found that TRF1 dimerization and its telomere binding can be increased by GNL3L, which is the vertebrate paralogue of nucleostemin (NS). Here, we show that NS and GNL3L bind TRF1 directly but competitively through two separate domains of TRF1. In contrast to GNL3L, NS prevents TRF1 dimerization through a mechanism not determined by its ability to displace TRF1-bound GNL3L. Furthermore, NS is capable of shortening the dynamic association of TRF1 with the telomere in normal and TRF2$^{\Delta B\Delta M}$-induced telomere-damaged cells without affecting the amount of telomere-bound TRF1 proteins in vivo. Importantly, NS displays a protective function against the formation of telomere-dysfunction-induced foci. This work demonstrates that TRF1 dimerization is actively and oppositely regulated by NS and GNL3L extrachromosomally. Changing the relative amount of TRF1 monomers versus dimers in the nucleoplasm might affect the dynamic association of TRF1 with the telomere and the repair of damaged telomeres.

Key words: Dimerization, FLIP, GNL3L, Nucleostemin, Telomere damage, TRF1

Introduction

Telomeric repeat-binding factor 1 (TRF1) is a component of the telomere-capping complex, also known as shelterin or telosome, which consists of six core proteins: TRF1, TRF2, TIN2 (TRF1-interacting nuclear protein 2), POT1 (protection of telomeres protein 1), TPP1 (also known as adrenocortical dysplasia homolog, ACD) and RAP1 (de Lange, 2005; Songyang and Liu, 2006). The telomere-capping complex organizes chromosomal ends into a high-order structure and has a crucial role in maintaining their stability. TRF1 serves the important functions of protecting telomeres (Martinez et al., 2009), preventing telomere elongation (van Steensel and de Lange, 1997), controlling the mitotic transit (Zhou et al., 2003) and regulating ALT (alternative lengthening of telomere)-associated PML body (APB) formation in telomerase-inactive cells (Jiang et al., 2007; Potts and Yu, 2005). TRF1 protein is post-translationally modified by phosphorylation, ADP ribosylation, ubiquitylation, and homodimerization (Chang et al., 2003; Chong et al., 1995; Kim et al., 2008; Lee et al., 2006; Smith et al., 1998; Wu et al., 2008). Dimerization allows TRF1 to form proper configuration and bind double-strand telomeric DNA repeats through its Myb domain (Bianchi et al., 1997; Broccoli et al., 1997). Even though TRF1 dimerization was observed both in a complex with DNA and by a yeast two-hybrid assay (Bianchi et al., 1997), it is not clear whether this event is actively regulated while TRF1 is in the nucleoplasm or occurs concomitantly with the formation of the telomere-capping complex.

We first discovered that nucleostemin (NS) is a TRF1-binding protein that accelerates the degradation of TRF1 (Zhu et al., 2006). NS belongs to a novel family of nucleolar GTP-binding proteins (Tsai and Meng, 2009), and is found preferentially expressed by multiple stem cell types, human cancers and adult regenerating tissues (Baddoo et al., 2003; Maki et al., 2007; Ohmura et al., 2008; Siddiqi et al., 2008; Tsai and McKay, 2002). It is required for early embryogenesis and the maintenance of continuous cell proliferation (Tsai and Meng, 2009; Zhu et al., 2006). In later studies, we found that its vertebrate paralogue, GNL3L (guanine nucleotide binding protein-like 3-like), can also bind TRF1 and promote its homodimerization and telomere association without being physically bound to the telomere (Zhu et al., 2009). In contrast to the NS effect on TRF1, GNL3L shows the ability to promote TRF1 stability by preventing its ubiquitylation and degradation. Those previous findings indicate that the TRF1 protein complex might be modulated actively and dynamically before it binds the telomere (Tsai, 2009).

To further our understanding of this new ‘pre-telomeric’ regulation of TRF1, we set out to investigate how NS controls the biochemical interaction and telomeric association of TRF1. Our results showed that NS and GNL3L both bind TRF1 directly but competitively. Whereas GNL3L promotes the dimerization and telomeric association of TRF1 (Zhu et al., 2009), NS diminishes TRF1 dimerization independently of its ability to dissociate GNL3L from TRF1. Functional studies demonstrated that NS is capable of shortening the dynamic association of TRF1 with the telomere in normal and TRF2$^{\Delta B\Delta M}$-induced telomere-damaged cells without affecting the amount of telomere-bound TRF1 proteins in vivo. TRF2$^{\Delta B\Delta M}$ is a TRF2 mutant deleted of its

Journal of Cell Science

N-terminal basic domain and C-terminal Myb domain. TRF2$^{\Delta B\Delta M}$ lacks telomere-binding activity, thus acting as a dominant-negative allele of TRF2, and has been used to destabilize the telomere-capping complex and trigger telomere damage (van Steensel et al., 1998). Importantly, we found that NS has a protective role against TRF2$^{\Delta B\Delta M}$-induced telomere damage. This work reveals a novel TRF1 regulatory mechanism that operates bidirectionally and extrachromosomally.

Results

NS and GNL3L bind directly to separate domains of TRF1

We have previously shown that TRF1 coexists in the same protein complex with NS or with GNL3L (Zhu et al., 2009; Zhu et al., 2006). To demonstrate that NS or GNL3L directly binds TRF1, we isolated bacterially expressed NS and GNL3L proteins and examined their binding with purified GST–TRF1 proteins by affinity pull-down assays. Immunoblotting of the input, unbound supernatant (Sup) and retained fractions (Ret) confirmed that both NS and GNL3L can specifically and directly bind TRF1 (Fig. 1A). The amounts of NS in the unbound (Sup) and bound (Ret) fractions relative to the input are less than that of GNL3L, which might be caused by the rapid degradation of purified NS proteins. The TRF1-interactive domain of NS was mapped by deletions made on the basic (B), coiled-coil (C), GTP-binding (G), intermediate (I) or A-domain of NS (Fig. 1B). Unlike the TRF1-interacting G-domain of GNL3L (Zhu et al., 2009), binding between TRF1 and NS requires the I-domain of NS. Conversely, the NS-interactive domain of TRF1 was determined by testing the NS binding of TRF1 mutants deleted of the A-domain, HBD (homodimerization domain), UD (undefined) or Myb domain (Fig. 1C). Whereas GNL3L interacts with the HBD domain of TRF1 (Zhu et al., 2009), binding between TRF1 and NS requires the UD domain of TRF1. The lack of binding capability of NSΔI or TRF1ΔUD should not be caused by protein misfolding because these proteins are capable of binding MDM2 and GNL3L, respectively (Meng et al., 2008; Zhu et al., 2009). To exclude another possibility that the differential NS-binding activities of TRF1 mutants might result from their distinct subcellular localization, confocal studies were conducted in HeLa cells and showed that both the NS binding (TRF1ΔMyb) and non-binding (TRF1ΔUD) mutants are located outside the nucleolus (Fig. 1D). Similar findings were observed in U2OS cells (data not shown). These results demonstrate that NS and GNL3L bind directly to separate domains of TRF1.

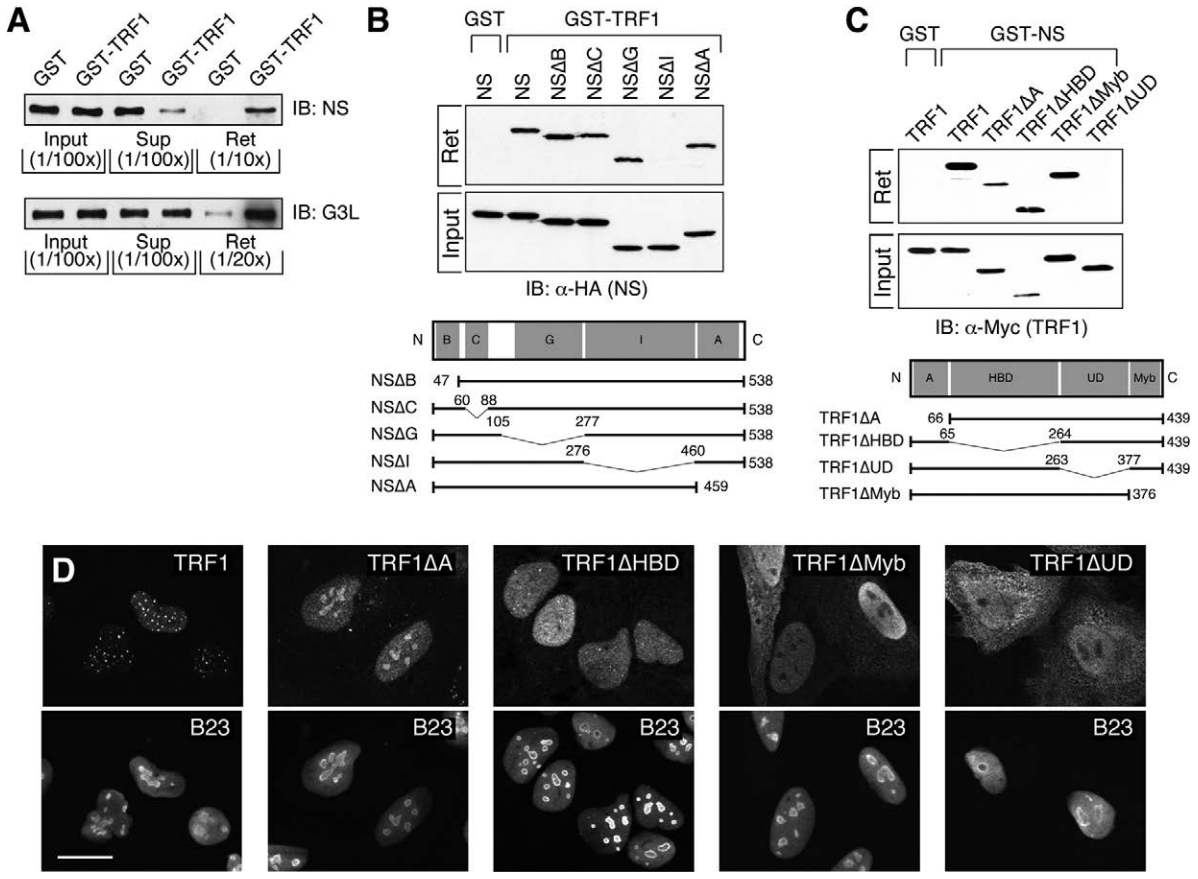

Fig. 1. NS and GNL3L bind directly to two separate domains of TRF1. (**A**) Purified NS and GNL3L proteins (40 μg) were incubated with purified Sepharose-bound GST–TRF1 protein (4 μg). Fractions of the input (1/100th), unbound supernatant (Sup, 1/100th), and retained lysates (Ret, 1/10th–1/20th) were immunoblotted (IB) with anti-NS and anti-GNL3L (G3L) antibodies. The pull-down results confirmed that NS and GNL3L bind TRF1 directly. (**B**) GST pull-down assays showing that the I-domain of NS is required for its TRF1 interaction. (**C**) Conversely, the UD domain of TRF1 is required for its interaction with NS. Bottom panels in B and C depict the deletion mutants of NS and TRF1. Bent lines and numbers denote the deleted regions and amino acid positions, respectively. B, basic; C, coiled-coil; G, GTP-binding; I, intermediate; A, acidic; HBD, homodimerization; UD, undefined domain. (**D**) Confocal images of GFP-fused wild-type and mutant TRF1 proteins in HeLa cells. Nucleoli are labeled by anti-B23 staining. Scale bar: 20 μm.

NS negatively regulates the GNL3L binding and homodimerization of TRF1

To interrogate the TRF1-binding relationship between NS and GNL3L, we asked whether NS and GNL3L form hetero-trimeric complexes with TRF1 or bind TRF1 as separate hetero-dimeric complexes. To address this issue, we first examined the coimmunoprecipitation of endogenous NS, TRF1 and GNL3L, and found only TRF1 in the NS protein complex (Fig. 2A). Next, we tested whether these three proteins can form hetero-trimeric complexes. NS (Myc), GNL3L (HA) and TRF1 (FLAG) were coexpressed in HEK293 cells, and the TRF1 and GNL3L co-complex was purified by sequential anti-FLAG and anti-HA immunoprecipitation. Anti-Myc western blots showed that the hetero-trimeric complex does exist, but accounts for only a small fraction of the hetero-dimeric complex of GNL3L and TRF1 even upon overexpression (Fig. 2B). These results indicate that the majority of NS and GNL3L bind TRF1 separately, but a small portion might form a heterotrimeric complex with TRF1. To examine the possibility that NS and GNL3L compete against each other for TRF1 binding, GST-fused TRF1 proteins were purified to pull down lysates containing a fixed amount of Myc-tagged GNL3L and increasing amounts of HA-tagged NS (Fig. 2C, left). The total protein concentrations were adjusted to the same levels in all samples. The results showed that NS is capable of blocking GNL3L binding to TRF1 in a dose-dependent manner. Reciprocally, GNL3L can also compete against NS for TRF1 binding (Fig. 2C, right). One major TRF1-binding protein in the telomere-capping complex is TIN2. GST-binding competition experiments showed that NS and TIN2 do not interfere with each other's binding to TRF1 (Fig. 2D). TRF1 is also known to form homodimers. To investigate the NS role in regulating TRF1 dimerization, GST–TRF1 was used to pull down lysates with the same amount of Myc-tagged TRF1 and increasing amounts of NS. In contrast to the effect of GNL3L on TRF1 dimerization (Zhu et al., 2009), addition of NS reduced the association between the Myc-tagged TRF1 and GST–TRF1 in a dose-dependent manner (Fig. 2E). Together, these results demonstrate that NS prevents TRF1 from binding to GNL3L and to itself, but does not interfere with the interaction of TRF1 with its partner at the telomere, TIN2.

NS structures required for its inhibition of GNL3L binding and dimerization of TRF1

NS inhibition of TRF1 homodimerization might be mediated by its role in competing against GNL3L for TRF1 binding, because GNL3L is known to promote TRF1 homodimerization (Zhu et al., 2009). If true, its abilities to block TRF1 dimerization and GNL3L binding should correlate. To test this idea, we examined the NS protein structures required to inhibit the GNL3L binding or dimerization of TRF1. Our results showed that the ability of NS to displace TRF1-bound GNL3L was mostly abolished by deleting its TRF1-interactive I-domain (Fig. 3A), but not affected by the deletion of the B-, G- or A-domain of NS, or by the G256V mutation that abolishes its GTP-binding capability (Fig. 3B–E). Reciprocally, the ability of GNL3L to displace TRF1-bound NS only required its TRF1-interactive G-domain (Fig. 3G), and was not decreased by the deletion of its BC- or I-domain (Fig. 3H,I) or the G253V mutation that corresponds to the G256V mutation of NS (Fig. 3J).

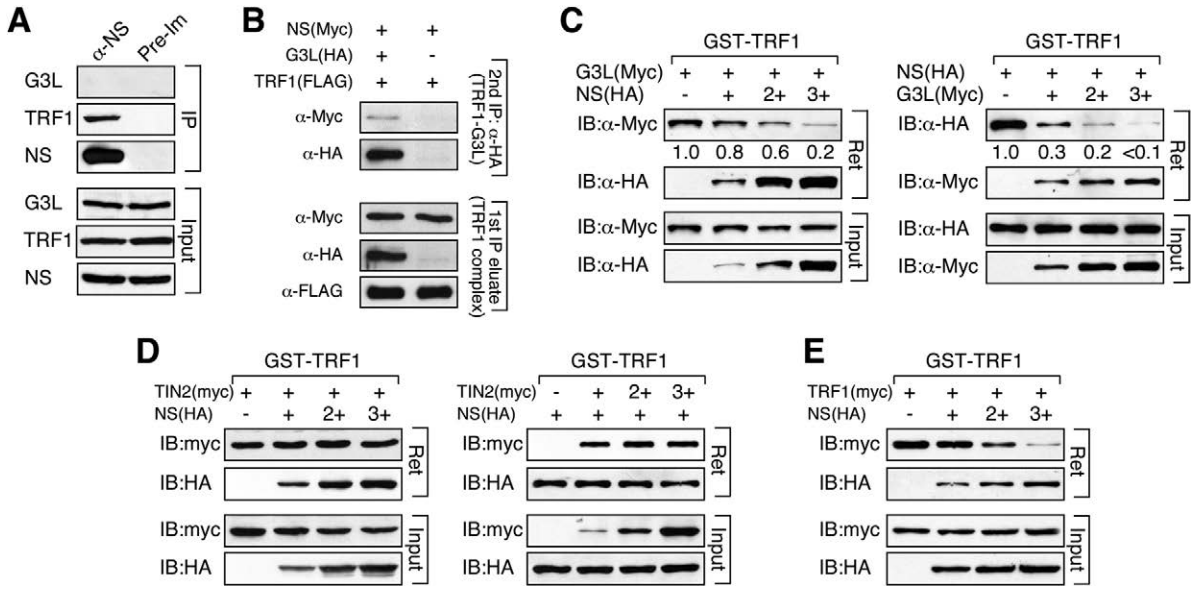

Fig. 2. NS inhibits GNL3L binding and homodimerization of TRF1. (**A**) Immunoprecipitation (IP) of endogenous NS complex copurified TRF1 but not GNL3L. (**B**) Two-step coimmunoprecipitation (coIP) was used to determine whether NS (Myc-tagged), GNL3L (HA-tagged) and TRF1 (FLAG-tagged) are capable of forming hetero-trimeric complexes. The TRF1 complex was precipitated using anti-FLAG antibody and eluted using FLAG peptide. Then the TRF1–GNL3L co-complex was purified by anti-HA immunoprecipitation. The amount of the hetero-trimeric complex (detected by immunoblotting the TRF1–GNL3L co-complex with anti-Myc antibody) represents a small fraction of the TRF1–GNL3L co-complex even upon overexpression. (**C**) Agarose-bound GST–TRF1 was incubated with lysates containing a fixed amount of GNL3L (Myc) and increasing amounts of NS (HA) or vice versa. Increasing the amount of NS significantly reduces the signal of TRF1-bound GNL3L (left). Reciprocally, increasing the amount of GNL3L also decreases NS binding to GST–TRF1 (right). (**D**) GST pull-down competition experiments show that NS (HA) does not affect the binding between TIN2 (Myc) and GST–TRF1 (left); nor does TIN2 (Myc) change the binding between NS (HA) and GST–TRF1 (right). (**E**) Increasing the amount of NS significantly decreases the binding efficiency between TRF1 (Myc) and GST–TRF1 in a dose-dependent manner.

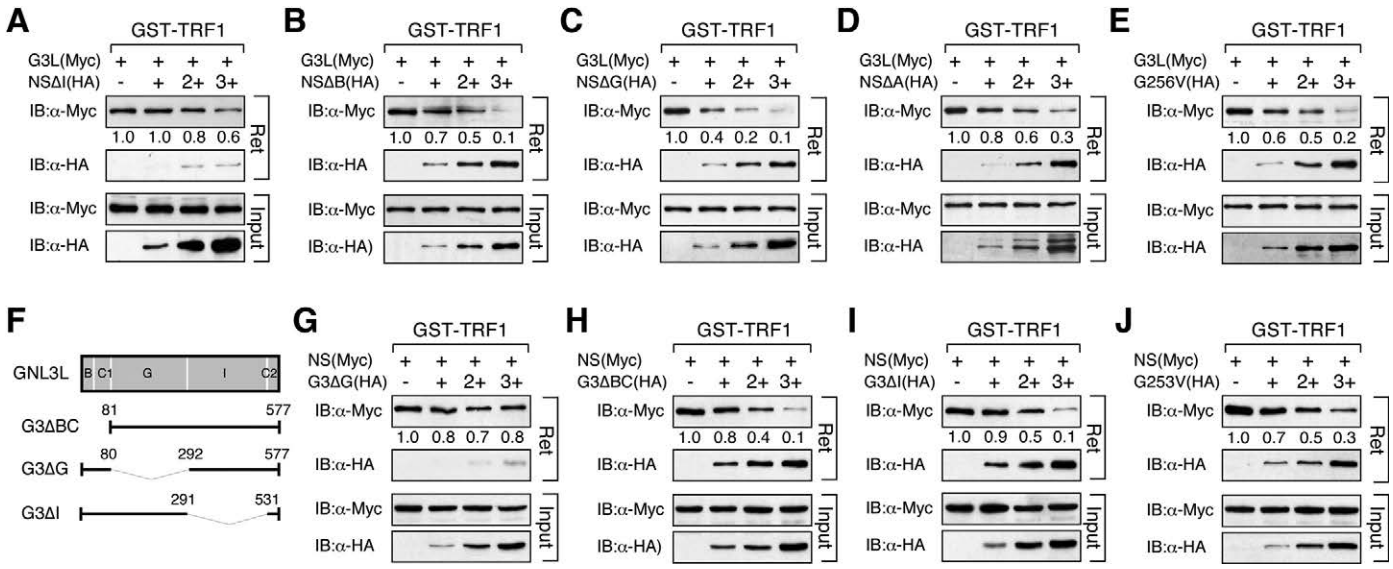

Fig. 3. Identification of NS domain required for its ability to inhibit GNL3L binding to TRF1 and vice versa. Affinity binding between GST–TRF1 and GNL3L (Myc) was conducted in the presence of different NS deletion mutants. The NS ability to block GNL3L binding to TRF1 requires its TRF1-interacting I-domain (**A**), but is unaffected by any other deletions (**B**–**D**) or the G256V mutation (**E**). (**F**) GNL3L mutants used to map the domain(s) required for its competition with NS for TRF1 binding. The ability of GNL3L to block NS binding to TRF1 requires only its TRF1-interacting G-domain (**G**) and does not depend on its BC-domain (**H**), I-domain (**I**) or GTP binding (**J**).

With respect to the NS effect on blocking TRF1 homodimerization, our data showed that this NS activity was completely abolished by deleting its I-domain (NSΔI, Fig. 4A), B-domain (NSΔB, Fig. 4B) or G-domain (NSΔG, Fig. 4C), and partially blocked by the non-GTP-binding mutation, G256V (Fig. 4D). This anti-TRF1 dimerization effect of NS was unaffected by the A-domain deletion (NSΔA, Fig. 4E). Given that the NSΔB and NSΔG mutants can both displace TRF1-bound GNL3L, but cannot block TRF1 homodimerization, we conclude that the anti-TRF1 dimerization effect of NS is not determined by its ability to compete against GNL3L for TRF1 binding.

NS decreases TRF1 binding to telomeric DNA in vitro

Because TRF1 binds telomeric DNA as homodimers, we speculate that NS might regulate the telomeric association of TRF1. To test whether NS has such a function, we first used the electrophoretic mobility shift assay (EMSA) to determine the direct effect of NS on TRF1 binding to double-stranded $(TTAGGG)_6$ probes. Compared with the probe alone (Fig. 5A1, lane 1) and vector-transfected sample (Fig. 5A1, lane 2), the Myc-tagged TRF1-transfected sample (Fig. 5A1, lane 3) yielded a specific TRF1–DNA complex (black arrow) that could be competed by excess unlabeled probes (Fig. 5A1, lane 4) and supershifted by anti-Myc antibody (Fig. 5A1, grey arrow in lane 5). NS by itself did not bind the $(TTAGGG)_6$

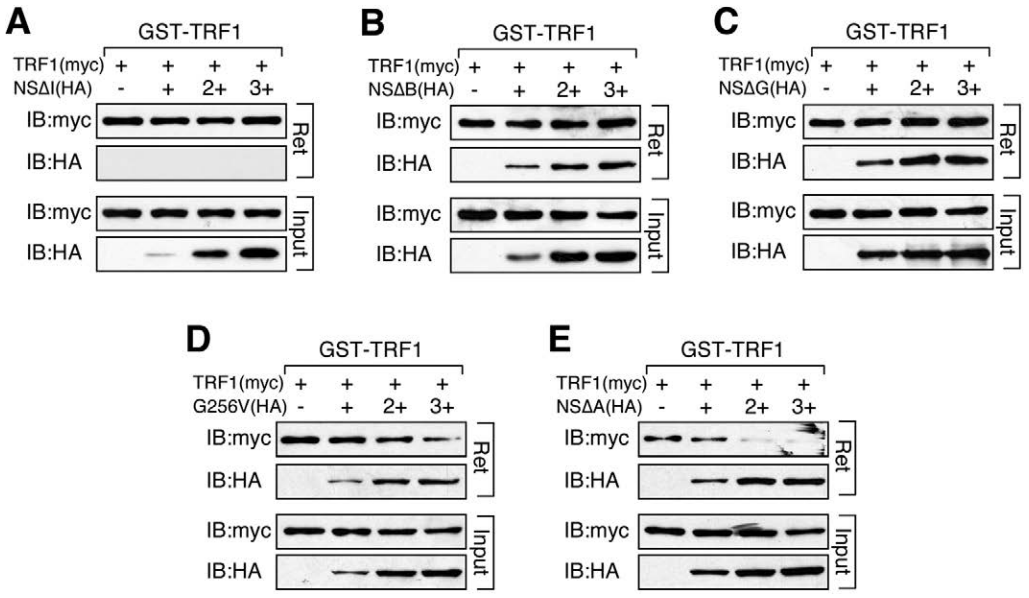

Fig. 4. The anti-TRF1 dimerization effect of NS requires its basic and GTP-binding domains, in addition to its TRF1-binding I-domain. Agarose-bound GST–TRF1 was incubated with lysates containing a fixed amount of TRF1 (Myc) and increasing amounts of NS deletion mutants (HA). The NS ability to block TRF1 dimerization is completely abolished by deletions of its I-domain (**A**), B-domain (**B**) or G-domain (**C**), partially blocked by the GTP-binding mutant (G256V, **D**), but is completely unaffected by the A-domain deletion of NS (**E**). Agarose-bound (R) and supernatant fractions (S) are indicated.

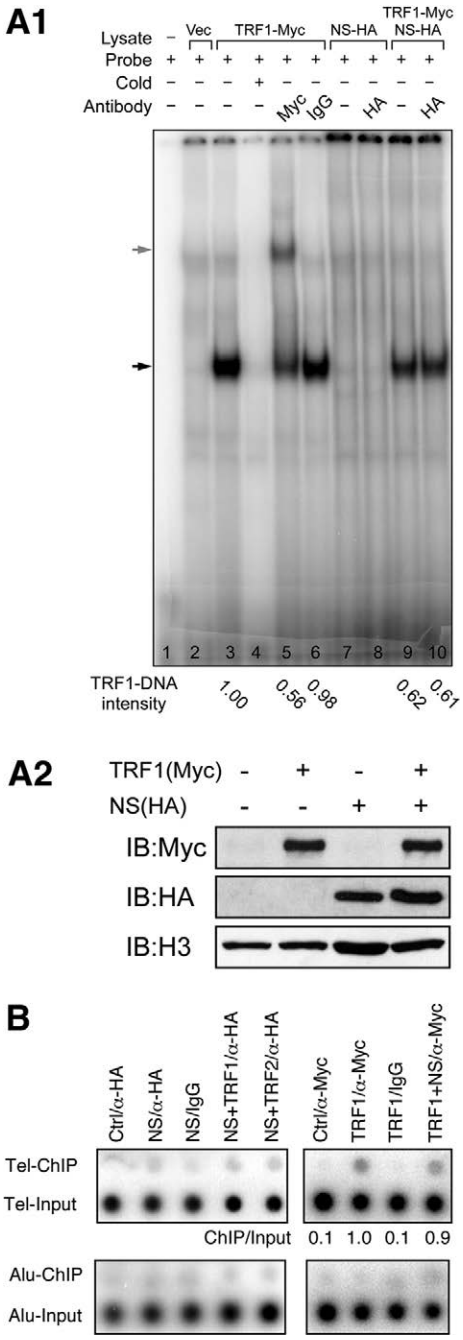

Fig. 5. NS reduces the amount of telomere-bound TRF1 in the electrophoretic mobility shift assay but not in the chromatin immunoprecipitation experiment. (**A1**) EMSA experiments identified a specific TRF1-probe complex (lane 3, indicated by black arrow) that can be competed by unlabeled probes (lane 4) and supershifted by anti-Myc antibody (lane 5, indicated by grey arrow). Coexpression of NS reduces the intensity of the TRF1-DNA complex by 40% (lanes 9 and 10). NS does not bind telomeric DNAs by itself (lanes 7 and 8) or through TRF1 (lane 10). (**A2**) Western blots show input HEK293 nuclear extracts expressing the indicated proteins used for EMSA experiments. (**B**) ChIP assays showed that immunoprecipitation of HA-tagged NS (NS/α-HA) does not co-purify telomeric DNAs (Tel-ChIP) more than the vector/α-HA (Ctrl/α-HA), NS/IgG, or Alu sequence controls (left). NS coexpression does not change the amount of telomere-bound TRF1 (TRF1+NS/α-Myc) in ChIP (right).

probe (Fig. 5A1, lanes 7 and 8). A 40% reduction in the TRF1–DNA complex intensity was noted in the NS overexpression samples (Fig. 5A1, lanes 9 and 10). Next, we performed chromatin immunoprecipitation (ChIP) to confirm that NS has an effect on the telomere binding of TRF1 in vivo. The ChIP results showed that NS does not bind the telomere by itself or through TRF1 or TRF2 (Fig. 5B, left). In addition, the ChIP experiments showed that NS does not change the amount of telomere-bound TRF1 (Fig. 5B, right). These results suggest that NS has little or no effect on regulating the amount of telomere-bound TRF1 proteins in vivo.

NS reduces the dynamic telomere association of TRF1

Because NS does not affect the static amount of telomere-bound TRF1, we decided to use the FLIP (fluorescence loss in photobleaching) approach to investigate whether NS regulates the dynamic telomere association of TRF1 in live cells. We chose U2OS cells for the dynamic study because their TRF1–GFP signals give the best telomere-to-nucleoplasmic ratios compared with other cell lines we tested. Consistent with the ChIP result, we found that NS overexpression did not change the static distribution pattern of TRF1 as detected by immunofluorescence (Fig. 6A). To study the dynamic telomere association of TRF1, a FLIP paradigm was designed to measure the telomeric retention time of TRF1–GFP proteins. In the FLIP experiments, a 17×4.6 μm rectangular region in the nucleoplasm was repetitively bleached and the loss of the TRF1–GFP fluorescent signals at non-bleached telomeres was recorded over a period of 136 seconds (Fig. 6B). The validity of using the C-terminally GFP-fused TRF1 to track the distribution of endogenous TRF1 proteins was previously verified (Zhu et al., 2009). The time to reach half-maximal loss of TRF1 signals (mean decay half-time [$T_{1/2}$]) was used as a measurement of its telomeric retention time. Our FLIP results showed that NS decreases the telomeric retention of TRF1 (Fig. 6C). The average $T_{1/2}$ of NS-overexpressing cells (22.6 seconds) was significantly shorter than the $T_{1/2}$ of control cells (33.8 seconds) ($P<0.0001$, Repeated Measures ANOVA). Together, our data demonstrate that NS regulates the dynamic telomere association of TRF1, but not the static amount of telomere-bound TRF1 proteins.

NS decreases the formation of telomere-dysfunction-induced foci

Because overexpressed TRF1 reduces the telomere length presumably by blocking the telomerase from gaining access to the telomere (van Steensel and de Lange, 1997), we speculated that NS might help the repair of damaged telomeres by reducing the telomeric retention of TRF1. To test this possibility, we measured the number of telomere-dysfunction-induced (TIF) foci per cell by confocal colocalization of 53BP1 (p53 binding protein 1) and TRF1–GFP signals in $TRF2^{\Delta B\Delta M}$-transfected U2OS cells (Fig. 7A). 53BP1 was originally identified as a p53 binding partner (Iwabuchi et al., 1994) and later shown to be a DNA damage response protein that is rapidly recruited to sites of DNA damage (Anderson et al., 2001; Schultz et al., 2000). Notably, we found that NS had a significant effect in protecting against TIF formation in $TRF2^{\Delta B\Delta M}$-transfected cells (Fig. 7B). NS overexpression (NS-OE) reduced the number of $TRF2^{\Delta B\Delta M}$-induced TIF per cell from 4.3 (± 0.2) down to 1.8 (± 0.2) ($P<0.0001$, *t*-test). This effect was TIF-specific, because NS did not change the number of non-telomere-related DNA damage foci per cell (non-TIF, defined by the $53BP1^{+}$/TRF1–GFP^{-}

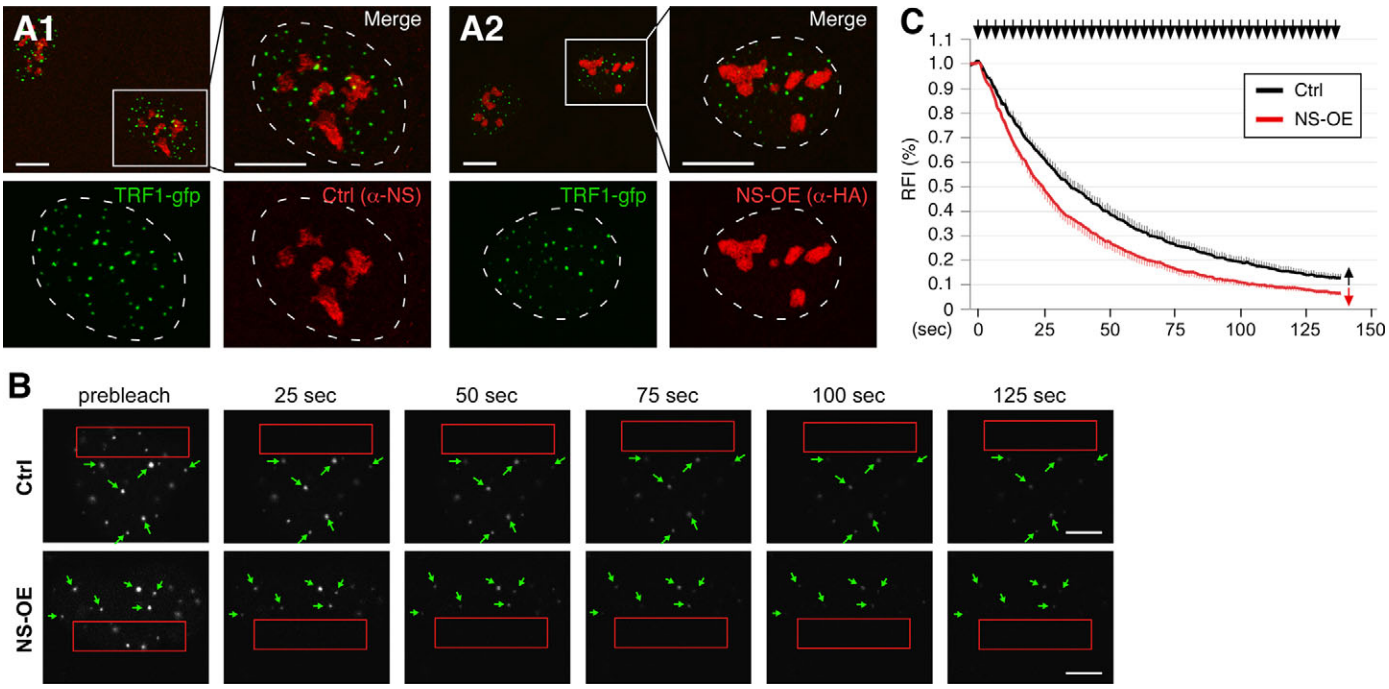

Fig. 6. NS shortens the telomeric retention time of TRF1. (**A**) Confocal studies show that the static distribution of TRF1–GFP is not changed by overexpression of HA-tagged NS (NS-OE) in U2OS cells. Right and bottom panels show enlarged areas indicated by the small rectangles in the left upper panels. Dashed lines demarcate the nucleo-cytoplasmic boundary. (**B**) The dynamic telomere association of TRF1 was measured its telomeric retention time using the fluorescence loss in photobleaching (FLIP) approach in U2OS cells. Time-sequenced images with labels indicating the bleached areas (red rectangles), measured telomeres (green arrows) and intervals between image acquisition and the first bleaching pulse (in seconds) are shown. (**C**) NS-OE significantly decreases the telomeric retention time of TRF1 ($P<0.0001$, by Repeated Measures ANOVA). Error bars represent s.e.m., shown on one side (indicated by arrows) of the curves. *Y*-axis represents the relative fluorescence index (RFI). Top arrows indicate bleaching pulses. Scale bars: 10 μm (A) and 5 μm (B).

signal). The numbers of non-TIF foci per cell are 6.5 ($\pm$0.5) and 6.2 ($\pm$0.4) in the control (Ctrl) and NS-OE groups, respectively ($P=0.56$). It is also not caused by changing the number of TRF1–GFP foci per cell (36.9$\pm$1.1 versus 35.5$\pm$1.0 in the control and NS-OE groups, respectively, $P=0.38$). To check whether this effect of NS correlates with its ability to decrease the telomeric retention of TRF1, we measured the FLIP rate of TRF1 in control and NS-overexpressing cells when telomeres were damaged (Fig. 7C). The FLIP results showed that the telomere-associated TRF1 was more dynamic under the TRF2$^{\Delta B\Delta M}$-transfected condition ($T_{1/2}=26.3$ seconds, black line) compared with the control condition ($T_{1/2}=33.8$ seconds, blue line) ($P<0.01$, Repeated Measures ANOVA) (Fig. 7D). Upon telomere damage, NS was capable of further lowering the telomeric retention time of TRF1 ($T_{1/2}=18.8$ seconds, red line) ($P<0.05$, Repeated Measures ANOVA). These results show that NS can shorten the dynamic association of TRF1 with the telomere and prevent the formation of TIF in TRF2$^{\Delta B\Delta M}$-transfected cells.

Discussion

NS and GNL3L regulate TRF1 dimerization in opposite directions

It is known that TRF1 binds telomeric DNAs as homodimers, but it is not clear whether non-telomere-bound TRF1 dimerizes first in the nucleoplasm or does so during its binding to the telomere. In an attempt to determine the differential activities of NS and GNL3L on TRF1 regulation, we uncovered an extrachromosomal mechanism that operates bidirectionally to inhibit or promote TRF1 dimerization (Fig. 8). Because NS and GNL3L do not bind telomeric DNAs by themselves or through TRF1 or TRF2, such activities most likely occur outside the telomere. In a previous report, we found that GNL3L can promote the dimerization and telomeric association of TRF1 (Zhu et al., 2009), Here, we discover that NS binding decreases the GNL3L binding and homodimerization of TRF1. The ability of NS and GNL3L to compete against each other for TRF1 binding is probably caused by a steric hindrance effect, because all NS and GNL3L mutants with the ability to bind TRF1 are capable of doing so. NS and GNL3L interact with separate domains of TRF1, that is, the undefined domain and homodimerization domain (HBD, also known as TRF homology or TRFH), respectively. Because the HBD domain of TRF1 also serves as its binding interface for TIN2 (Chen et al., 2008), this might explain why GNL3L can compete against TIN2 for TRF1 binding but NS cannot. Mutant analyses showed that NSΔB and NSΔG have the ability to block the GNL3L binding but not the dimerization of TRF1, indicating that the NS ability to perturb TRF1 dimerization is not determined by its ability to displace TRF1-bound GNL3L.

NS reduces the telomeric retention time of TRF1

Since TRF1 binds telomeric DNAs as dimers, the NS-mediated inhibition on TRF1 dimerization may decrease its telomeric association. Even though this idea is consistent with our EMSA result, it is not supported by the telomere ChIP data, which show that the amount of telomere-bound TRF1 in vivo is not affected by NS perturbation. Instead, the NS effect is mainly on the dynamic association between TRF1 and the telomere. Based on these findings, we speculate that NS might have a function in

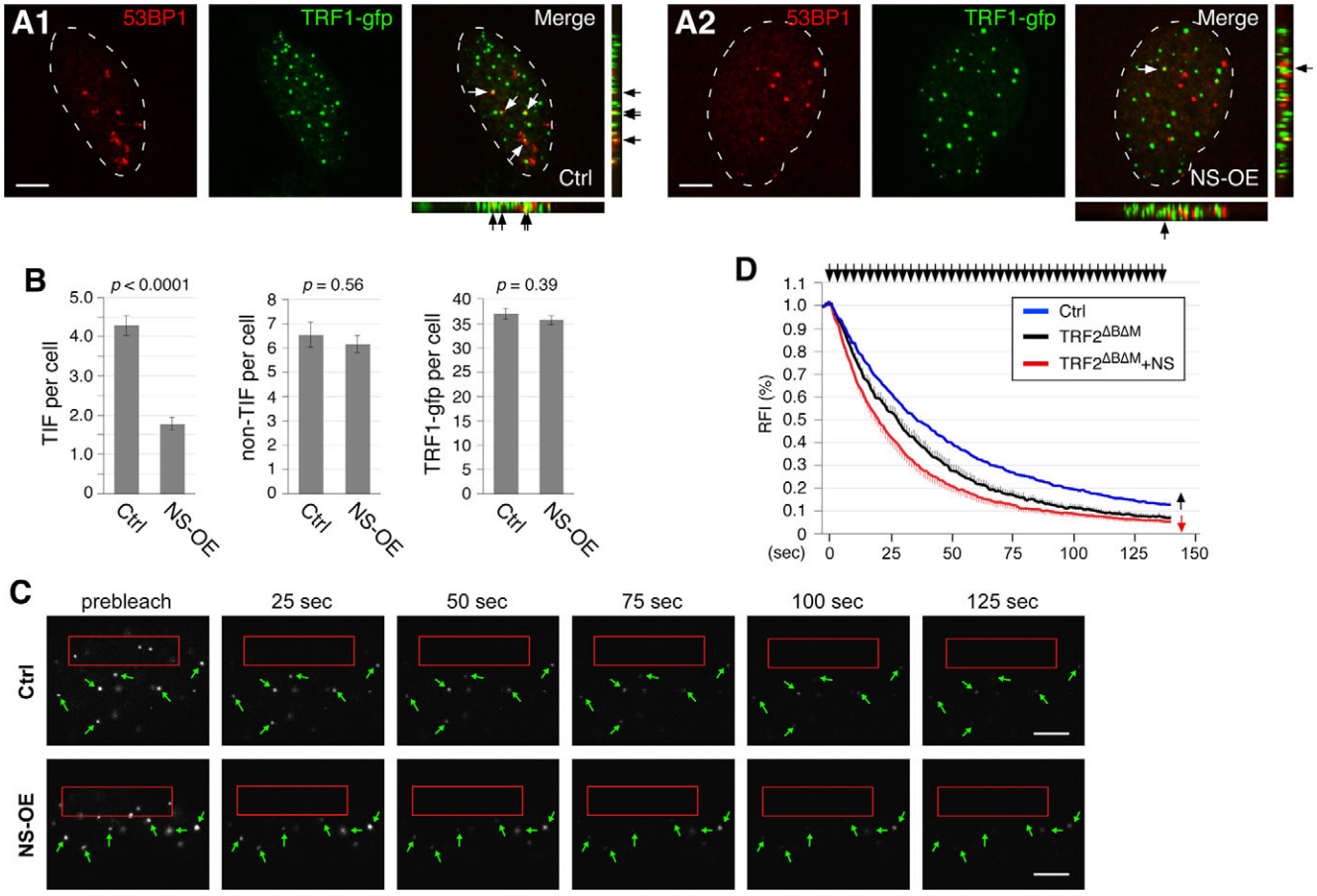

Fig. 7. NS decreases formation of telomere-dysfunction-induced foci and the telomeric retention time of TRF1 in TRF2$^{\Delta B\Delta M}$-transfected cells. (**A**) TIF formation was induced by TRF2$^{\Delta B\Delta M}$ transfection in U2OS cells. The number of TIF per cell was measured by confocal colocalization of 53BP1 and TRF1–GFP signals in control (A1) and NS-OE (A2) cells. (**B**) NS shows a significant effect in reducing the number of TIF per cell (left), but has no effect on the number of non-telomere-related DNA damage foci (non-TIF, middle), as defined by the 53BP1^{+}/TRF1–GFP^{-} signal, or the number of total TRF1–GFP foci per cell (right). (**C**) Time-sequenced FLIP images of TRF2$^{\Delta B\Delta M}$-transfected U2OS cells (see Fig. 6B for label description). (**D**) The FLIP results show that TRF2$^{\Delta B\Delta M}$ expression decreases the telomeric retention time of TRF1 (black line) compared with the control-transfected cells (blue line) ($P<0.01$), which supports the idea that TRF2$^{\Delta B\Delta M}$ destabilizes the telomere-capping complex. Overexpression of NS further accelerates the exchange rate between telomere-bound and unbound TRF1 proteins (red line) ($P=0.02$). Scale bars: 5 μm.

promoting the dynamic exchange between the telomere-bound and unbound TRF1 proteins by shifting the nucleoplasmic TRF1 from the dimer pool to the monomer pool.

Biological implications of NS-regulated TRF1 dynamics

It has been shown that one of the functions of TRF1 is to block the telomere access by the telomerase, which negatively affects the telomere length (van Steensel and de Lange, 1997). At the same time, TRF1 also has a crucial role in protecting the integrity of the telomere (Martinez et al., 2009). How these two activities of TRF1 work in sync at the cellular level needs further clarification. We propose that the telomere-bound TRF1 consists of two dynamically distinct pools of proteins. The dynamic TRF1 population is constantly shifting between the telomere-bound state and the non-telomere-bound state, whereas the stabilized TRF1 population is held in place by the formation of the telomere-capping complex and undergoes little exchange with the non-telomere-bound TRF1. We speculate that the fast-exchanging component of the telomere-bound TRF1 serves as the precursor of the highly organized telomere complex on one hand and prevent the telomere access by the telomere remodelling or repair machinery on the other hand.

The NS function described in this study primarily affects the retention time of the dynamic (or destabilized) pool of telomere-bound TRF1, and, therefore, might allow the remodelling and repair proteins better access to the telomeric DNAs. Given the preferential expression of NS and GNL3L in the undifferentiated and differentiated cells, respectively, and their opposite roles in regulating TRF1 dimerization, one might infer that the telomere-remodeling capability differs from cell to cell. Undifferentiated cells, which express high levels of NS and low levels of GNL3L, might be more active in telomere remodeling and repair than differentiated cells, which express low levels of NS and high levels of GNL3L. Because NS and GNL3L are separate genes only in vertebrates (Tsai and Meng, 2009), such expansion of the functional repertoire in telomere regulation probably arose during the evolution of the vertebrate lineage. Of note, the NS effect on telomere damage prevention was determined in U2OS cells, chosen for their superior imaging quality of TRF1–GFP and 53BP1 signals for both static and dynamic studies. U2OS cells belong to the alternative lengthening of telomeres (ALT) cell type that uses the homologous recombination (HR) instead of the telomerase-dependent mechanism for telomere remodeling and repair (Bryan

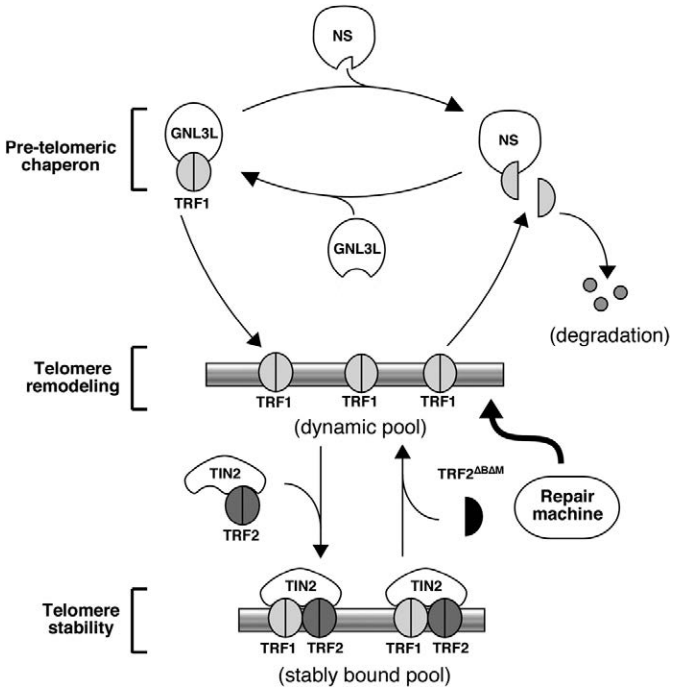

Fig. 8. Opposing regulation of TRF1 dimerization and telomere association by NS and GNL3L. We propose that the dimerization of TRF1 is oppositely regulated by NS and GNL3L before it binds to the telomere. In this pre-telomeric phase, GNL3L promotes and NS inhibits the dimerization of non-telomere-bound TRF1. The relative amount of TRF1 monomers versus dimers in the nucleoplasm determines the telomeric retention time of a dynamic pool of telomere-bound TRF1, which might serve the function of blocking the telomeric access of telomere remodelling and repair proteins and as the precursor for the stably bound TRF1 that protects the integrity of the telomere.

et al., 1997; Bryan et al., 1995). Therefore, it is possible that if TRF1 differentially affects the telomere access of telomerase and HR proteins in telomerase-active and ALT cells, respectively, the function of NS on telomere damage prevention might also differ in these two cell types.

In conclusion, this study shows that NS and GNL3L act as chaperone proteins that regulate the monomeric versus dimeric forms of non-telomere-bound TRF1. Even though NS and GNL3L do not take part in the formation of the telomere-capping complex, they modulate the dynamics of telomere-bound TRF1, and NS, in particular, has the ability to prevent telomere damage in TRF2$^{\Delta B\Delta M}$-transfected cells.

Materials and Methods

cDNA constructs and antibodies

Deletions, point mutations and epitope tagging were introduced using the stitching PCR strategy as described previously (Meng et al., 2007; Tsai and McKay, 2005). The N-terminal FLAG-tagged TRF2$^{\Delta B\Delta M}$ construct (containing aa 45–454) was obtained from Zhou Songyang (Baylor College of Medicine, Houston, TX). Primary antibodies used here include those against HA (HA.11, Covance), Myc (9E10, Covance), FLAG (M2, Sigma), TRF1 (TRF-78, Chemicon), 53BP1 (4937, Cell Signaling), NS (Ab2438, Ab1164 and Ab138) and GNL3L (Ab134).

Cell culture

Procedures for cell culture and plasmid transfection were described in our previous work (Meng et al., 2007). All biochemical studies were performed in vitro or in HEK293 cells (Figs 1–5). Dynamic studies were conducted in U2OS cells (Figs 6, 7).

GST pull-down assays and protein purification

For pull-down experiments, GST fusion proteins were expressed using the pGEX 4T-2 vector in BL21/DE3 cells (Tsai and McKay, 2002). Epitope-tagged proteins were expressed in HEK293 cells and extracted in phosphate-buffered saline (PBS) with Triton X-100 (1%). Sepharose-bound GST fusion proteins (1–2 μg) were used for each reaction. To purify NS and GNL3L proteins, GST-fused recombinant proteins were expressed in BL21/DE3 bacteria, purified by glutathione beads, and released from the GST backbone by thrombin cleavage.

Coimmunoprecipitation

Protein lysates were extracted in NTEN buffer and incubated with primary antibody and Protein-G–Sepharose beads (Amersham) for 4 hours at 4℃. Immunoprecipitates were washed with RIPA buffer before SDS-PAGE. For two-step coimmunoprecipitation, the TRF1 (FLAG-tagged) complex was precipitated using anti-FLAG antibody and eluted by FLAG peptide incubation. The co-complex of TRF1 (FLAG-tagged) and GNL3L (HA-tagged) was subsequently immunoprecipitated from the TRF1 complex using the anti-HA antibody.

Electrophoretic mobility shift assay

EMSA experiments were carried out based on the protocol described previously. Nuclear extracts were prepared from HEK293 cells transfected with the indicated constructs. To generate EMSA probes, the $(TTAGGG)_6$ primer was radiolabeled with [γ-^{32}P]ATP in a T4 kinase reaction, annealed with excess amounts of the $(CCCTAA)_6$ primer, and purified through QIAquick nucleotide removal columns (Qiagen). Reaction and gel electrophoresis conditions were described previously (Yasumoto et al., 2007; Zhu et al., 2009).

Chromatin immunoprecipitation

Cells were crosslinked using 1% formaldehyde, lysed in 50 mM Tris buffer with 1% SDS and sonicated to obtain chromatin fragments from 300 bp to 1 kb. The resulting lysates were incubated with antibodies and Protein-G–Sepharose. Chromosomal DNA was extracted from the immunoprecipitates by RNase-A and proteinase-K treatment and reverse crosslinking. DNA samples were dot blotted and hybridized with a ^{32}P-labeled $(TTAGGG)_4$ or Alu (5′-GGC CGG GCG CGG TGG CTC ACG CCT GTA ATC CCA GCA-3′) oligonucleotide probe. All lysates were normalized based on protein concentrations. A part of the lysate (1/20th) was used to measure the input DNA amount.

Fluorescence loss in photobleaching

Bleaching experiments were performed in U2OS cells grown on Nalgene Lab Tek II chamber slides by using a Zeiss LSM510 confocal microscope equipped with a 63× plan-apochromat oil objective, as described previously (Meng et al., 2007). The FLIP paradigm was modified based on a previously published method (Mattern et al., 2004). Specifically, we measured the dynamic telomere association of TRF1 by the rate of fluorescence loss of TRF1–GFP signals on unbleached telomeres while bleaching a 17×4.6 μm rectangular region within the nucleoplasm with repetitive bleaching pulses of 150 msecond duration and 787 msecond interval. Images were acquired with 3× confocal zoom. The telomeric relative fluorescence index (RFI) in bleached cells was normalized to the telomeric intensity of neighboring non-bleached cells after background subtraction using the calculation: $RFI=(I_t/I_0)*(C_0/C_t)$, where I_t and I_0 are the background-subtracted intensities of the telomere in the bleached cell at time-point t and before photobleaching, respectively (Phair and Misteli, 2000). C_t and C_0 are the background-subtracted intensities of the telomere in the neighboring non-bleached cell at time-point t and before photobleaching, respectively. The telomeric RFI were measured from 24 cells collected from two independent experiments. For every cell, the RFI represents the average of six telomeres in random positions.

Confocal quantification of telomere dysfunction-induced foci

TIF were determined by the colocalization of 53BP1 and TRF1–GFP signals. Images were acquired using a Zeiss LSM510 confocal microscope using a 63× plan-apochromat oil objective (1.4 NA). Scanning was set with a 512×512 frame size, 3× zoom, and <1.0 μm optical thickness. Stacked images of 60 cells were collected at 0.5 μm intervals from three independent experimental repeats, and using ImageJ 1.36b software.

Acknowledgements

We gratefully thank Zhou Songyang (Baylor College of Medicine, Houston, TX) for his gift of the TRF2$^{\Delta B\Delta M}$ construct. Special thanks go to His-Wen Tsai for his unwavering support of our work.

Funding

This work was supported by the National Institutes of Health [grant number RO1 CA113750]. Deposited in PMC for release after 12 months.

References

Anderson, L., Henderson, C. and Adachi, Y. (2001). Phosphorylation and rapid relocalization of 53BP1 to nuclear foci upon DNA damage. *Mol. Cell Biol.* **21**, 1719-1729.

Baddoo, M., Hill, K., Wilkinson, R., Gaupp, D., Hughes, C., Kopen, G. C. and Phinney, D. G. (2003). Characterization of mesenchymal stem cells isolated from murine bone marrow by negative selection. *J. Cell Biochem.* **89**, 1235-1249.

Bianchi, A., Smith, S., Chong, L., Elias, P. and de Lange, T. (1997). TRF1 is a dimer and bends telomeric DNA. *EMBO. J.* **16**, 1785-1794.

Broccoli, D., Smogorzewska, A., Chong, L. and de Lange, T. (1997). Human telomeres contain two distinct Myb-related proteins, TRF1 and TRF2. *Nat. Genet* **17**, 231-235.

Bryan, T. M., Englezou, A., Gupta, J., Bacchetti, S. and Reddel, R. R. (1995). Telomere elongation in immortal human cells without detectable telomerase activity. *EMBO. J.* **14**, 4240-4248.

Bryan, T. M., Englezou, A., Dalla-Pozza, L., Dunham, M. A. and Reddel, R. R. (1997). Evidence for an alternative mechanism for maintaining telomere length in human tumors and tumor-derived cell lines. *Nat. Med.* **3**, 1271-1274.

Chang, W., Dynek, J. N. and Smith, S. (2003). TRF1 is degraded by ubiquitin-mediated proteolysis after release from telomeres. *Genes Dev.* **17**, 1328-1333.

Chen, Y., Yang, Y., van Overbeek, M., Donigian, J. R., Baciu, P., de Lange, T. and Lei, M. (2008). A shared docking motif in TRF1 and TRF2 used for differential recruitment of telomeric proteins. *Science* **319**, 1092-1096.

Chong, L., van Steensel, B., Broccoli, D., Erdjument-Bromage, H., Hanish, J., Tempst, P. and de Lange, T. (1995). A human telomeric protein. *Science* **270**, 1663-1667.

de Lange, T. (2005). Shelterin: the protein complex that shapes and safeguards human telomeres. *Genes Dev.* **19**, 2100-2110.

Iwabuchi, K., Bartel, P. L., Li, B., Marraccino, R. and Fields, S. (1994). Two cellular proteins that bind to wild-type but not mutant p53. *Proc. Natl. Acad. Sci. USA* **91**, 6098-6102.

Jiang, W. Q., Zhong, Z. H., Henson, J. D. and Reddel, R. R. (2007). Identification of candidate alternative lengthening of telomeres genes by methionine restriction and RNA interference. *Oncogene* **26**, 4635-4647.

Kim, M. K., Kang, M. R., Nam, H. W., Bae, Y. S., Kim, Y. S. and Chung, I. K. (2008). Regulation of telomeric repeat binding factor 1 binding to telomeres by casein kinase 2-mediated phosphorylation. *J. Biol. Chem.* **283**, 14144-14152.

Lee, T. H., Perrem, K., Harper, J. W., Lu, K. P. and Zhou, X. Z. (2006). The F-box protein FBX4 targets PIN2/TRF1 for ubiquitin-mediated degradation and regulates telomere maintenance. *J. Biol. Chem.* **281**, 759-768.

Maki, N., Takechi, K., Sano, S., Tarui, H., Sasai, Y. and Agata, K. (2007). Rapid accumulation of nucleostemin in nucleolus during newt regeneration. *Dev. Dyn.* **236**, 941-950.

Martinez, P., Thanasoula, M., Munoz, P., Liao, C., Tejera, A., McNees, C. Flores, J. M., Fernández-Capetillo, O., Tarsounas, M. and Blasco, M. A. (2009). Increased telomere fragility and fusions resulting from TRF1 deficiency lead to degenerative pathologies and increased cancer in mice. *Genes Dev.* **23**, 2060-2075.

Mattern, K. A., Swiggers, S. J., Nigg, A. L., Lowenberg, B., Houtsmuller, A. B. and Zijlmans, J. M. (2004). Dynamics of protein binding to telomeres in living cells: implications for telomere structure and function. *Mol. Cell Biol.* **24**, 5587-5594.

Meng, L., Zhu, Q. and Tsai, R. Y. (2007). Nucleolar trafficking of nucleostemin family proteins: common versus protein-specific mechanisms. *Mol. Cell Biol.* **27**, 8670-8682.

Meng, L., Lin, T. and Tsai, R. Y. (2008). Nucloplasmic mobilization of nucleostemin stabilizes MDM2 and promotes G2-M progression and cell survival. *J. Cell Sci.* **121**, 4037-4046.

Ohmura, M., Naka, K., Hoshii, T., Muraguchi, T., Shugo, H., Tamase, A. et al. (2008). Identification of stem cells during prepubertal spermatogenesis via monitoring of nucleostemin promoter activity. *Stem. Cells* **26**, 3237-3246.

Phair, R. D. and Misteli, T. (2000). High mobility of proteins in the mammalian cell nucleus. *Nature* **404**, 604-609.

Potts, P. R. and Yu, H. (2005). Human MMS21/NSE2 is a SUMO ligase required for DNA repair. *Mol. Cell Biol.* **25**, 7021-7032.

Schultz, L. B., Chehab, N. H., Malikzay, A. and Halazonetis, T. D. (2000). p53 binding protein 1 (53BP1) is an early participant in the cellular response to DNA double-strand breaks. *J. Cell Biol.* **151**, 1381-1390.

Siddiqi, S., Gude, N., Hosoda, T., Muraski, J., Rubio, M., Emmanuel, G., Fransioli, J., Vitale, S., Parolin, C., D'Amario, D. et al. (2008). Myocardial induction of nucleostemin in response to postnatal growth and pathological challenge. *Circ. Res.* **103**, 89-97.

Smith, S., Giriat, I., Schmitt, A. and de Lange, T. (1998). Tankyrase, a poly(ADP-ribose) polymerase at human telomeres. *Science* **282**, 1484-1487.

Songyang, Z. and Liu, D. (2006). Inside the mammalian telomere interactome: regulation and regulatory activities of telomeres. *Crit. Rev. Eukaryot. Gene Expr.* **16,** 103-118.

Tsai, R. Y. (2009). Nucleolar modulation of TRF1: a dynamic way to regulate telomere and cell cycle by nucleostemin and GNL3L. *Cell Cycle.* **8**, 2912-2916.

Tsai, R. Y. and McKay, R. D. (2002). A nucleolar mechanism controlling cell proliferation in stem cells and cancer cells. *Genes Dev.* **16**, 2991-3003.

Tsai, R. Y. and McKay, R. D. (2005). A multistep, GTP-driven mechanism controlling the dynamic cycling of nucleostemin. *J. Cell Biol.* **168**, 179-184.

Tsai, R. Y. and Meng, L. (2009). Nucleostemin: A latecomer with new tricks. *Int. J. Biochem. Cell Biol.* **41**, 2122-2124.

van Steensel, B. and de Lange, T. (1997). Control of telomere length by the human telomeric protein TRF1. *Nature* **385**, 740-743.

van Steensel, B., Smogorzewska, A. and de Lange, T. (1998). TRF2 protects human telomeres from end-to-end fusions. *Cell* **92**, 401-413.

Wu, Z. Q., Yang, X., Weber, G. and Liu, X. (2008). Plk1 phosphorylation of TRF1 is essential for its binding to telomeres. *J. Biol. Chem.* **283**, 25503-25513.

Yasumoto, H., Meng, L., Lin, T., Zhu, Q. and Tsai, R. Y. (2007). GNL3L inhibits activity of estrogen-related receptor {gamma} by competing for coactivator binding. *J. Cell Sci.* **120**, 2532-2543.

Zhou, X. Z., Perrem, K. and Lu, K. P. (2003). Role of Pin2/TRF1 in telomere maintenance and cell cycle control. *J. Cell Biochem.* **89**, 19-37.

Zhu, Q., Yasumoto, H. and Tsai, R. Y. (2006). Nucleostemin delays cellular senescence and negatively regulates TRF1 protein stability. *Mol. Cell Biol.* **26**, 9279-9290.

Zhu, Q., Meng, L., Hsu, J. K., Lin, T., Teishima, J. and Tsai, R. Y. (2009). GNL3L stabilizes the TRF1 complex and promotes mitotic transition. *J. Cell Biol.* **185**, 827-839.

Oncogene (2011) 30, 1716–1726

www.nature.com/onc

ORIGINAL ARTICLE

GNL3L depletion destabilizes MDM2 and induces p53-dependent G2/M arrest

L Meng, JK Hsu and RYL Tsai

Center for Cancer and Stem Cell Biology, Alkek Institute of Biosciences and Technology, Texas A and M Health Science Center, Houston, TX, USA

Guanine nucleotide binding protein-like 3-like (GNL3L) is a nucleolar protein and the vertebrate paralogue of nucleostemin (NS). We previously reported that nucleoplasmic mobilization of NS stabilizes MDM2 (*mouse double minute 2*). Here, we investigated the role of GNL3L as a novel MDM2 regulator. We found that GNL3L binds MDM2 *in vivo* and displays the same function as NS in stabilizing MDM2 protein and preventing its ubiquitylation. The interaction between GNL3L and MDM2 also takes place in the nucleoplasm. However, the MDM2 regulatory activity of GNL3L occurs constitutively and does not so much depend on the nucleolar release mechanism as NS does. GNL3L depletion triggers G2/M arrest in the p53-wild-type HCT116 cells more than in the p53-null cells, and upregulates specific p53 targets (that is, Bax, 14-3-3σ and p21) without affecting the ubiquitylation or stability of p53 proteins. The inhibitory activity of GNL3L on p53-mediated transcription correlates with the increased expression of GNL3L and reduced expression of 14-3-3σ and p21 in human gastrointestinal tumors. This work shows that in contrast to most nucleolar proteins that negatively control MDM2, GNL3L and NS are the only two that are designed to stabilize MDM2 protein under basal or induced condition, respectively, and may act as tumor-promoting genes.
Oncogene (2011) **30,** 1716–1726; doi:10.1038/onc.2010.550; published online 6 December 2010

Keywords: colorectal carcinoma; G2/M arrest; GNL3L; MDM2; nucleostemin; p53

Introduction

As proteins residing in the nucleolus are being cataloged systematically, so is the focus on this classic organelle turned from its ribosomal function to non-ribosomal role (Pederson and Tsai, 2009). Nucleostemin (NS) is one of the nucleolar proteins shown to be capable of exercising non-ribosomal activities. It is preferentially expressed by undifferentiated stem/progenitor cells undergoing active proliferation, and has an essential role in early embryogenesis and self-renewal. The vertebrate NS family includes three members—NS, guanine nucleotide binding protein-like 3-like (GNL3L) and Ngp-1, all of which contain a unique MMR1_HSR1 domain of five guanosine-5′-triphosphate-binding motifs arranged in a circularly permuted order (Tsai and Meng, 2009). NS and GNL3L are vertebrate paralogues that share a common invertebrate orthologue, whereas Ngp-1 exists as a single gene from yeast to human.

Mammalian NS was first cloned as a neural stem cell-enriched gene (Tsai and McKay, 2002), and was later found to be abundantly expressed by other stem cell types, cancer cells and the adult testis (Baddoo *et al*., 2003; Maki *et al*., 2007; Ohmura *et al*., 2008; Siddiqi *et al*., 2008). In contrast, GNL3L is expressed at lower levels in the undifferentiated neural stem cells than in their differentiated progeny during neural development, and is preferentially expressed by the cerebellum and forebrain in adult animals (Yasumoto *et al*., 2007). At the subcellular level, NS is highly concentrated in the nucleolus, whereas GNL3L displays a higher nucleoplasmic intensity and a much shorter nucleolar retention time than NS (Meng *et al*., 2007). Among the NS-interacting proteins, functional outcomes have been shown for p53 (Tsai and McKay, 2002; Ma and Pederson, 2007), MDM2 (*mouse double minute 2*) (Dai *et al*., 2008; Meng *et al*., 2008), TRF1 (telomeric repeat binding factor 1) (Zhu *et al*., 2006), ARF (alternative reading frame) (Ma and Pederson, 2007) and RSL1D1 (ribosomal L1 domain containing 1) (Meng *et al*., 2006). So far, only three proteins, that is, the estrogen receptor-related protein, TERT (telomerase reverse transcriptase) and TRF1, have been shown to interact with GNL3L (Fu and Collins, 2007; Yasumoto *et al*., 2007; Zhu *et al*., 2009).

The biological importance of NS is best demonstrated by the early embryonic lethal phenotype of NS-null mice (Beekman *et al*., 2006; Zhu *et al*., 2006) and also by multiple studies showing its function in maintaining the continuous proliferation of cancer and stem cells. One of the proposed mechanisms for the NS activity is via MDM2 regulation. A study reported that NS depletion enhances MDM2 interaction with L5 and L11 and induces p53 activation (Dai *et al*., 2008). We found that nucleoplasmic mobilization of NS stabilizes MDM2 protein and inhibits the p53 transcription activity

Correspondence: Dr RYL Tsai, Center for Cancer and Stem Cell Biology, Alkek Institute of Biosciences and Technology, Texas A&M Health Science Center, 2121 W. Holcombe Blvd, Houston, TX 77030, USA.
E-mail: rtsai@ibt.tamhsc.edu
Received 2 April 2010; revised 1 October 2010; accepted 20 October 2010; published online 6 December 2010

(Meng *et al*., 2008). Reciprocally, MDM2 is responsible for the degradation of NS protein induced by guanine nucleotide depletion (Huang *et al*., 2009). Compared with NS, the GNL3L function is much less explored. It has been shown to negatively regulate the telomere length (Fu and Collins, 2007) and to promote the metaphase-to-anaphase transition via TRF1 stabilization (Zhu *et al*., 2009). So far, it is not clear whether GNL3L regulates the MDM2/p53 pathway or how it relates to the MDM2-stabilizing activity of NS.

Given the paralogous relationship between NS and GNL3L, we began to investigate the possibility that GNL3L may be a novel MDM2 regulator that functions redundantly with or distinctively from NS. Here, we report that GNL3L can stabilize MDM2 protein by preventing its ubiquitylation, and rescue the NS-knockdown-induced MDM2 ubiquitylation. Unlike NS, the anti-MDM2-ubiquitylation activity of GNL3L occurs constitutively and is not as much controlled by the nucleolar release mechanism as in the case of NS. Consistent with its MDM2-stabilizing ability, GNL3L knockdown triggers G2/M arrest and upregulates specific p53 downstream targets, that is, Bax, 14-3-3σ and p21, more so in the p53-wild-type than in the p53-null HCT116 cells. In accordance, high percentages of human colorectal and gastric cancers express high levels of GNL3L and low levels of 14-3-3σ and p21. This work indicates a potential role of GNL3L as a tumor-promoting factor via MDM2 stabilization.

Results

GNL3L binds MDM2 via its G- or I-domain and the central domain of MDM2

A connection between GNL3L and MDM2 was first revealed by coimmunoprecipitation (coIP) of MDM2 (Myc-tagged) and NS family proteins (hemagglutinin (HA)-tagged), which showed that both NS and GNL3L can be coimmunoprecitated with MDM2 by anti-Myc (rows 1 and 2) or anti-HA antibody (rows 3 and 4) (Figure 1a). In contrast, little or no Ngp-1 interacts with MDM2. Endogenous coIP further confirmed that GNL3L and MDM2 coreside in the same protein complex immunoprecipitated by anti-MDM2 or anti-GNL3L antibody in HeLa cells (Figure 1b). To investigate the MDM2-binding relationship between NS and GNL3L, anti-FLAG coIP of expressed MDM2 (FLAG), GNL3L (HA) and/or NS (Myc) was performed in

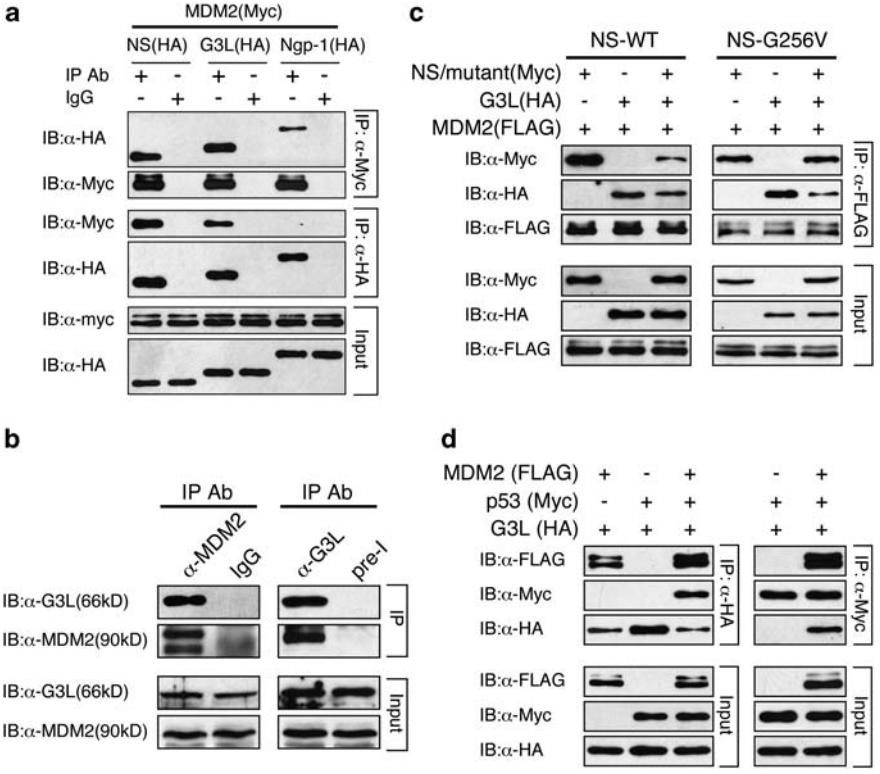

Figure 1 GNL3L competes against NS for MDM2 binding. (**a**) MDM2 (Myc) and NS family proteins (HA) were coimmunoprecipitated and immunoblotted (IB) by antitag antibodies in HEK293 cells. The results showed that MDM2 preferentially interacts with NS and GNL3L. (**b**) Endogenous binding between MDM2 and GNL3L was demonstrated by anti-MDM2 (*left panel*) and anti-GNL3L (*right panel*) coIP experiments. Immunoglobulin G and preimmune serum-precipitated (pre-I) samples were used as controls. (**c**) Anti-FLAG coIP of GNL3L (HA), NS (Myc) and MDM2 (FLAG) showed that GNL3L and NS compete against each other for MDM2 binding. By comparison, GNL3L shows more binding with MDM2 than wild-type NS does (*left panel*) and less binding with MDM2 than NS-G256V does (*right panel*). NS-G256V is a nucleoplasm-mislocalized mutant of NS (Supplementary Figure S1b3). (**d**) Triple coIP of GNL3L (HA), MDM2 (FLAG) and p53 (Myc) by anti-HA (*left panel*) or anti-Myc antibody (*right panel*) shows that GNL3L may bind p53 indirectly through MDM2.

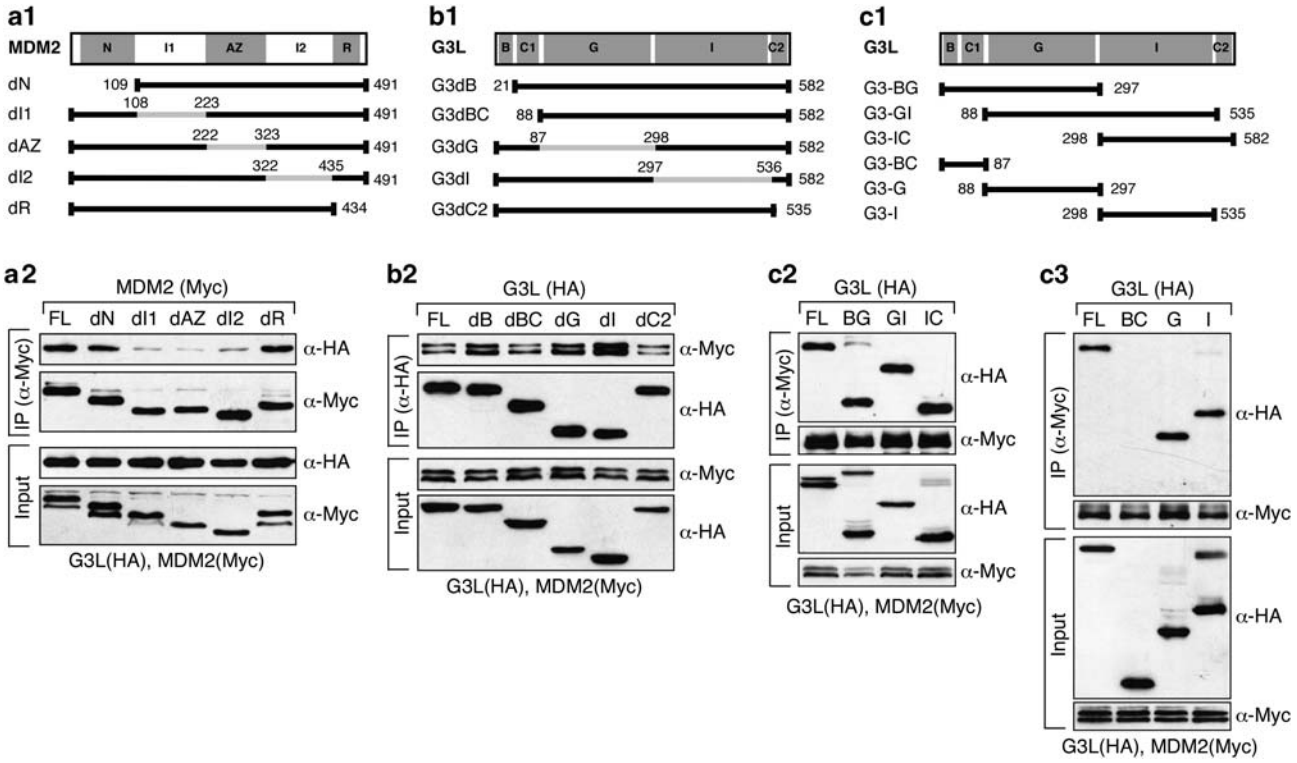

Figure 2 GNL3L binds the central domain of MDM2 via its guanosine-5′-triphosphate (GTP)-binding or intermediate domain. Diagrams show MDM2 (**a1**) and GNL3L single- (**b1**) or multi-domain (**c1**) deletion mutants. Gray lines and numbers indicate the deleted regions and amino acid positions. CoIP showed that binding between GNL3L and MDM2 requires the I1, AZ and I2 domains of MDM2 (**a2**) and the G- or I-domain of GNL3L (**b2**, **c2**, **c3**). N, p53-binding; I1 and I2, intermediate-1 and -2; AZ, acidic zinc-finger; R, RING-finger; B, basic; C, coiled-coil; G, GTP-binding and I, intermediate.

HEK293 cells and showed that GNL3L appears to have a stronger activity in competing against NS for MDM2 binding than NS does against GNL3L (Figure 1c, *left panel*). The better MDM2 binding of GNL3L than that of NS may be caused by their differential nucleoplasmic distribution (see Supplementary Figure S1). To examine this possibility, we conducted the same competitive coIP experiment using wild-type GNL3L and NS-G256V mutant, which is mislocalized to the nucleoplasm but still maintains its MDM2-binding activity. The results showed that NS-G256V displays a stronger MDM2-binding activity compared with GNL3L (Figure 1c, *right panel*). Finally, triple coIP demonstrated that GNL3L does not bind p53 directly but does so in the presence of MDM2, suggesting that MDM2 may bridge between GNL3L and p53 (Figure 1d).

The binding interface between MDM2 and GNL3L was defined by non-overlapping deletion mutants of MDM2 on its p53-binding (N, aa (amino acid) 1–108), intermediate-1 (aa 109–222), acidic zinc-finger (aa 223–322), intermediate-2 (aa 323–434) and RING-finger domains (R, aa 435–491) (Figure 2a1). Anti-Myc coIP of MDM2 mutants (Myc) and full-length GNL3L-HA showed that deleting the intermediate-1 (dI1), acidic zinc-finger (dAZ) or intermediate-2 domain (dI2) of MDM2 reduces its ability to bind GNL3L (Figure 2a2). To map the MDM2-binding site(s) on GNL3L, GNL3L mutants lacking the basic (B, aa 1–20), basic-coiled-coil (BC, aa 1–87), guanosine-5′-triphosphate-binding (G, aa 88–297), intermediate (I, aa 298–535) or C2 (aa 536–582) domain were created (Figure 2b1). Anti-HA coIP of full-length MDM2-Myc and mutant GNL3L (HA) showed that none of the single domain deletion mutants of GNL3L lose their ability to bind MDM2 and suggested the involvement of multiple GNL3L domains (Figure 2b2). CoIP of complex deletion mutants of GNL3L (Figure 2c1) confirmed that both the G and I-domains of GNL3L are sufficient to bind MDM2 (Figure 2c2 and c3). These data demonstrate that the interaction between GNL3L and MDM2 is mediated by the central region of MDM2 and the G or I domain of GNL3L.

GNL3L stabilizes MDM2 protein by reducing its ubiquitylation

We investigated how GNL3L affects MDM2 and found that small interfering (si)RNA knockdown of GNL3L (siG3-2) reduces the amount of endogenous MDM2 protein in p53-inactive HeLa cells, which can be reversed by putting back a siG3-2-resistant GNL3L construct (G3L-siR) (Figure 3a). In consistence, GNL3L overexpression increases the endogenous MDM2 protein level in a dose-dependent manner (Figure 3b). We next determined the effect of GNL3L overexpression on MDM2 protein stability in cyclohexamide-treated H1299 cells expressing recombinant MDM2 proteins. Western results showed that MDM2

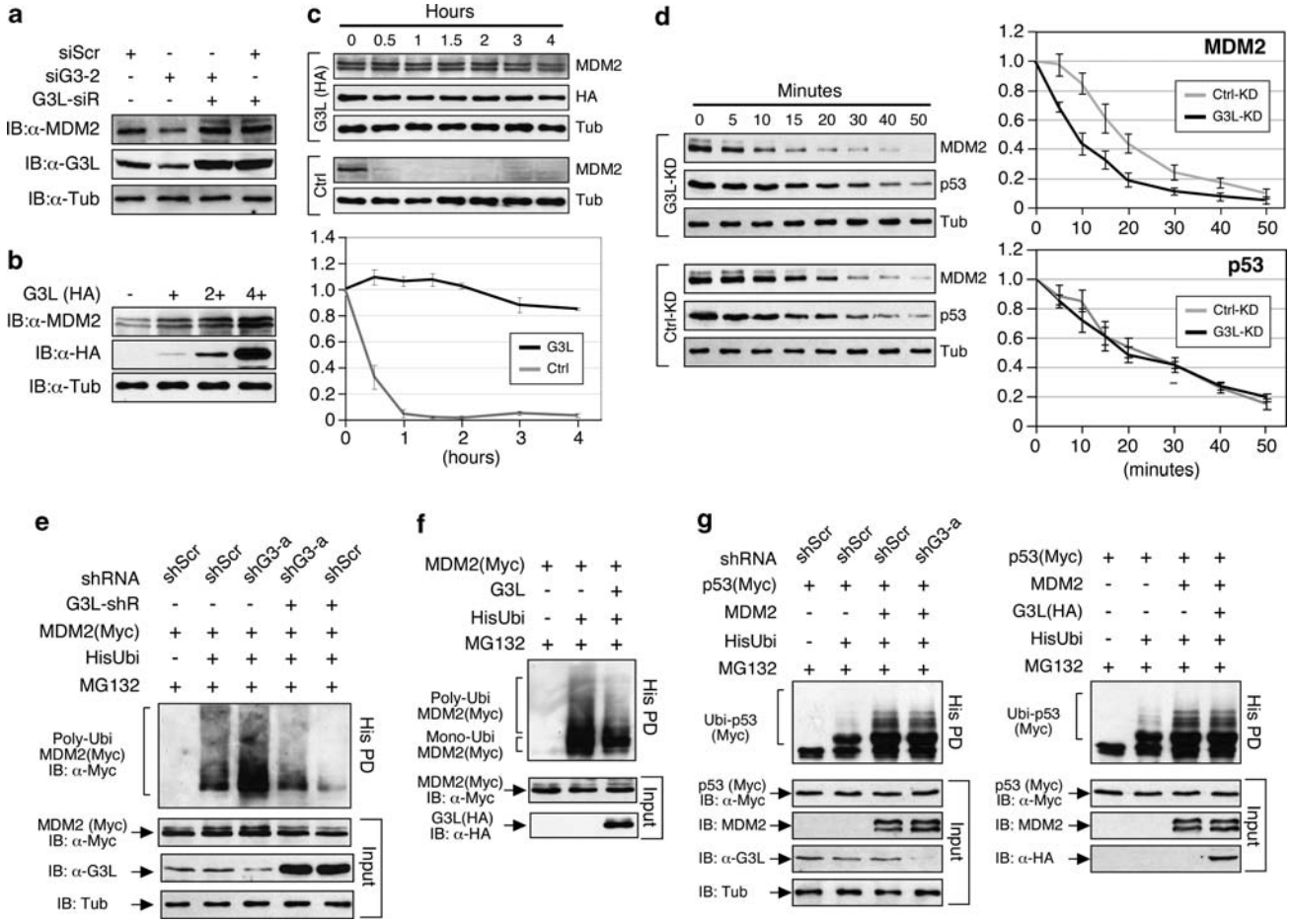

Figure 3 GNL3L stabilizes MDM2 protein by preventing its ubiquitylation. (**a**) Transient siRNA knockdown of GNL3L (siG3-2) in HeLa cells decreases the level of endogenous MDM2 proteins. This effect can be reversed by coexpression of a siG3-2-resistant GNL3L, G3L-siR. (**b**) Coexpression of GNL3L (HA) increases the protein level of endogenous MDM2 in a dose-dependent manner. (**c**) The effect of GNL3L on MDM2 protein stability was determined in H1299 cells transfected with MDM2 alone (Ctrl) or cotransfected with MDM2 and GNL3L (G3L). After cycloheximide treatment, the MDM2 protein amounts were measured, adjusted by their α-tubulin amounts, and expressed as percentages of the MDM2 protein amount at the 0 h time-point (bottom). (**d**) The cycloheximide experiment showed that GNL3L knockdown in HCT116-8 cells significantly reduces the protein stability of endogenous MDM2 ($n=3$, $P<0.005$, repeated measures analysis of variance) without affecting the stability of endogenous p53 ($P=0.27$). (**e**) HEK293 cells were transfected with the $(His)_6$-tagged ubiquitin, MDM2 and a control (shScr) or GNL3L-specific (shG3-a) shRNAmir construct. Ubiquitylated MDM2 products were precipitated by Ni^{2+} sepharose (His PD) and detected by anti-MDM2 antibody. GNL3L depletion increases the ubiquitylation of MDM2, and this effect can be rescued by a short-hairpin RNA-resistant GNL3L (G3L-shR). (**f**) Overexpression of wild-type GNL3L decreases MDM2 polyubiquitylation compared with the control sample. (**g**) GNL3L knockdown (*left panel*) or overexpression (*right panel*) has no effect on the MDM2-induced p53 ubiquitylation.

proteins in the GNL3L-overexpressing cells are degraded much slower than that in the control cells (Figure 3c, $P<0.0001$ by repeated measures analysis of variance). To confirm this finding, the endogenous MDM2 protein stability was measured in cycloheximide-treated HCT116-8 cells. GNL3L knockdown significantly reduces the stability of the endogenous MDM2 protein (protein half-life ($T_{1/2}$) = 8.4 min) as compared with the control knockdown ($T_{1/2}=17.2$ min, $n=3$, $P<0.005$ by repeated measures analysis of variance), but has no effect on the endogenous p53 protein stability ($P=0.27$) (Figure 3d). To investigate whether GNL3L regulates MDM2 ubiquitylation, HEK293 cells were transfected with $(His)_6$-tagged ubiquitin, MDM2 and GNL3L-targeting shRNAmir (shG3-a) constructs. Ubiquitylated proteins were captured by Ni^{2+}-chelating sepharose and detected by anti-MDM2 western blots. The results showed that GNL3L knockdown significantly increases the ubiquitylation of MDM2, and that this effect can be rescued by the shG3-a-resistant GNL3L (G3L-shR) (Figure 3e). Similarly, GNL3L overexpression decreases the amount of ubiquitylated MDM2 (Figure 3f). In consistence with the lack of effect of GNL3L on p53 protein stability, neither knockdown nor overexpression of GNL3L changes the amount of MDM2-mediated p53 ubiquitylation (Figure 3g).

GNL3L constitutively interacts with MDM2 in the nucleoplasm

To determine where GNL3L and MDM2 interact within the cell, HCT116-8 cells were transfected with green fluorescent protein-fused GNL3L and FLAG-tagged

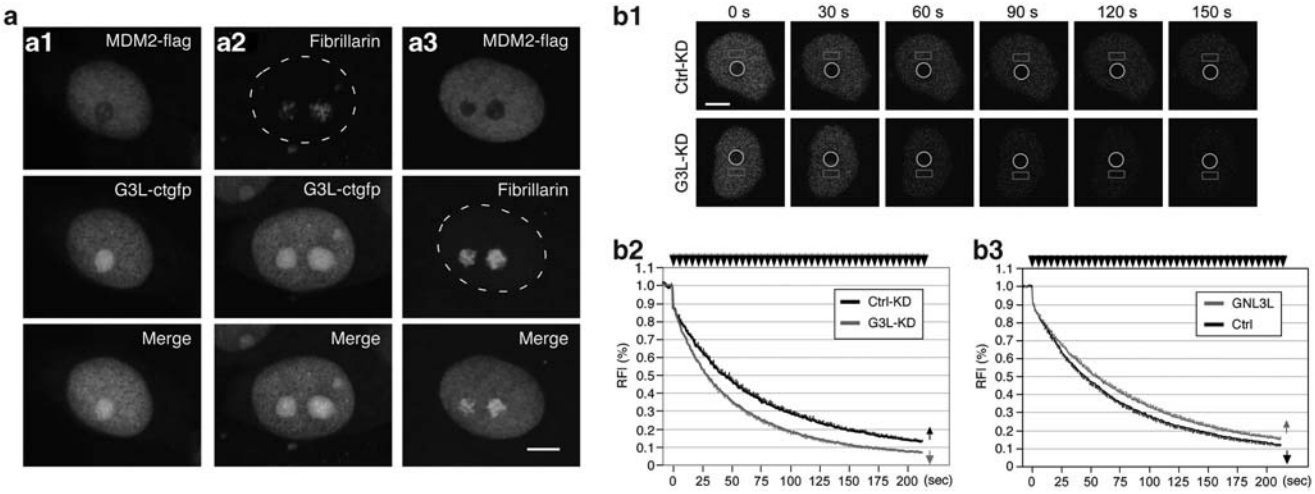

Figure 4 GNL3L colocalizes with MDM2 in the nucleoplasm. Knockdown of GNL3L increases the nucleolar-nucleoplasmic exchange rate of MDM2. (**a**) Confocal studies showed that green fluorescent protein (GFP)-fused GNL3L and FLAG-tagged MDM2 colocalize in the nucleoplasm of HCT116-8 cells and that coexpression of these two proteins does not change each other's distributions. Antifibrillarin staining labels the nucleolus in singly transfected cells. Bars show 5 μm. (**b1**) The exchange rate between the nucleolar and nucleoplasmic pools of MDM2 was measured in HCT116-8 cells by FLIP (fluorescence loss in photobleaching). The nucleolar signal of GFP-fused MDM2 was bleached repeatedly (circle) and the nucleoplasmic signal was recorded (rectangle). Time-sequenced images and their time intervals (in seconds) to the first bleaching pulse were shown. (**b2**) Knockdown of GNL3L (G3L-KD, in red) significantly increases the nucleolar-nucleoplasmic exchange rate of MDM2 ($P<0.01$). (**b3**) Overexpression of GNL3L exerts only a small effect on decreasing the exchange rate of MDM2 ($P=0.05$). Error bars represent s.e.m. shown in one direction (arrows in graph). The *y* axis represents the relative fluorescence index. Top arrows indicate bleaching pulses.

MDM2 individually or together. Confocal studies showed that GNL3L and MDM2 overlap considerably in the nucleoplasm but not in the nucleolus (Figure 4a). To show their dynamic interaction in living cells, FLIP (fluorescence loss during photobleaching) was used to determine the nucleolar-nucleoplasmic exchange rate of green fluorescent protein-fused MDM2, represented by the disappearance of its nucleoplasmic signal while bleaching the nucleolus (Meng *et al*., 2007). We reasoned that if GNL3L complexes with MDM2 in the nucleoplasm, the exchange rate of MDM2 will be increased by GNL3L knockdown. Indeed, the nucleolar-nucleoplasmic exchange rate of MDM2 is significantly increased by GNL3L knockdown (mean decay half-time ($T_{1/2}$) = 45.1 s) compared with the control-knockdown samples (Ctrl-KD, $T_{1/2}=28.7$ s, $P<0.01$ by repeated measures analysis of variance, $n=27$) (Figures 4b1 and b2). By contrast, overexpression of GNL3L has only a small effect on reducing the exchange rate of MDM2 ($P=0.05$ by repeated measures analysis of variance, $n=30$) (Figure 4b3), which may be due to the constitutive interaction between MDM2 and the endogenous GNL3L. This is in contrast to what we have found in NS, which shows a much clearer effect on the MDM2 FLIP rate when overexpressed than knocked down (Meng *et al*., 2008). These results demonstrate that GNL3L constitutively interacts with MDM2 in the nucleoplasm.

The MDM2-regulatory activity of GNL3L is constitutively active and does not depend on the nucleolar release mechanism

The FLIP results indicate that GNL3L binds MDM2 constitutively. We therefore hypothesize that the MDM2 ubiquitylation activity of GNL3L may also be constantly active and less regulated by the nucleolar release mechanism compared with that of NS. To test this, we first measured the effect of GNL3L and NS knockdown on MDM2 ubiquitylation and showed that GNL3L knockdown has a more profound effect in increasing MDM2 ubiquitylation than NS knockdown (Figure 5a). Next, we compared the MDM2 ubiquitylation effects of wild-type GNL3L and its nucleoplasm-mislocalized mutants. These mutations include deletion of its nucleolar localization signal (G3L-dB) or point mutation on the conserved guanosine-5′-triphosphate-binding residue (G3L-G253V) (Supplementary Figure S1). The results showed that these two nucleoplasmic forms of GNL3L show comparable activities in reducing MDM2 ubiquitylation to the wild-type GNL3L (Figure 5b). The effect of NS overexpression in reducing MDM2 ubiquitylation is slightly less than that of GNL3L overexpression. Notably, the MDM2-regulatory activity of NS nucleoplasmic mutants is significantly stronger compared not only with wild-type NS but also with wild-type and mutant GNL3L, indicating that after being released from the nucleolus, NS may exert a stronger effect in reducing MDM2 ubiquitylation than GNL3L does. The release of nucleolar proteins from the nucleolus can be triggered by the mitotic entry. As more NS is partitioned in the nucleolus than GNL3L, one may expect this event to increase the NS-MDM2 binding more than the GNL3L-MDM2 binding. To compare the effect of mitosis-induced nucleolar disassembly on the NS-MDM2 and GNL3L-MDM2 interactions, we measured the endogenous binding between MDM2 and GNL3L (or NS) in S-phase and M-phase synchronized cells, and found that the mitosis-induced increase of coIP efficiency is more

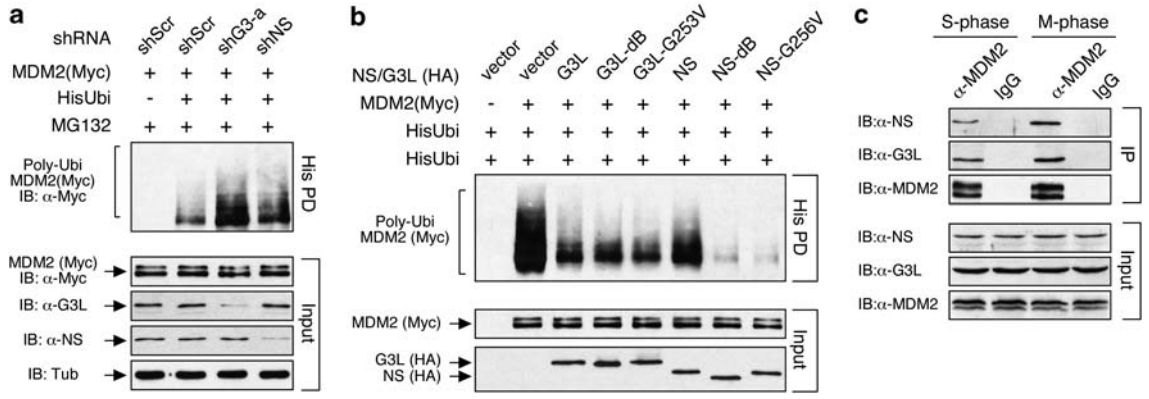

Figure 5 The activity of GNL3L in regulating MDM2 ubiquitylation is constitutively active and less controlled by the nucleolar release mechanism than in the case of NS. (**a**) For *in vivo* ubiquitylation assays, HEK293 cells were transfected with the $(His)_6$-tagged ubiquitin, MDM2 (Myc) and GNL3L or NS-specific short-hairpin RNA constructs. GNL3L knockdown shows a stronger effect in increasing MDM2 ubiquitylation than NS does. (**b**) The effects of GNL3L and NS overexpression on MDM2 ubiquitylation were compared using the same assay. Overexpression of wild-type and nucleoplasmic forms (G3L-dB and G3L-G253V) of GNL3L shows the same effect in decreasing the ubiquitylation of MDM2. On the other hand, nucleoplasmic forms of NS (NS-dB and NS-G256V) show much stronger effects compared not only with wild-type NS but also with wild-type and mutant GNL3L. (**c**) Endogenous coIP of MDM2 and GNL3L (or NS) showed that mitosis increases the coIP efficiency of NS and MDM2 more than it does on the coIP of GNL3L and MDM2.

evident in the NS-MDM2 binding than in the GNL3L-MDM2 binding (Figure 5c). Together, these data demonstrate that despite the common activity of NS and GNL3L in preventing MDM2 ubiquitylation, they differ in that the GNL3L effect is constitutively active and the NS effect is triggered by the nucleolar release mechanism.

GNL3L knockdown induced G2/M arrest and p53 activation

One frequently debated issue concerning the NS activity is whether its cell cycle effect is p53 dependent or not. To clarify this issue for GNL3L, we examined the cell cycle profiles of GNL3L knockdown in two isogenic cell lines that differ only in their p53 status. The parental HCT116-8 cells were derived from human colorectal carcinoma with normal p53 functions and a mutation in the *ras* proto-oncogene. The HCT116-2 line is a derivative of the HCT116-8 line, in which p53 is inactivated by homologous recombination (Bunz *et al*., 1998). In HCT116-8 ($p53^{+/+}$) cells, GNL3L knockdown decreases the G1 cell percentage ($P<0.0001$) and increases the percentage of G2/M cells ($P=0.001$) (Figure 6a). In HCT116-2 ($p53^{-/-}$) cells, the G2/M arrest effect of GNL3L knockdown is less significant ($P=0.07$). The differential sensitivity of $p53^{+/+}$ and $p53^{-/-}$ cells to GNL3L knockdown is not caused by differences in their GNL3L knockdown efficiencies, as western blots confirmed a more effective GNL3L knockdown in the $p53^{-/-}$ cells than in the $p53^{+/+}$ cells (Figure 6b). Western blots also showed that GNL3L knockdown decreases the amount of MDM2 protein in both p53-wild-type and null cells and increases the amount of phospho-Cdc2 (Y15) (an inhibitor of mitotic entry) mainly in the p53-wild-type cells, but does not change the p53 protein level. To determine how GNL3L depletion affects the p53 activity, we measured the mRNA levels of several p53-regulated genes by real-time reverse transcriptase PCR (quantitative reverse transcriptase PCR) (Figure 6c). The results first confirmed that the GNL3L knockdown efficiencies in p53-wild-type and null cells are 25 and 50%, respectively. Notably, GNL3L depletion induces a significant upregulation of Bax ($P<0.0001$), 14-3-3-σ ($P<0.0001$) and p21 ($P<0.01$) in a p53-dependent manner, but does not affect the expression levels of MDM2, Gadd45 or Apaf-1.

NS depletion triggers a compensatory upregulation of GNL3L

To determine whether the expressions of NS and GNL3L are coregulated, we compared their mRNA and protein levels in control (siScr), NS-knockdown (siNS) and GNL3L-knockdown (siG3L) cells (Figure 7a). Quantitative reverse transcriptase PCR and western assays showed that NS depletion induces a significant upregulation of GNL3L transcripts and proteins in both p53-wild-type and null HCT116 cells ($P<0.001$) and a moderate increase of GNL3L in U2OS cells ($P=0.04$). The increase of GNL3L following NS knockdown is cell type-specific, as NS-knockdown HeLa and HEK293 cells show no such effect, and does not work reciprocally on NS when GNL3L is depleted. NS can also be decreased by guanine nucleotide depletion at the protein level (Huang *et al*., 2009). Interestingly, mycophenolic acid treatment, which depletes the endogenous guanine nucleotide by blocking the *de novo* guanine nucleotide biosynthesis, concomitantly decreases the NS protein and increases the GNL3L protein levels (Figure 7b). This increase of GNL3L protein can be reversed by adding a 26S proteasome inhibitor, MG132, but not by restoring the NS level, indicating that the mycophenolic acid effect on GNL3L is not directly controlled by the level of NS protein. To further examine whether GNL3L can

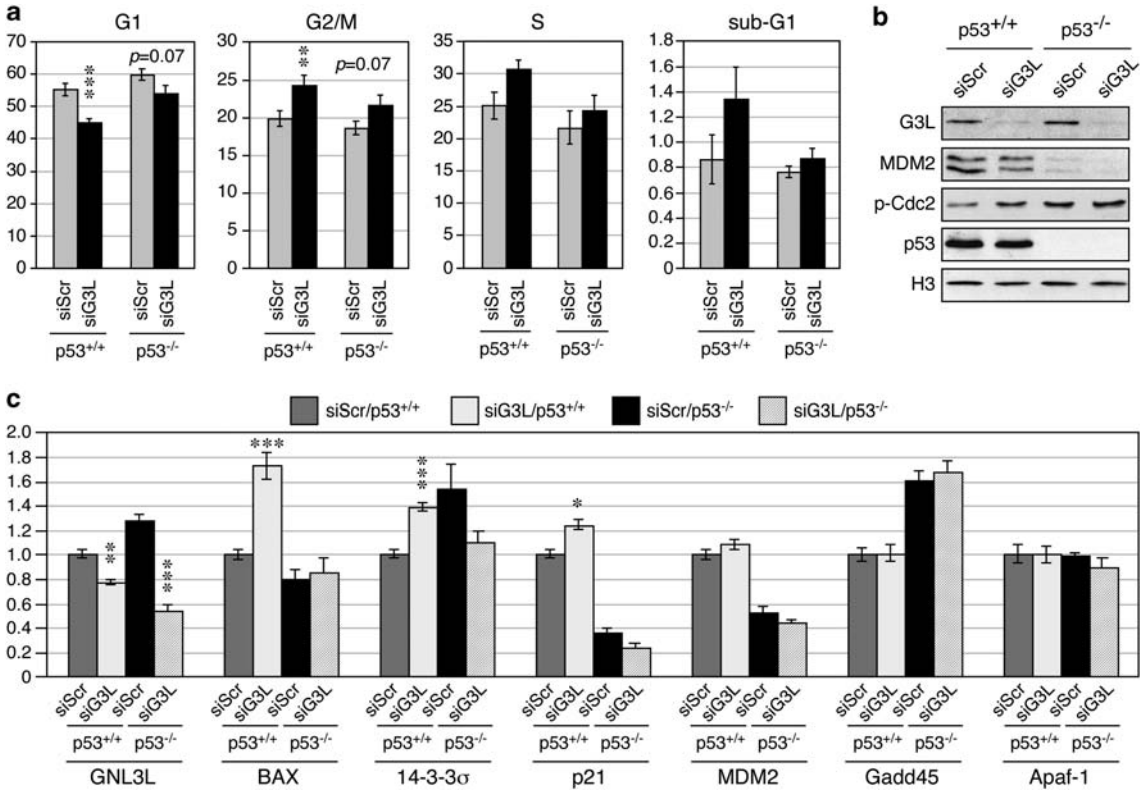

Figure 6 GNL3L knockdown triggers G2/M arrest and p53 activation. (**a**) The cell cycle phenotypes of control (siScr) and GNL3L (siG3L) knockdown were analyzed by propidium-iodide-labeled flow cytometry in HCT116-8 ($p53^{+/+}$) and HCT116-2 ($p53^{-/-}$) cells. GNL3L knockdown triggers G2/M arrest more in the $p53^{+/+}$ cells than in the $p53^{-/-}$ cells. (**b**) Western blots confirm GNL3L knockdown efficiencies and reveal a slight decrease of MDM2 proteins in the p53-wild-type and null cells and an increase of phospho-Cdc2 (Y15) in the p53-wild-type cells by GNL3L knockdown. (**c**) The GNL3L knockdown effect on the p53 activity was determined by quantitative reverse transcriptase PCR assays of several p53 downstream targets. GNL3L depletion upregulates Bax, 14-3-3-σ and p21 in a p53-dependent manner. $^{*}P<0.01$; $^{**}P<0.001$; $^{***}P<0.0001$.

functionally compensate for the loss-of-NS effect on MDM2 ubiquitylation, we performed rescue experiments and showed that the NS-knockdown-induced MDM2 ubiquitylation increase can be fully reversed by coexpression of GNL3L (Figure 7c). These results indicate that some cells may upregulate GNL3L to functionally compensate for the loss of NS.

Correlation between GNL3L expression and p53 activities in human cancers

To establish the relevance of GNL3L and its p53 regulatory activity in human cancers, we first analyzed the expression levels of GNL3L in primary tumor samples using the Oncomine 4.3 (http://www.oncomine.org). We set the threshold of our analysis at *P*-value <0.05 and fold-change >1.5, and calculated the percentage of tumor samples showing upregulation or downregulation of the target genes (Figure 8). We found that a significant portion of the bladder, brain, colorectal, esophageal, gastric, head and neck, kidney, ovarian and sarcoma tumors show increased levels of GNL3L compared with the normal tissues. Particularly, the colorectal, esophageal and gastric tumors display the highest percentages of samples with increased GNL3L expression. Notably, it is also in these three types of tumors that we found downregulation of 14-3-3σ and p21. The decrease of 14-3-3σ and p21 in colorectal carcinomas indicates p53 suppression, which cannot be explained by the transcript changes in MDM2, p53 and other nucleolar proteins that stabilize p53, including ARF, B23, L5, L11 and L23 (Supplementary Figure S2). The expression of Bax, however, is increased in most tumor types. Together, these expression patterns support the idea that high levels of GNL3L may suppress p53 activities in human colorectal cancers.

Discussion

GNL3L and NS both stabilize MDM2 protein by preventing its ubiquitylation

This study reveals that GNL3L, like its vertebrate paralogue, NS, is a novel MDM2 regulator (Figure 7d). GNL3L and NS share similar MDM2-binding characteristics, that is, both occur in the nucleoplasm and bind to the central domain of MDM2. The MDM2 interaction of GNL3L is mediated by its G- or I-domain, which is different from the MDM2-interactive C- and A-domains of NS. Functionally, GNL3L shows the same ability as NS in stabilizing MDM2 protein and preventing its ubiquitylation, and is capable of rescuing the MDM2

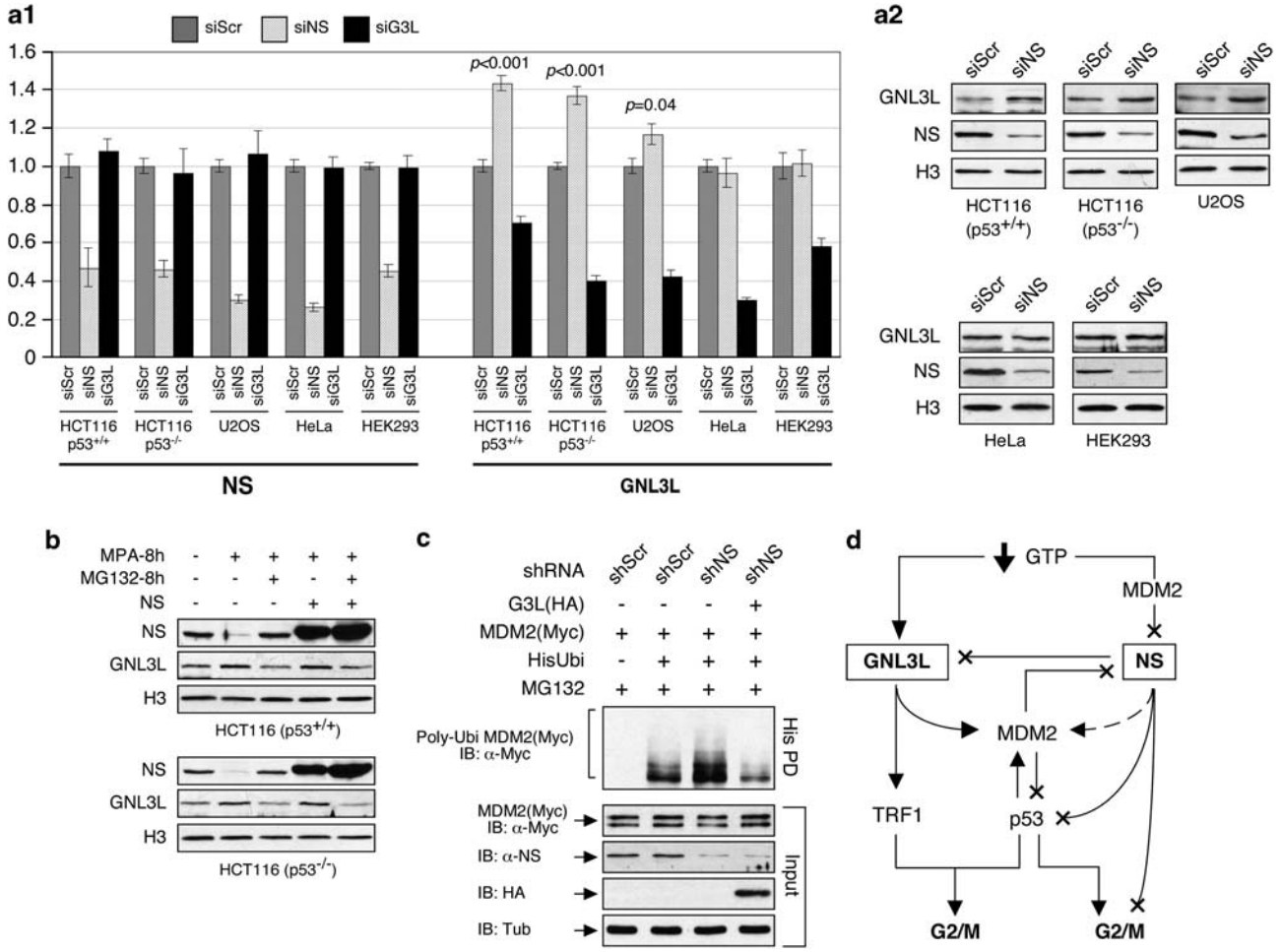

Figure 7 NS depletion triggers a compensatory upregulation of GNL3L in HCT116 and U2OS cells. (**a1**) Quantitative reverse transcriptase PCR measurements revealed a compensatory upregulation of GNL3L transcripts following NS knockdown in p53-wild-type and null HCT116 cells and U2OS cells, but not in HeLa or HEK293 cells. Conversely, GNL3L knockdown shows no such effect on NS. (**a2**) The increase of GNL3L expression by NS knockdown was confirmed by western blots. (**b**) Mycophenolic acid (MPA) treatment triggers an increase of GNL3L and a decrease of NS in HCT116-8 and 2 cells. The MPA-induced GNL3L upregulation can be reversed by MG132 treatment but not by NS overexpression. (**c**) GNL3L can functionally rescue the MDM2 ubiquitylation phenotype of NS-knockdown cells. (**d**) GNL3L and NS form a complex regulatory network on the MDM2-p53 pathway. Both proteins show similar activities in MDM2 stabilization but differ in their modes of regulation. Multiple points of feedback and cross-regulation exist. Arrows and X's indicate excitatory or inhibitory functions, respectively, and the dashed line represents an event regulated by the nucleolar release mechanism.

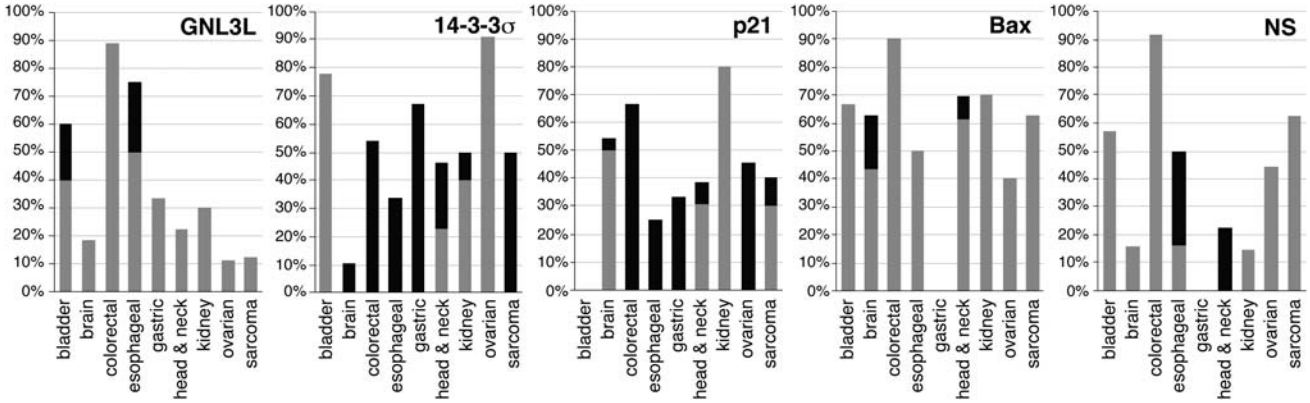

Figure 8 Correlation between GNL3L expression and p53 activities in human cancers. Nine types of human cancers show a significant percentage of samples with increased GNL3L expression. Among them, the colorectal, gastric and esophageal carcinomas also show a downregulation of 14-3-3σ and p21. Bax expression is increased in most tumors. The *y* axis represents the percentage of tumor samples whose expression of the target gene is 1.5-fold higher (gray bars) or lower (black bars) than that of normal tissues.

ubiquitylation effect caused by NS depletion. Like NS, MDM2 destabilization by GNL3L knockdown affects neither the ubiquitylation nor the stability of p53 proteins. Therefore, the GNL3L-stabilized MDM2 may inhibit the transcriptional activation of p53 through a direct binding mechanism without affecting the p53 protein level. Previous reports have shown that deletion of the acidic zinc-finger domain of MDM2 blocks its p53 degradation activity (Kubbutat *et al*., 1999) and that p53 ubiquitylation can be inhibited by peptide binding to the acidic domain of MDM2 (Wallace *et al*., 2006). Considering that GNL3L also binds to the central domain of MDM2, the lack of effect on p53 stability and ubiquitylation by GNL3L indicates that GNL3L binding to MDM2 may disrupt the E3 ligase activity of MDM2, which may also explain how NS and GNL3L prevent MDM2 ubiquitylation, as MDM2 also serves as its own E3 ligase (Fang *et al*., 2000).

Distinct features in GNL3L- and NS-mediated MDM2 regulation

Despite their similar effects on MDM2 stabilization, GNL3L and NS are designed to operate under distinct biological contexts. The binding and ubiquitylation activity of GNL3L on MDM2 is constitutive and does not so much depend on the nucleolar release mechanism. In contrast, the MDM2-stabilizing effect of NS is only active when the nucleolar release mechanism is triggered and therefore is mainly used in the context of cell cycle counting or stress response. Such a difference in the GNL3L- and NS-mediated MDM2 regulation may be due to their differential nucleolar-nucleoplasmic partitioning dynamics (Meng *et al*., 2007). Consistent with the idea that the MDM2-stabilizing effect of GNL3L is constitutively active and the NS effect is kept inactive in normal growing interphase cells, GNL3L knockdown shows a stronger effect on the FLIP kinetics and ubiquitylation of MDM2 than NS knockdown does. Even though wild-type NS is mostly inactive in MDM2 regulation in unstressed interphase cells, a significant amount of NS protein can still be seen in the nucleoplasm when overexpressed. This nucleoplasmic overflow of overexpressed NS and the constitutive binding of endogenous GNL3L and MDM2 may explain why NS and GNL3L overexpression show only a small difference in MDM2 ubiquitylation. It should be noted that the MDM2-regulatory activity of NS nucleoplasmic mutants (NS-dB and NS-G256V) is significantly stronger than that of wild-type and mutant GNL3L, and that NS-G256V shows a stronger MDM2-binding ability than GNL3L. These two results indicate that once released from the nucleolus, NS may exert a stronger effect in reducing MDM2 ubiquitylation than GNL3L does. Besides MDM2 regulation, NS and GNL3L also exercise distinct biological activities in TRF1 and estrogen receptor-related protein-γ regulation, wherein they show opposite effects on TRF1 protein stability (Zhu *et al*., 2009), and only GNL3L can inhibit the transcription activity of estrogen receptor-related protein-γ (Yasumoto *et al*., 2007).

Relationship between MDM2 destabilization and p53 activation in GNL3L-depleted cells

GNL3L knockdown produces a more prominent G2/M arrest phenotype in the p53-wild-type cells ($P<0.001$) than in the p53-null cells ($P=0.07$), showing that the p53 pathway clearly contributes to the cell cycle phenotype of GNL3L-knockdown cells. GNL3L knockdown also leads to an increase in phospho-Cdc2 (Y15) and several p53 downstream targets, including Bax, 14-3-3σ and p21. Upregulation of 14-3-3σ or p21 can trigger G2/M arrest by retaining the Cdc2/cyclin B1 complex in the cytoplasm (Hermeking *et al*., 1997; Taylor and Stark, 2001) or by directly inhibiting Cdc2 (Bunz *et al*., 1998; Taylor and Stark, 2001), respectively. Notably, the expression profiles of GNL3L, 14-3-3σ and p21 in primary tumor samples fit the idea that GNL3L has a role in suppressing p53 activities in the colorectal, esophageal and gastric cancers. However, most human tumors with increased GNL3L also show a paradoxical increase of Bax, even though GNL3L knockdown increases Bax more than it does on 14-3-3σ or p21 in HCT116 cells. Considering the cell type complexity of human cancer samples, this result may not exclude the role of Bax in mediating the GNL3L effect in primary tumors. It is worthy of note that MDM2 can also be regulated by other nucleolar proteins, including ARF, B23, L5, L11 and L23 (Tao and Levine, 1999; Zhang *et al*., 2003; Dai *et al*., 2004, 2008; Jin *et al*., 2004; Kurki *et al*., 2004; Meng *et al*., 2008). Most of these proteins stabilize p53 by inhibiting or sequestering MDM2 in the nucleolus. In colorectal tumors, the levels of *ARF*, *B23*, *L5*, *L11* and *L23* genes are either upregulated or not changed, which raises the possibility that GNL3L may be a key factor in suppressing the p53 activity in these tumors.

NS depletion is associated with a compensatory upregulation of GNL3L

This new discovery was first made in the knockdown experiment. Besides siRNA knockdown, there are only two physiological events known so far that can reduce the expression of NS, that is, cell differentiation (Tsai and McKay, 2002) and guanine nucleotide depletion (Huang *et al*., 2009). Indeed, the decrease of NS expression during neural differentiation is accompanied by a reciprocal increase of GNL3L expression (RYL Tsai, unpublished data). Here, we also observe that guanine nucleotide depletion can trigger NS decrease and GNL3L increase simultaneously, and that this increase of GNL3L can be reversed by MG132 treatment but not by restoring the level of NS protein, which argues against a direct control over GNL3L expression by NS. Importantly, this phenomenon does not occur in all cancer cell lines. It appears in HCT116 and U2OS cells, but not in HeLa or HEK293 cells. Considering that HCT116 and U2OS cells are Rb1-wildtype and p16-inactive, HeLa cells are Rb1-inactive and p16-wildtype and HEK293 cells are Rb1-wildtype and p16-wildtype, this cell type-dependent upregulation of GNL3L by NS knockdown should not involve the p53 and Rb1 pathways and may explain some of the cell

type-specific phenotypes of NS knockdown (Nikpour *et al*., 2009). It also suggests that some cells may survive the consequence of NS depletion better than others in the events wherein NS and GNL3L share redundant functions, such as MDM2 regulation.

Conclusion

MDM2 is a key regulator of p53, which arguably is the most important tumor suppressor gene in the genome. Our data demonstrate that GNL3L stabilizes MDM2 by inhibiting its ubiquitylation and that depletion of GNL3L causes G2/M arrest and upregulation of Bax, 14-3-3σ and p21. Compared with the NS effect, the MDM2-regulatory activity of GNL3L does not so much depend on the nucleolar release mechanism as NS does and behaves as a basal regulator of MDM2. Our work shows that NS and GNL3L are two nucleolar proteins that uniquely stabilize MDM2 and suppress p53 activities, and may have a role in promoting tumor formation in human colorectal carcinomas.

Materials and methods

Cell culture and antibodies

HCT116 and U2OS cells were cultured in McCoy's 5A medium plus 10% fetal bovine serum. Other cell lines were maintained in Dulbecco's modified Eagle's medium plus 10% fetal bovine serum. Early S-phase synchronization was achieved by incubation with 2 mM thymidine for 20 h. Mitotic arrest was done by incubation with 0.5 μM nocodazole for 20 h. Primary antibodies include anti-HA (HA.11), Myc (9E10), FLAG (M2), α-tubulin (Sigma, St Louis, MO, USA), MDM2 (SMP-14), p53 (DO-1), p-Cdc2 (Y15, Cell Signaling, Beverly, MA, USA), p-Histone H3 (S10, Millipore-Upstate, Billerica, MA, USA), NS (Ab2438, Ab1164 and Ab138) and GNL3L (Ab134 and Ab3404).

coIP

Cells were harvested in NTEN (150 mM NaCl, 20 mM Tris–Cl (pH 7.4), 1 mM EDTA (pH 8.0), and 0.5% NP-40) buffer. Lysates were incubated with primary antibody for 1 h at 4C, followed by incubation with protein G sepharose beads (Pharmacia, Saint Paul, MN, USA) for an additional 4 h at 4C. Immunoprecipitates were washed three times with radioimmunoprecipitation assay buffer before SDS–polyacrylamide gel electrophoresis and western detection.

siRNA knockdown of NS and GNL3L

Transient knockdown experiments were performed by either Lipofectamine-mediated transfection of shRNAmir constructs or Oligofectamine-mediated transfection of siRNA duplexes. Designs for NS and GNL3L-specific siRNAs and short-hairpin RNAs were described previously (Meng *et al*., 2008; Zhu *et al*., 2009).

FLIP

FLIP experiments were performed in HCT116-8 cells using the same setup as described previously (Meng *et al*., 2007). A nucleolus of 3-μm diameter was bleached with repetitive pulses at 70% power of the 488 nm Argon laser (Carl Zeiss, Jena, Germany). The relative fluorescence index in the nucleoplasm of bleached cells was normalized to the nucleoplasmic intensity of neighboring non-bleached cells after background subtraction using the following calculation: relative fluorescence index $= (I_{(t)}/I_{(0)})^*(C_{(0)}/C_{(t)})$, wherein $I_{(t)}$ and $I_{(0)}$ are the background-subtracted intensities in the bleached cell at time point t and before photobleaching. $C_{(t)}$ and $C_{(0)}$ are the background-subtracted intensities in the neighboring control cell at time point t and before photobleaching. FLIP data represent the average of 27–30 cells from four to five independent experiments.

Protein degradation and in vivo *ubiquitylation assays*

The cycloheximide protein degradation and *in vivo* ubiquitylation assays were performed as described before (Meng *et al*., 2008). For overexpression protein degradation experiments, Myc-tagged MDM2 was coexpressed with GNL3L in H1299 cells, which express little MDM2. For knockdown protein degradation experiments, the endogenous MDM2 and p53 proteins were measured in HCT116-8 cells.

Cell-cycle analysis

Cell-cycle profiles were analyzed by counting the PI-labeled cells with a Coulter Epics XL flow cytometer (Brea, CA, USA) and the XL System II software. Each cell-cycle profile was compiled from 2×10^4-gated events and analyzed using the Multi Cycle AV software.

Quantitative reverse transcriptase PCR analyses

Total RNAs (5 μg) were reversed transcribed into first strand complementary DNAs using random hexamers and moloney murine leukemia virus reverse transcriptase. For quantitative PCR, the ΔC(t) values between the target message and the reference message (Rplp0) were determined by the MyiQ single-color real-time PCR (Hercules, CA, USA) detection system and supermix SYBR green reagent. The ΔΔC(t) values were measured from three biological replicates and two technical repeats ($n = 6$) to compare the relative expression levels of target sequences between different groups. All final results were confirmed by comparing with a second reference message, HMG-14.

Conflict of interest

The authors declare no conflict of interest.

Acknowledgements

We gratefully acknowledge Bert Vogelstein of the Johns Hopkins Oncology Center for providing the HCT116 cells. This work is supported by NCI-PHS grant R01 CA113750 to RY Tsai.

References

Baddoo M, Hill K, Wilkinson R, Gaupp D, Hughes C, Kopen GC *et al*. (2003). Characterization of mesenchymal stem cells isolated from murine bone marrow by negative selection. *J Cell Biochem* **89**: 1235–1249.

Beekman C, Nichane M, De Clercq S, Maetens M, Floss T, Wurst W *et al*. (2006). Evolutionarily conserved role of nucleostemin: controlling proliferation of stem/progenitor cells during early vertebrate development. *Mol Cell Biol* **26**: 9291–9301.

Bunz F, Dutriaux A, Lengauer C, Waldman T, Zhou S, Brown JP *et al*. (1998). Requirement for p53 and p21 to sustain G2 arrest after DNA damage. *Science* **282**: 1497–1501.

Dai MS, Sun XX, Lu H. (2008). Aberrant expression of nucleostemin activates p53 and induces cell cycle arrest via inhibition of MDM2. *Mol Cell Biol* **28**: 4365–4376.

Dai MS, Zeng SX, Jin Y, Sun XX, David L, Lu H. (2004). Ribosomal protein L23 activates p53 by inhibiting MDM2 function in response to ribosomal perturbation but not to translation inhibition. *Mol Cell Biol* **24**: 7654–7668.

Fang S, Jensen JP, Ludwig RL, Vousden KH, Weissman AM. (2000). Mdm2 is a RING finger-dependent ubiquitin protein ligase for itself and p53. *J Biol Chem* **275**: 8945–8951.

Fu D, Collins K. (2007). Purification of human telomerase complexes identifies factors involved in telomerase biogenesis and telomere length regulation. *Mol Cell* **28**: 773–785.

Hermeking H, Lengauer C, Polyak K, He TC, Zhang L, Thiagalingam S *et al*. (1997). 14-3-3 sigma is a p53-regulated inhibitor of G2/M progression. *Mol Cell* **1**: 3–11.

Huang M, Itahana K, Zhang Y, Mitchell BS. (2009). Depletion of guanine nucleotides leads to the Mdm2-dependent proteasomal degradation of nucleostemin. *Cancer Res* **69**: 3004–3012.

Jin A, Itahana K, O'Keefe K, Zhang Y. (2004). Inhibition of HDM2 and activation of p53 by ribosomal protein L23. *Mol Cell Biol* **24**: 7669–7680.

Kubbutat MH, Ludwig RL, Levine AJ, Vousden KH. (1999). Analysis of the degradation function of Mdm2. *Cell Growth Differ* **10**: 87–92.

Kurki S, Peltonen K, Latonen L, Kiviharju TM, Ojala PM, Meek D *et al*. (2004). Nucleolar protein NPM interacts with HDM2 and protects tumor suppressor protein p53 from HDM2-mediated degradation. *Cancer Cell* **5**: 465–475.

Ma H, Pederson T. (2007). Depletion of the nucleolar protein nucleostemin causes G1 cell cycle arrest via the p53 pathway. *Mol Biol Cell* **18**: 2630–2635.

Maki N, Takechi K, Sano S, Tarui H, Sasai Y, Agata K. (2007). Rapid accumulation of nucleostemin in nucleolus during newt regeneration. *Dev Dyn* **236**: 941–950.

Meng L, Lin T, Tsai RY. (2008). Nucleoplasmic mobilization of nucleostemin stabilizes MDM2 and promotes G2-M progression and cell survival. *J Cell Sci* **121**: 4037–4046.

Meng L, Yasumoto H, Tsai RY. (2006). Multiple controls regulate nucleostemin partitioning between nucleolus and nucleoplasm. *J Cell Sci* **119**: 5124–5136.

Meng L, Zhu Q, Tsai RY. (2007). Nucleolar trafficking of nucleostemin family proteins: common versus protein-specific mechanisms. *Mol Cell Biol* **27**: 8670–8682.

Nikpour P, Mowla SJ, Jafarnejad SM, Fischer U, Schulz WA. (2009). Differential effects of nucleostemin suppression on cell cycle arrest and apoptosis in the bladder cancer cell lines 5637 and SW1710. *Cell Prolif* **42**: 762–769.

Ohmura M, Naka K, Hoshii T, Muraguchi T, Shugo H, Tamase A *et al*. (2008). Identification of stem cells during prepubertal spermatogenesis via monitoring of nucleostemin promoter activity. *Stem Cells* **26**: 3237–3246.

Pederson T, Tsai RY. (2009). In search of nonribosomal nucleolar protein function and regulation. *J Cell Biol* **184**: 771–776.

Siddiqi S, Gude N, Hosoda T, Muraski J, Rubio M, Emmanuel G *et al*. (2008). Myocardial induction of nucleostemin in response to postnatal growth and pathological challenge. *Circ Res* **103**: 89–97.

Tao W, Levine AJ. (1999). P19(ARF) stabilizes p53 by blocking nucleo-cytoplasmic shuttling of Mdm2. *Proc Natl Acad Sci USA* **96**: 6937–6941.

Taylor WR, Stark GR. (2001). Regulation of the G2/M transition by p53. *Oncogene* **20**: 1803–1815.

Tsai RY, McKay RD. (2002). A nucleolar mechanism controlling cell proliferation in stem cells and cancer cells. *Genes Dev* **16**: 2991–3003.

Tsai RY, Meng L. (2009). Nucleostemin: a latecomer with new tricks. *Int J Biochem Cell Biol* **41**: 2122–2124.

Wallace M, Worrall E, Pettersson S, Hupp TR, Ball KL. (2006). Dual-site regulation of MDM2 E3-ubiquitin ligase activity. *Mol Cell* **23**: 251–263.

Yasumoto H, Meng L, Lin T, Zhu Q, Tsai RY. (2007). GNL3L inhibits activity of estrogen-related receptor gamma by competing for coactivator binding. *J Cell Sci* **120**: 2532–2543.

Zhang Y, Wolf GW, Bhat K, Jin A, Allio T, Burkhart WA *et al*. (2003). Ribosomal protein L11 negatively regulates oncoprotein MDM2 and mediates a p53-dependent ribosomal-stress checkpoint pathway. *Mol Cell Biol* **23**: 8902–8912.

Zhu Q, Meng L, Hsu JK, Lin T, Teishima J, Tsai RY. (2009). GNL3L stabilizes the TRF1 complex and promotes mitotic transition. *J Cell Biol* **185**: 827–839.

Zhu Q, Yasumoto H, Tsai RY. (2006). Nucleostemin delays cellular senescence and negatively regulates TRF1 protein stability. *Mol Cell Biol* **26**: 9279–9290.

Supplementary Information accompanies the paper on the Oncogene website (http://www.nature.com/onc)